INFORMATION TO USERS

This manuscript has been reproduced from the microfilm master. UMI films the text directly from the original or copy submitted. Thus, some thesis and dissertation copies are in typewriter face, while others may be from any type of computer printer.

The quality of this reproduction is dependent upon the quality of the copy submitted. Broken or indistinct print, colored or poor quality illustrations and photographs, print bleedthrough, substandard margins, and improper alignment can adversely affect reproduction.

In the unlikely event that the author did not send UMI a complete manuscript and there are missing pages, these will be noted. Also, if unauthorized copyright material had to be removed, a note will indicate the deletion.

Oversize materials (e.g., maps, drawings, charts) are reproduced by sectioning the original, beginning at the upper left-hand corner and continuing from left to right in equal sections with small overlaps.

Photographs included in the original manuscript have been reproduced xerographically in this copy. Higher quality 6" x 9" black and white photographic prints are available for any photographs or illustrations appearing in this copy for an additional charge. Contact UMI directly to order.

ProQuest Information and Learning
300 North Zeeb Road, Ann Arbor, MI 48106-1346 USA
800-521-0600

RANDOM WALKS ON A FLUCTUATING LATTICE

by

Gerald John Lapeyre

A Dissertation Submitted to the Faculty of the

DEPARTMENT OF PHYSICS

In Partial Fulfillment of the Requirements
For the Degree of

DOCTOR OF PHILOSOPHY

In the Graduate College

THE UNIVERSITY OF ARIZONA

2001

UMI Number: 3010238

UMI Microform 3010238

Bell & Howell Information and Learning Company
300 North Zeeb Road
P.O. Box 1346
Ann Arbor, MI 48106-1346

THE UNIVERSITY OF ARIZONA ®
GRADUATE COLLEGE

As members of the Final Examination Committee, we certify that we have read the dissertation prepared by Gerald John Lapeyre

entitled Random Walks on a Fluctuating Lattice

and recommend that it be accepted as fulfilling the dissertation requirement for the Degree of Doctor of Philisophy

Daniel B. Stein — Date 4/4/01

C. David Levermore — Date 4/16/01

Koen Visscher — Date 04/04/01

Date

Date

Final approval and acceptance of this dissertation is contingent upon the candidate's submission of the final copy of the dissertation to the Graduate College.

I hereby certify that I have read this dissertation prepared under my direction and recommend that it be accepted as fulfilling the dissertation requirement.

Dissertation Director — Date 4/4/01

STATEMENT BY AUTHOR

This dissertation has been submitted in partial fulfillment of requirements for an advanced degree at The University of Arizona and is deposited in the University Library to be made available to borrowers under rules of the library.

Brief quotations from this dissertation are allowable without special permission, provided that accurate acknowledgment of source is made. Requests for permission for extended quotation from or reproduction of this manuscript in whole or in part may be granted by the head of the major department or the Dean of the Graduate College when in his or her judgment the proposed use of the material is in the interests of scholarship. In all other instances, however, permission must be obtained from the author.

SIGNED: 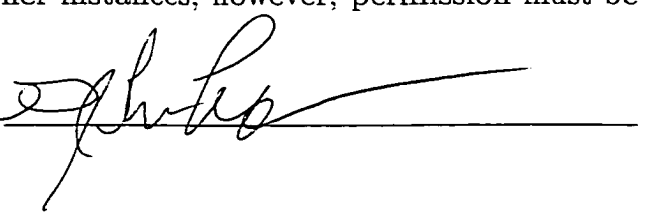

TABLE OF CONTENTS

LIST OF FIGURES

ABSTRACT

In recent years, studies of diffusion in random media have been extended to include the effects of media in which the defects fluctuate randomly in time. Typically, the diffusive motion of particles in a static medium persists when the medium is allowed to fluctuate, with the diffusivity (diffusion constant) D depending on the character of the fluctuations. In the present work, we study random walks on lattices in which the bonds connecting vertices open and close randomly in time, and the walker is not allowed to cross a closed bond. Variations of the model studied here have been used to model the diffusion of CO through myoglobin, the transport of ions in polymer solutions, and conduction in hydrogenated amorphous silicon. The major objective in analyzing these systems is to find efficient methods for computing the diffusivity. In this dissertation, we focus mainly on methods of computing the diffusivity in our model. In addition, we study the critical behavior of the model and present a demonstration, valid for a restricted range of model parameters, that the distribution of the displacement converges in time to a Gaussian with width D.

To compute the diffusivity, we use a numerical renormalization group (RG) method, power series expansions in model parameters, and Monte Carlo simulations. We choose a model with two parameters characterizing the bond fluctuations— the time scale of fluctuations τ and the mean open-bond density p. We calculate a series expansion of the diffusivity to about 10th order in the parameter $\nu = \exp(-1/\tau)$ on the hypercubic lattice $\mathbb{Z}^d$ for $d = 1, 2, 3$, as well as on the Bethe lattice. We compute

the same power series expansion to 3rd order in ν for arbitrary d. We compute estimates of the diffusivity on the Bethe lattice using the RG methods and show by comparison to Monte Carlo data that the RG provides excellent quantitative predictions of D when τ is not too large.

CHAPTER 1

Introduction

The fundamental importance of the idea of diffusion is well known, as it appears in nearly every field of science and engineering. In the past several years workers have attempted to extend older work to diffusion in a broad range of disordered media. Until recently, these studies of transport in disordered media included the assumption that the disorder is static during the time of observation. The first such studies gave rise in the early 1960's to percolation theory (3; 8) which is mainly concerned with the connectivity properties of sites in the medium and neglects the motion of the diffusing particles. After about 1970, studies of random walks on (static) percolation processes began to appear (4; 12; 16; 17; 27; 28; 29). In the 1980's and continuing to the present, models of transport in fluctuating random media have become common in the physics, chemistry, and biology literatures (2; 6; 5; 10; 12; 13; 18; 19; 20; 21; 22; 23).

Our model is derived from the ordinary random walk, with dynamic disorder introduced in a simple and natural way. We begin by recalling the simple random walk. For simplicity, we restrict our attention for the moment to the hypercubic lattices $\mathbb{Z}^d$. The lattice consists of vertices connected by bonds. Each bond connects two vertices, while each vertex is connected to $2d$ bonds. (The number $z = 2d$ is called the coordination number.) The walker begins at the vertex at the origin and

takes a step across one of the $2d$ adjacent bonds, chosen with equal probability, occupying the vertex at the other end. This process is repeated, with the walker hopping to a new vertex at the end of each unit time interval. At the end of n time intervals, the walker occupies a random vertex $S_n \in \mathbb{Z}^d$. It is well known that the motion in an ordinary random walk is diffusive, that is $\langle S_n^2 \rangle / n = 1$, where angle brackets denote an average over all possible paths. Now we add fluctuations to the model, allowing each bond to fluctuate in time between two states; open and closed. If the walker attempts to cross a bond in the open state, it is successful. But if the bond is closed, the attempt fails and the walker remains on the same vertex for that time step. Two parameters characterize the bond fluctuations, the bond correlation time τ and the mean bond density p. There are no spatial correlations in the states of the bonds, but each bond state fluctuates on the time scale τ. At any time a fraction p of the bonds are in the open state. We call this model the fluctuating bond random walk (FBRW). As in the case of the ordinary random walk, we study the distribution of the displacement S_n. But the distribution now depends on the parameters p and τ. If the bond correlation time $\tau < \infty$, the walker may find a bond closed at one time, but open at a later time, so that its motion is not bounded. Our Monte Carlo evidence, and that presented in other work (19), suggests that if $\tau < \infty$, the motion is asymptotically diffusive, which means that the mean square displacement is proportional to time; that is, $\lim \langle S_n^2 \rangle / n \to D$ as $n \to \infty$, where the angle brackets here and in the remainder of this dissertation denote an average over all possible paths and bond histories. The diffusion coefficient $D = D(p, \nu)$ is called the diffusivity. The convergence to diffusive behavior is shown in Fig. 1.1.

In the present work, we address two questions; Firstly, assuming the motion is diffusive, how can one obtain numerical estimates of D? Secondly, can one make

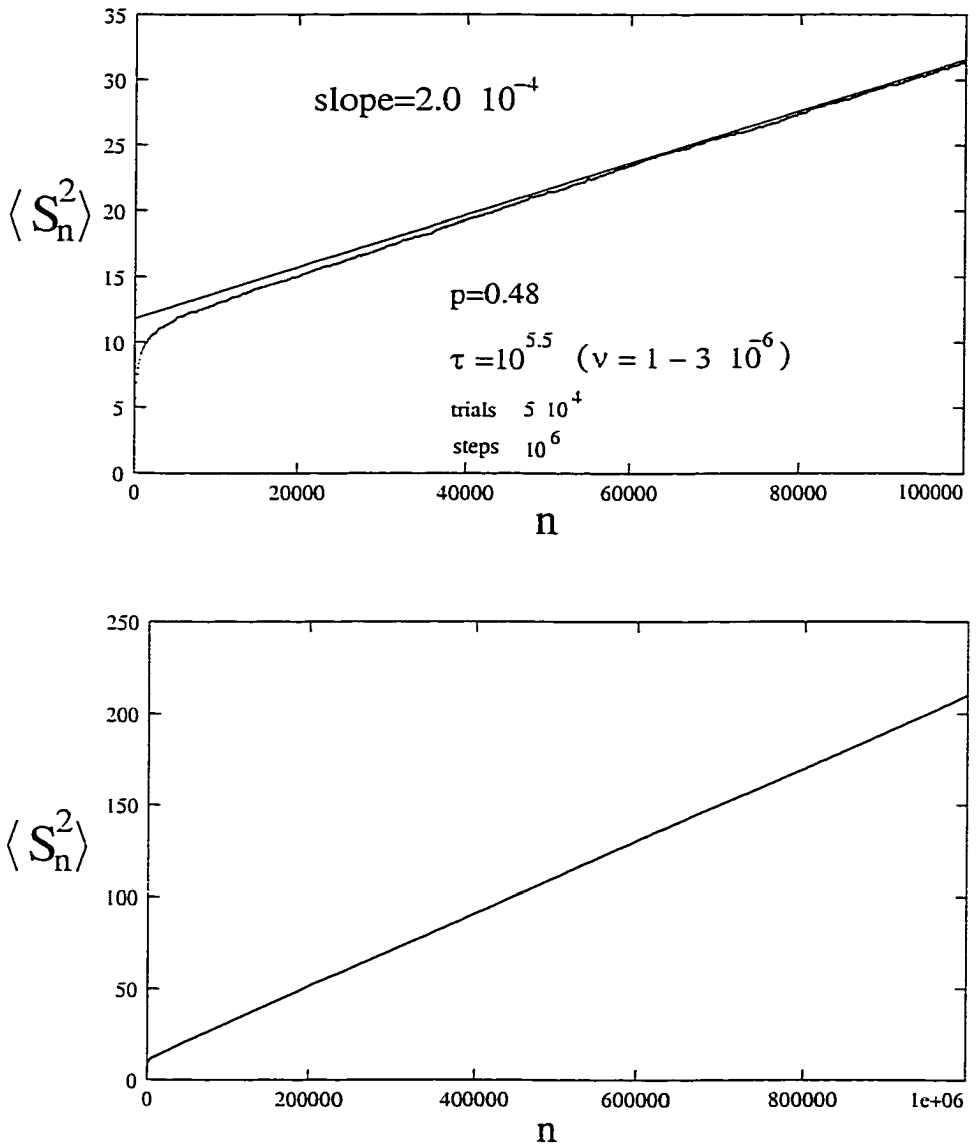

Figure 1.1: Mean square displacement on the Bethe lattice (z=3) as a function of time. The Bethe lattice is described in section 2.7 on page 49. Note the convergence to diffusive motion. The diffusivity is equal to the slope of the curve at long times. Both plots are drawn from the same Monte Carlo data, but the scale in the upper plot shows the non-diffusive regime more clearly. The qualitative shape of the curve, *i.e.* the slope decreasing to a constant value, is the same in d-dimensional lattices and for most parameter values.

the stronger statement that the asymptotic probability distribution is normal? We will see that the answer to the first question is "yes" and will present two analytical approaches to computing D: a series expansion and a renormalization group (RG) procedure. In answer to the second question, we show that, for τ small enough, the asymptotic probability distribution is indeed normal, although numerical evidence suggests that the distribution is in fact normal for all finite τ. The numerical estimates of D are obtained via series expansions, and a related renormalization group procedure. For several lattices, we compute power series expansions in $\nu = \exp(-1/\tau)$ about $\nu = 0$, and in p about $p = 0$. Note that if $\nu = 0$ (that is, $\tau = 0$), the bond fluctuations are infinitely rapid. If $\nu = 1$ (that is $\tau = \infty$), the bond states are static. The expansions in ν are computed to third order for walks on $\mathbb{Z}^d$ for arbitrary d and to about tenth order for $d = 1, 2, 3$ and the Bethe lattice. The expansions in p are valid for all ν, and the expansions in ν are valid for all p. Next, we present an RG procedure that is based on estimates of D obtained from the expansion in ν. The results of the RG calculations are best when ν is small, but generally improve upon the expansion. While numerical evidence indicates that the probability distribution is asymptotically normal for $\nu < 1$, we present a proof valid for p and ν such that $8(2^d)\max(p, 1-p)\,\nu < p$. This restriction is related to a lower bound on the radius of convergence of an expansion of D, and can be improved systematically by computing terms in the expansion in D.

We now describe how the present work fits in the context of the existing literature on transport in disordered media. We mention some physical systems and the models used to describe them. Then, we focus on models most similar to the fluctuating bond random walk and compare their behavior.

The theory of percolation grew out of attempts to explain fluid flow and charge transport in disordered media (3; 8). When the bond disorder is static ($\tau = \infty$), the fluctuating bond random walk becomes a random walk on a bond percolation process. We make use of the large body of work on this subject. In particular, in section 2.6 we discuss the critical behavior observed when $\tau \to \infty$ and $p \to p_c$.

Models such as the FBRW are relevant because in many diffusive systems, motions of the background, as well as of the diffusing particle, must be included in a useful description. One example is diffusion of ions of salts dissolved in polar polymers (6; 21), where it is believed that local motions of the polymer are necessary for long range ion transport. Another example is the diffusion of ligands (*e.g.* O_2 or CO_2) from a solute, through myoglobin, to an active site in the heme pocket (for a review see (15)). In this case there is evidence that a path does not exist through the myoglobin at any moment in time, making fluctuations of the molecule necessary for transport (1; 24). It may be necessary to modify the simplest models in order to describe some systems. This was found to be the case by Lust and Kakalios (LK) (20) when studying the conduction of electrons in films of silicon doped with hydrogen. The dynamic nature of the medium arises from motion of hydrogen atoms, which they model with a bond percolation process in which the bonds are allowed to fluctuate (These models are sometimes called dynamic bond percolation.) However, the experimentally observed conduction is not reproduced if one assumes that all bonds fluctuate with the same rate. It is believed that the hydrogen occupies wells with exponentially distributed energies. LK reported that computer simulations of their model reproduced experimental conduction traces only when they allowed the bonds to fluctuate with waiting times calculated from

a distribution of well depths obtained from other experiments on Si:H.

We discuss the details of only a few models that are closely related to the fluctuating bond random walk. (There are many models of transport in dynamically disordered media that we do not discuss here, including some with site disorder, rather than bond disorder, models with ballistic motion and random scattering centers, and models with continuous random media.) Harrison and Zwanzig (13) applied an effective medium approximation (EMA) to a continuous-time version of the FBRW (the HZ model). In both HZ and the FBRW, the bonds fluctuate between two states, open and closed, with rates p/τ and $(1-p)/\tau$. In the HZ model, the attempted hops occur after exponentially distributed waiting times with mean waiting time 1. We describe briefly the treatment given in HZ. One of several approaches to the effective medium approximation begins with two processes with differing random media. In the first process the independent transition rates are replaced by an effective medium with a spatially uniform transition rate that changes in time. In the second process, each bond has the effective medium transition rate except for one bond, which is allowed to fluctuate as in the original model. The effective transition rate is chosen so that the probability distribution of the walker's position is the same in the two processes. In HZ this condition is actually applied in Laplace transform space to find an effective transition rate $\tilde{\psi}(z)$, where z is the Laplace transform variable conjugate to the time t. The stationary transition rate $\tilde{\psi}(0)$ is then the estimate of the diffusivity for $t = \infty$. The main result of HZ is that $\tilde{\psi}(z) = \psi(z + \frac{1}{\tau})$, where $\psi(z)$ is the transition rate for the EMA on the static lattice. Thus the diffusivity is given by $\tilde{\psi}(0) = \psi(\frac{1}{\tau})$. The EMA for the static lattice has been treated extensively, for instance by Odagaki and Lax (22). Their solution correctly describes some qualitative behaviors. A critical point is predicted (in (22)

and (13), $p_c = 1/d$), but as in mean field theories, the critical exponents are usually incorrect. The walker moves with a time-dependent diffusivity that begins at the value p and decreases to an asymptotic value, which is 0 if $p < p_c$. We see that the effective medium approximation for the fluctuating lattice takes as an estimate of D the time-dependent diffusivity computed in the EMA on the static lattice at time τ.

Levermore, Nadler, and Stein (19) (LNS), made numerical estimates of the diffusivity in the one dimensional FBRW using renormalization group (RG) techniques. They compare the results with the EMA for the HZ model (equation 1.4) and Monte Carlo estimates for several values of p and τ in the regime in which the two models are nearly identical. They found that in one dimension the RG method gives estimates that are significantly better than those given by the EMA. In chapter 4 we give the details of improvements on their RG method. While the RG was successful in one dimension, its use is limited in higher dimensions. The main problem, as we will see, is that when τ is large, it fails to capture the behavior for $p > p_c$, a regime which is inaccessible in one dimension. Still, the RG is successfully applied in higher dimensions, particularly when τ is not too large, or when $p < p_c$.

The expansions developed in chapter 3 give numerical predictions that are much more accurate than the EMA for parameters away from the critical point $(p, \tau) = (p_c, \infty)$. However, the EMA does have some advantages: It has a simple form in one dimension that correctly describes the behavior when $p = 0$ or $p = 1$ as well as at $\tau = 0$; It correctly yields $D \propto 1/\tau$ for large τ; It predicts a critical point in the parameter p when $\tau = \infty$. However, as noted below, the expansion of the EMA for large τ does not have the correct p dependence and in one dimension

the RG method, which uses the correct expansion as a starting point, gives more accurate numerical predictions for the diffusivity.

Druger, Nitzan, and Ratner (6; 5; 21), and Granek and Nitzan (10) have studied random walks in dynamic random environments that generally differ from the FBRW in that the states of all bonds are updated simultaneously at regular or random intervals. Druger, Nitzan, and Ratner (DRN) (6; 5; 21), give particular attention to a simple model. In the DRN model, the walker steps at unit time intervals and the bonds are updated at time intervals of length τ (the renewal period), which is an integral number of unit time intervals. During each renewal period, the bond states remain static. At the end of each renewal period, the state of each bond is chosen to be open with probability p and closed with probability $1-p$. The fact that the states of the bonds during one renewal period are independent from the states during another renewal period makes analysis of the DRN easier than that of the FBRW. Nitzan and Ratner (21) give a review discussing the HZ, the DRN, and other models.

Now we compare the models discussed above. Monte Carlo evidence shows that each of the HZ, the FBRW, and the DRN models have effective diffusivities. A definition of effective diffusivity suitable for all of these models is $D = \lim\langle S_n^2\rangle/n$ as $n \to \infty$. The HZ and FBRW models appear to satisfy the stronger condition that $d\langle S^2\rangle/dn$ tends to a constant, as illustrated in Fig. 2.1 on page 28. (The derivative is periodic with period τ for the DRN model.) One might expect that the HZ model and the FBRW yield the same effective diffusivity as long as τ is much larger than the (mean) step time so that many steps are attempted before a cluster of mutually connected open bonds changes. We performed Monte Carlo simulations

on both models that show that this is indeed the case. But as τ approaches the mean step time, the diffusivities in the two models differ (Fig. 1.2). (The Monte Carlo technique is discussed in chapter 2.)

For both the DRN and the EMA of the HZ model the frequency dependent diffusivity

$$D(\omega) = -\lim_{\epsilon \to 0^+} \omega^2 \int_0^\infty e^{-i\omega t - \epsilon t} \langle S^2 \rangle(t)\, dt \tag{1.1}$$

obeys the simple relation

$$D(\omega, \tau) = D_0 \left(\omega - \frac{i}{\tau} \right), \tag{1.2}$$

where $D_0(\omega)$ is the frequency dependent diffusivity in the limit $\tau \to \infty$ (13; 21). This agrees with the discussion of the HZ model above, but the exact solution of HZ does not obey this relation. Although we have not computed the equivalent of (1.1) for the FBRW, the similarity of the HZ model and the FBRW (specifically correlations over long times) leads us to expect that (1.2) does not hold for the FBRW. In the DRN model, the diffusivity satisfies

$$D = \frac{\langle S_\tau^2 \rangle}{\tau}, \tag{1.3}$$

where the mean square displacement is computed over the first renewal period. Because the bonds are static during a renewal period, the numerator in (1.3) is the mean square displacement on the static lattice after a time τ. This simple behavior can be understood by noticing that, for the DRN model, during each renewal period we have a walk on a static lattice with the final distribution from the previous period taken as the initial distribution. Notice the similarity between the diffusivity given by (1.3) and the diffusivity in the EMA of the HZ model above. Both take a diffusivity computed after a time τ on the static lattice as an estimate.

(The estimate is exact for the DRN.) Consider the case that $p < p_c$ and τ is large, so that the numerator in (1.3) depends only weakly on τ and is approximately $\langle S_\infty^2 \rangle$. In LNS, the expression for the diffusivity given by the EMA in HZ was calculated explicitly in one dimension, with the result

$$D_{eff}^{EM} = 1 + 2\tau(1-p)^2 - \sqrt{\left[1 + 2\tau(1-p)^2\right]^2 - p(2-p)}\,. \tag{1.4}$$

To lowest order in $1/\tau$ and to order p^2 in p, this formula becomes

$$D_{eff}^{EM} \approx \left(\frac{p}{2} + \frac{3p^2}{4}\right)\frac{1}{\tau}. \tag{1.5}$$

As we mentioned before, the FBRW and the HZ model behave the same in this limit (that is for large τ), but (1.5) does not give the correct p dependence as it does not agree with our exact expansion given in (3.12) on page 69. We also ask if substituting the exact expression for $\langle S_\infty^2 \rangle$ with $p < p_c$ and $\tau = \infty$ into (1.3) gives the correct result for the FBRW. In section 3.2 we give the exact expression for $\langle S_\infty^2 \rangle$ in one dimension and show that it does not agree with the exact expression for D in the limit of small p. Finally, we examine (1.3) on the Bethe lattice near the critical point, with $p < p_c$. An exact calculation shows that $\langle S_\infty^2 \rangle \propto \ln(p_c - p)$ for $\tau = \infty$. However, in section 2.6, we will see that the true behavior in this case obeys $D \approx (p_c - p)^{-1.5}/\tau$, which disagrees with (1.3).

Druger, Nitzan, and Ratner (6) have shown that the DRN is diffusive. Calculations for the FBRW, such as the proof of diffusivity, are more difficult than they are for the DRN because all bonds are updated simultaneously for the DRN. Still, we are able to derive an expansion for the effective diffusivity D about the rapid bond-fluctuation limit, which is shown to converge for ν small enough. (There is no reason to suspect that it fails to converge for any $\nu < 1$. For instance, Monte

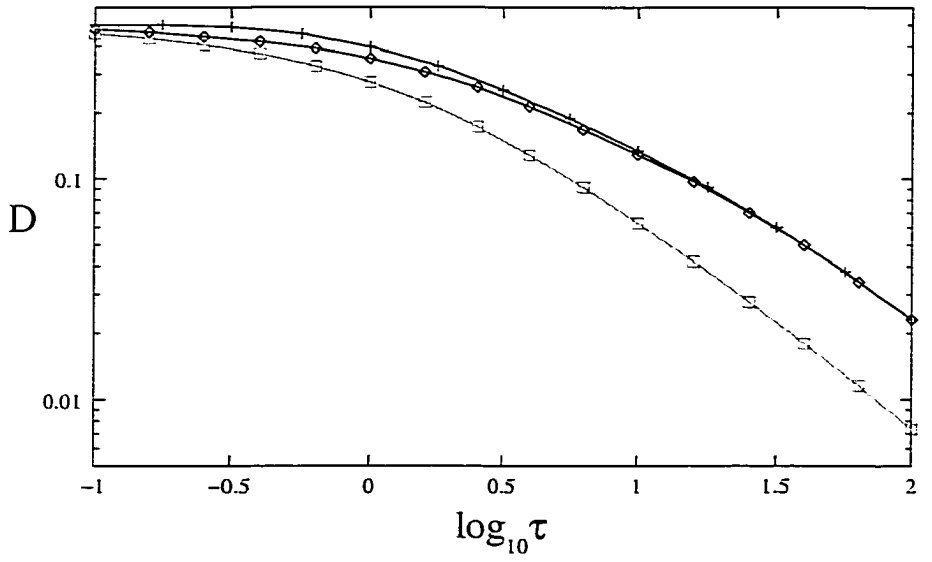

Figure 1.2: Diffusivity D in one dimension for $p = 0.5$. Pluses are MC simulations of the FBRW, diamonds are MC simulations of the exact HZ model, and squares are the effective medium approximation from (1.4). The Monte Carlo estimates show that the diffusivity in the FBRW model approaches that in the HZ model as τ becomes large, while the relative error in the effective medium estimate grows.

Carlo evidence shows that the only qualitative change in behavior occurs at $\nu = 1$.) The proof that the asymptotic distribution is normal is based on the expansion and is valid for ν small enough.

The remainder of this dissertation is organized as follows. In Chapter 2, we describe the model, and discuss its general behavior. In Chapter 3, we present expansions of D about the limit of rapid fluctuations, as well as expansions about the low bond-density limit. In Chapter 4, we describe the RG procedure and present the results. In Chapter 5, we give a proof, valid for small ν, that the asymptotic distribution of the walker's position is normal.

CHAPTER 2

The Fluctuating Bond Random Walk

In this chapter we give a description of the fluctuating bond random walk (FBRW) and some of its properties. We begin by defining the model. Next, we discuss its general behavior including information obtained from Monte Carlo simulations and scaling theory. We predict scaling behavior on different time scales, supported by Monte Carlo evidence. Finally, we discuss the implementation of the model on the Bethe lattice. The structure of the Bethe lattice requires that we define the distance function so that the statistical properties of the walk are similar to those on the Euclidean lattices.

2.1 Definition of the Model

Before explaining the behavior of the FBRW, we present a more detailed description. Except where noted, we make no assumptions on the structure of the lattice. The lattice is a collection sites together with bonds connecting pairs of sites (In the language of graph theory, these are vertices and edges.) We provide the lattice with an origin and a metric so that we can measure distance from the origin. There is a state associated with each bond which can take two values: open or closed. The walker begins at time $n = 0$ at the origin and attempts to make steps in random directions, independent of the states of the bonds, at times $n = 1, 2, 3, \ldots$. If the

bond attempted at time n is open, then the walker crosses that bond and occupies the site at the other end. If the attempted bond is closed, then the walker waits at the same site and makes an attempt in a random direction at time $n+1$. Thus, the walker may attempt the same bond several times, finding it at times open and at other times closed. We denote the displacement from the origin after n time steps by S_n; for walks on $\mathbb{Z}^d$, we have $S_n \in \mathbb{Z}^d$. The definition of S_n on the Bethe lattice is discussed in section 2.7. We denote the mean square displacement after n time steps by $\langle S_n^2 \rangle$.

We now describe the bond fluctuations in greater detail. Each bond fluctuates independently between two states. There are no spatial correlations among the bonds, and the states of the bonds are independent of the state of the walker. The bond fluctuations are characterized by two parameters, the mean bond density p and the relaxation time τ. We denote by $p_{i,j}^{(n)}$ the probability that a bond is in the state j at time $n+n_0$ given that it was in the state i at time n_0. We define the bond state transition matrix as in reference (19)

$$\mathbf{p^{(n)}} = \begin{pmatrix} p_{0,0}^{(n)} & p_{0,1}^{(n)} \\ p_{1,0}^{(n)} & p_{1,1}^{(n)} \end{pmatrix} = \begin{pmatrix} q+p\nu^n & p-p\nu^n \\ q-q\nu^n & p+q\nu^n \end{pmatrix}, \tag{2.1}$$

where $q = 1-p$ and $\nu = \exp(-1/\tau)$. Initially, all bonds are in the stationary state, that is, each is open with probability p. Notice that a power series expansion of ν in τ about $\tau = 0$ does not exist. It follows that a function of ν, such as the diffusivity, cannot be expanded in both τ and ν at $\nu = \tau = 0$. We will see below that the parameter ν is a natural choice for the expansion of the diffusivity. The parameters p and ν both take values on $[0,1]$.

2.2 Monte Carlo Simulations

The main lesson to be learned from our Monte Carlo simulations is that the FBRW is diffusive at long times. To obtain an estimate of D for a particular pair of parameters (p, ν), we used the following procedure. We performed 10^5 — 10^6 trials of a walk of 10^5 — 10^7 time steps. We estimated $\langle S_n^2 \rangle$ by computing S_n^2 for each trial and averaging over the trials. We then plotted the average *v.s.* n, and fit a line to the portion of the resulting curve at long times. We found that slope decays roughly exponentially (at the longest times) to a constant, with a time constant that diverges as $(p, \nu) \to (p_c, 1)$. When the parameter values are close enough to this critical point, the walk will not have converged within the number of time steps simulated. For the case that τ is greater than the maximum value of n in the simulation, we used the following method to determine if the walk has converged. We have exact expressions for the asymptotic mean square displacement on the static lattice for 1-d and the Bethe lattice when $p < p_c$. It seems reasonable that the walk will converge more quickly when $\nu < 1$ than when $\nu = 1$. Indeed the curves showed this behavior. Because we know the asymptotic value of $\langle S_n^2 \rangle$ in the static case exactly, we can measure the time constant of the decay to $\langle S_n^2 \rangle$ in this case. We then discard curves in which the maximum time is less than three times the time constant from the static case. For $p > p_c$ on the Bethe lattice, we have to use a cruder method, such as fitting a line to the end of the data and measuring the decay constant from the decay to this line.

2.3 Diffusive Behavior of the Model

In this section, we are concerned with the qualitative behavior of the diffusivity (diffusion coefficient) as a function of the parameters τ and p. We use two approximates to the diffusivity for finite time n, the average approximate

$$D_n^A(p,\nu) = \frac{1}{n}\langle S_n^2\rangle, \quad n = 1, 2, \ldots, \tag{2.2}$$

and the incremental approximate

$$D_n^I(p,\nu) = \langle S_n^2\rangle - \langle S_{n-1}^2\rangle, \quad n = 1, 2, \ldots, \tag{2.3}$$

where we set $D_0^A(p,\nu) = 0$. The reason for the names of these approximates becomes more clear when we note that

$$D_n^A(p,\nu) = \frac{1}{n}\sum_{i=1}^{n} D_i^I(p,\nu) = \frac{\langle S_n^2\rangle - \langle S_0^2\rangle}{n}, \tag{2.4}$$

and that

$$D_n^I(p,\nu) = nD_n^A(p,\nu) - (n-1)D_{n-1}^A(p,\nu). \tag{2.5}$$

We define the diffusivity by

$$D(p,\nu) = \lim_{n\to\infty} D_n^I(p,\nu). \tag{2.6}$$

As mentioned above, we assume that the limit exists for all p and ν. It is easy to show that the existence of the limit in in (2.6) implies that the average approximate defined in (2.2) approaches the same limit as $n \to \infty$. The converse is not true. For instance, for the dynamic bond percolation model, the limit of the average approximate exists but not the limit of the incremental approximate (5).

We now discuss the qualitative behavior of the mean square displacement and the approximates to the diffusivity, as well as trivial behavior that occurs

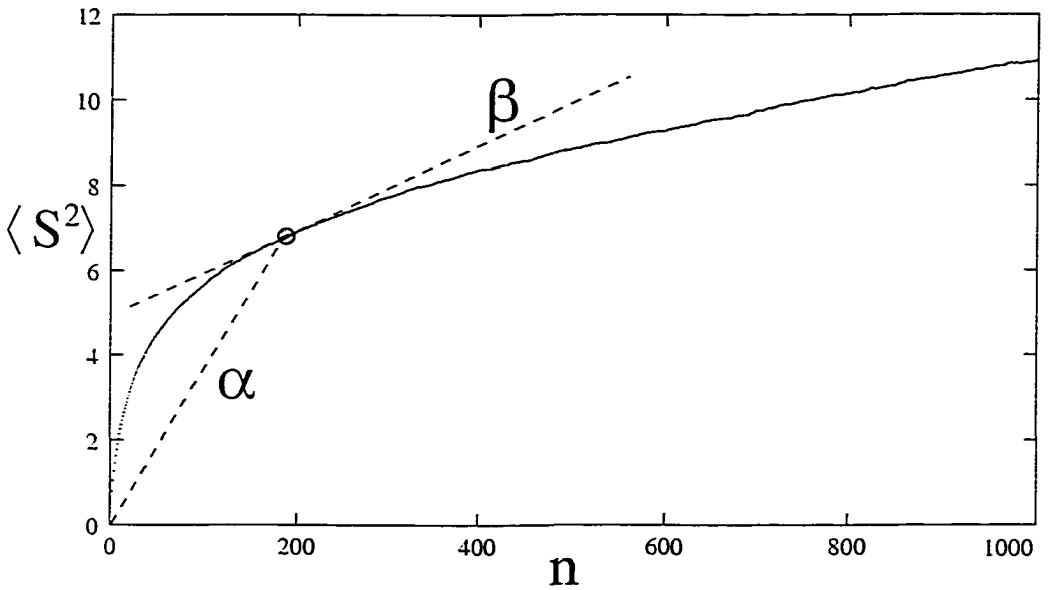

Figure 2.1: Mean square displacement $\langle S_n^2 \rangle$ *v.s.* time n. The incremental approximate $D_n^I(p,\nu)$ at the indicated point is given by the slope of the line marked β, which is tangent to the curve. The average approximate $D_n^A(p,\nu)$ is given by the slope of the line marked α, which passes through the origin. Note $\langle S_n^2 \rangle$ is linear for large times and the two approximates approach the same limit for large times. $D_n^I(p,\nu)$ is a better approximation than $D_n^A(p,\nu)$. This is a section of Monte Carlo data in which the linear behavior persisted for 10^6 time steps.

for certain parameter values. The statements that follow hold for the FBRW on $\mathbb{Z}^d$ and the Bethe lattice (if we use the metric on the Bethe lattice described in section 2.7). The bonds all begin in the stationary state, which means that they are open with probability p. Thus, on the first step, the walker is successful with probability p, regardless of the value of ν. So $\langle S_1^2 \rangle = D_1^A(p,\nu) = D_1^I(p,\nu) = p$. On the second step, there is a chance that the walker will attempt to cross the same bond that it attempted on the first step. So if $\nu > 0$, correlations enter into $\langle S_2^2 \rangle$ and therefore into the approximates to the diffusivity. Monte Carlo simulations and exact calculations for $n = 10$ show that, because of correlations, $D_n^A(p,\nu)$ and $D_n^I(p,\nu)$ decrease monotonically in n. However, the rate of decrease slows and the two approximates approach the same limit. This situation is depicted in Fig. 2.1. It is evident from the figure and equation (2.3) that $D_n^I(p,\nu)$ is roughly the derivative of the mean square displacement for large n.

Now we examine the behavior of the diffusivity at long times, which is illustrated in Fig. 2.2. For certain values of the parameters, the behavior of the model is trivial. When $p = 0$, all bonds are closed all of the time, so $D(0,\nu) = 0$. When $p = 1$, we have an ordinary random walk and $D(1,\nu) = 1$. When $\nu = 0$, the state of a bond at any particular time is independent of its state at other times. At each step, the walker proceeds with probability p. On average, this amounts to waiting a fraction $1 - p$ of the time; we have an ordinary random walk with time rescaled by a factor of p. So $D(p,0) = p$. When p increases, more bonds open and the diffusivity increases. It is not so obvious that the diffusivity should increase with decreasing ν. One can think of the walker as being trapped on clusters of open bonds, with the lifetime of the traps decreasing as bonds fluctuate more rapidly.

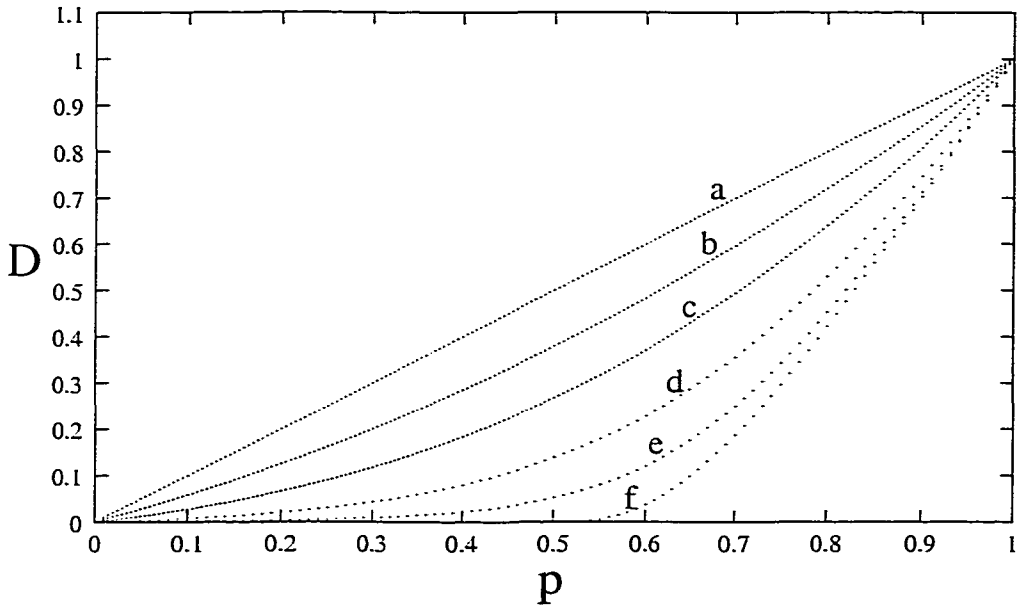

Figure 2.2: Diffusivity D on the Bethe lattice with $z = 3$. Curves are for different values of ν: (a) 10^{-4}; (b) 0.57; (c) 0.83; (d) 0.97; (e) 0.994; (f) 1.0. Notice the critical point $(p, \nu) = (1/2, 1)$. Curves a–c are obtained from expansions, and d–f are obtained from Monte Carlo simulations.

As $\tau \to \infty$ (that is $\nu \to 1$) the behavior of the model approaches that of a random walk on a static lattice. We discuss the walk on the static lattice in more detail in the next section. When τ is large the critical density for percolation on the static lattice becomes important. We find that, for $p < p_c$, $D \propto 1/\tau$ to leading order as τ increases (Fig. 3.3). For $p > p_c$, D approaches a non-zero constant as τ increases. If we fix $p = p_c$ and approach the critical point by increasing τ, we expect the diffusivity to decay more slowly than it does for $p < p_c$. Monte Carlo simulations on the Bethe lattice show that this is the case, with D decaying as $\tau^{-\alpha}$, with $\alpha \approx 0.66$. Because critical exponents on the Bethe lattice are typically ratios of small integers, it seems likely that $\alpha = 2/3$. This decay is shown in Fig. 2.3. Before discussing the critical behavior of the walk in more detail, we must review some of the elements of percolation theory.

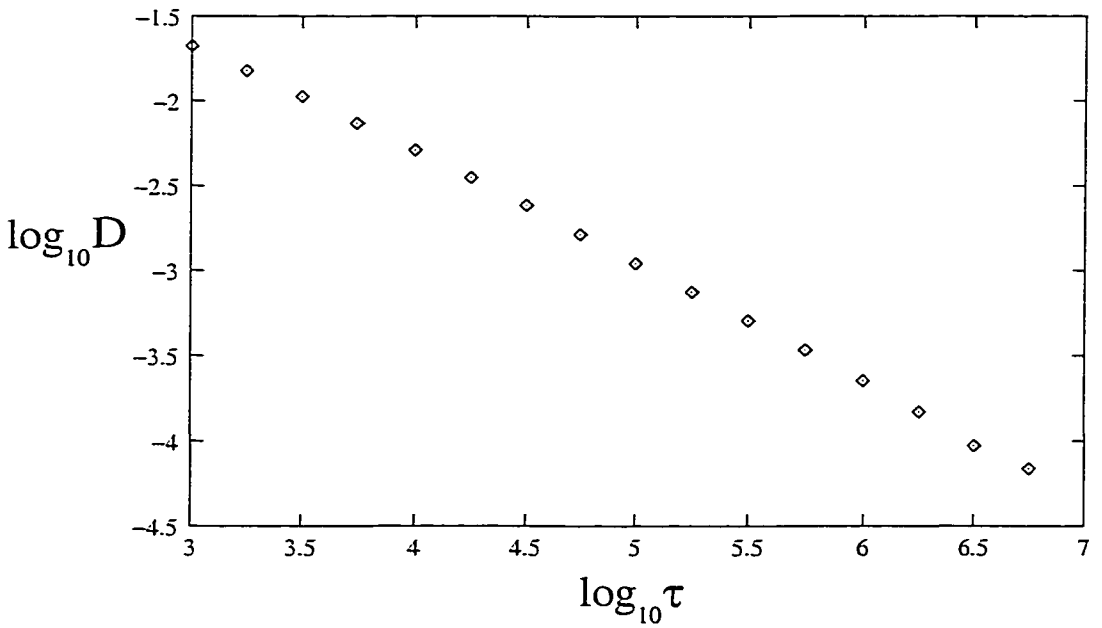

Figure 2.3: Diffusivity at $p = p_c$ for various τ on the Bethe lattice for $z = 3$. The slope of a line fit to the points is approximately -0.66. Each point is computed from Monte Carlo simulations of 10^5 trials of walks of 10^5 steps. For larger values of τ a systematic error occurs because of the increasing time of relaxation to diffusive motion. The error in the points for the largest values of τ shown here is largely statistical.

2.4 Percolation Theory

On the longest time scales, the pattern of open bonds in the FBRW is completely changed many times. However, if $\tau \gg 1$, then the walker takes many steps on an essentially static lattice. In order to understand how the properties of the static disordered lattice appear in the FBRW, we must understand some of the basic facts of percolation theory. In this section, we discuss briefly bond percolation on $\mathbb{Z}^d$, presenting those features that bear on the FBRW. A more detailed treatment of the material in this section can be found in references (11) and (25).

In percolation theory, each bond on the lattice is open with probability p and closed with probability $1-p$. One then studies the connectivity properties of sites on the lattice; for instance, one can ask for the probability that two particular sites are connected by a path of open bonds. The basic fact of percolation theory is that the system exhibits only two phases separated by a single critical point $p = p_c$. In the super-critical phase ($p > p_c$), there is a cluster containing an infinite number of sites that are connected by unbroken paths of open bonds. In the sub-critical phase, no such infinite cluster exists.

Before explaining the phases in more detail, we define the percolation process more carefully. We call the elements of $\mathbb{Z}^d$ sites. The set of bonds is the set of all (unordered) pairs $\langle x, y \rangle$ with $x, y \in \mathbb{Z}^d$ such that $\delta(x, y) = 1$, where δ is the Euclidean distance. Typically, as in this dissertation, the phrase "bond percolation on $\mathbb{Z}^d$ ", means percolation on this structure of sites and bonds. In a realization of the percolation process, each bond is chosen independently to be in one of two states. Each bond is open with probability p and is closed with probability $1-p$.

One can also study site percolation, in which the bonds play no role, but the sites are taken to be randomly open or closed.

The main object of study in percolation is the open cluster (often called simply a "cluster"). The open cluster can be defined in terms of open paths. An open path is a (possibly infinite) sequence of adjacent open edges $\{\langle w,x\rangle, \langle x,y\rangle, \langle y,z\rangle, \ldots\}$, together with the sites $\{w,x,y,z,\ldots\}$. The open cluster at the site x, denoted by $C(x)$, is the set of all sites and edges in every open path containing x. If x is in no open path, then we let $C(x) = \{x\}$. We denote the number of sites in $C(x)$ by $|C(x)|$. Because $\mathbb{Z}^d$ and the probability distribution are translationally invariant, statements about the cluster at an arbitrary site x are equivalent to statements about the cluster at the origin $C(0)$, which we denote by C. In this section, we use the notation $P(A)$ for the probability that the event A occurs in the percolation process. We use the notation $\langle X\rangle$ for the expectation (average) of the random variable X in the percolation process.

Percolation theory consists of the study of statistics of clusters. As mentioned above, the most important fact is that there exists a single critical point $p_c = p_c(d)$ that separates two phases in which clusters differ qualitatively. When $p > p_c$, $P(|C| = \infty) > 0$, that is, the origin is in an infinite cluster with strictly positive probability. When $p < p_c$, $P(|C| = \infty) = 0$. Application of a standard theorem from probability theory (the Kolmogorov zero-one law) gives immediately that an infinite cluster exists with probability 1 when $p > p_c$. Furthermore, it can be shown that the infinite cluster is unique. When $p = p_c$ it is believed that no infinite cluster exists, although this has been proven only for $d = 2$. In the remainder of this section, we shall assume $d < 6$, the upper critical dimension. The distribution

of cluster sizes differs between the super- and sub-critical phases. It is believed that asymptotically

$$P(|C| < s < \infty) \approx e^{-\gamma_1 s} \quad \text{for } p < p_c, \tag{2.7}$$

$$P(|C| < s < \infty) \approx e^{-\gamma_2 s^{(d-1)/d}} \quad \text{for } p > p_c, \tag{2.8}$$

for some constants γ_1 and γ_2. Next, we describe results of scaling theory. Most of the conjectures of scaling theory are not proven, but they are widely believed and well supported, for instance, by Monte Carlo simulations.

Scaling theory provides a phenomenological explanation for cluster structure when p is near p_c. If p changes by a small amount, one expects that the connectivity properties of bonds on a relatively small sub-lattice will change proportionately. But, if p is near p_c and the sub-lattice is large, changing p by a small amount, and hence the state of just a few bonds, may affect connectivity over large distances. This behavior is seen empirically and is quantified in scaling theory. The main idea in scaling theory is that there is a length scale, the correlation length $\xi(p)$, below which the percolation process does not differ qualitatively from the process at $p = p_c$. The correlation length diverges as p approaches p_c. Furthermore, the correlation length is the only macroscopic (that is, larger than the lattice spacing) length scale. On scales much larger than ξ, the process appears homogeneous with a granularity of order ξ. On scales smaller than ξ, structures have no typical size, rather blobs and holes occur on all length scales, leading to a (statistical) fractal structure. For instance, consider drawing a box of linear dimension L in a large cluster. If $L < \xi$, then the mass of the cluster in the box is proportional to L^D, with $D < d$. But if $L > \xi$, the mass is proportional to L^d. Because, for $L > \xi$, the cluster is homogeneous, but regions of linear size ξ have mass ξ^D, the mass is

proportional to $\xi^D L^d$.

One assumption of scaling theory is that all reasonable definitions of the correlation length are equivalent. Consider the event that the origin is connected to a site located n units from the origin on the first axis. We denote this site by $x_n = (n, 0, \ldots, 0)$. This is the same as the event that the origin and x_n are in the same open cluster. It is believed that the probability of this event decays exponentially when $p \neq p_c$. One can take, for instance,

$$\xi^{-1} = \lim_{n\to\infty} \left\{ -\frac{1}{n} \log P\left(x_n \in C; |C| < \infty\right) \right\}. \tag{2.9}$$

In the definition we have excluded events for which the origin is in the infinite cluster, otherwise the correlation would not decay when $p > p_c$.

Near the critical point, many cluster properties vary as $|p - p_c|$ to a power. The power laws that concern us here follow from two assumptions. The first assumption is that the correlation length obeys

$$\xi \approx |p - p_c|^{-\phi} \quad \text{as } p \to p_c, \tag{2.10}$$

for some $\phi > 0$, where $a \approx b$ means $\log a / \log b \to 1$. The exponent ϕ depends on d but not on the details of the percolation model.[1] For instance, site percolation on a hexagonal lattice and bond percolation on $\mathbb{Z}^2$ have the same value for ϕ. Equation 2.10 is valid for p near p_c. As $|p - p_c|$ grows, corrections to scaling become important. The second assumption, which concerns the form of the distribution of cluster masses, is

$$P(|C| = s) \sim s^{-\theta} f[(p - p_c)s^{\sigma}], \tag{2.11}$$

[1] In the literature, this exponent is usually usually denoted by ν.

where $\theta, \sigma > 0$, and the relation "$\sim$" means that the ratio of the left hand side to the right hand side approaches 1 as $p \to p_c$ and $s \to \infty$. The function $f(z)$ behaves roughly like an exponential. It approaches a constant at $z = 0$ and decays faster than any power of z when z is large. Equation 2.11 is an example of a scaling ansatz. Assumptions similar to (2.11) are made repeatedly in percolation theory, as well as in the study of other critical phenomena. A common feature is the presence of a cross-over phenomenon. In this case, $P(|C| = n)$ decays roughly algebraically when the mass n is smaller than $|p - p_c|^{1/\sigma}$, but decays exponentially for much larger n.

These two assumptions provide a unified basis for understanding the scaling laws that we state below. Furthermore, one can use the scaling ansatz to calculate the asymptotics of the moments of the cluster size distribution and to relate the resulting critical exponents to three fundamental exponents. Below, we will give an example of such a calculation. But here, we only state some of the results. The percolation probability $\theta(p) = P(|C| = \infty)$ is the probability that the origin is in the infinite cluster. For $p < p_c$, $\theta(p) = 0$. As p increases from p_c to 1, $\theta(p)$ increases from 0 to 1. It is believed that $\theta(p)$ vanishes at p_c according to

$$\theta(p) \approx (p - p_c)^{\beta} \quad \text{as } p \downarrow p_c, \tag{2.12}$$

for some $\beta > 0$. As mentioned above, it is likely that $\theta(p_c) = 0$ [as required by (2.12).] However, one still finds references to the cluster at $p = p_c$, the "incipient infinite cluster". To understand the incipient infinite cluster, one can define a new process by considering a box of linear size L centered on the origin of a percolation process at $p = p_c$. One deletes all configurations that contain no path joining the origin to the surface of the box and considers the process in the limit $L \to \infty$. The resulting process has an infinite cluster with probability one. This infinite cluster

is believed to have the same properties that the non-critical infinite cluster in the original process has on length scales smaller than ξ. Kesten (16) has proved some statements showing that the distribution of a walk on this object is not Gaussian.

The average cluster size is defined by $\chi(p) = \langle |C|; |C| < \infty \rangle$, where the average is taken over all bond configurations. We exclude configurations with an infinite cluster from the average in order that $\chi(p)$ remain finite when $p > p_c$. Although there is no infinite cluster at $p = p_c$, $\chi(p)$ diverges at this point because the cluster size distribution decays slowly. The average cluster size diverges at $p = p_c$ according to

$$\chi(p) \approx |p - p_c|^{-\gamma} \quad \text{as } p \to p_c, \tag{2.13}$$

for some $\gamma > 0$. We will find scaling theory useful in understanding the random walk on the static lattice.

2.5 Random Walks on the Static Lattice

In this section, we discuss random walks on the static lattice (*i.e.* on a percolation process), giving particular attention to the critical behavior. A review of the subject can be found in reference (25). We consider a random walk on the bond percolation process on $\mathbb{Z}^d$. The process is equivalent to the fluctuating bond random walk when the bond fluctuation time $\tau = \infty$. One can imagine executing a random walk on a realization of the percolation process on an infinite lattice. However it is useful to review the process in the context of the FBRW. The walker begins at the origin and attempts to step at unit time intervals from the site it occupies to one of its nearest neighbors chosen at random. If the bond connecting the occupied site to the chosen nearest neighbor has not been attempted before, then this bond's state

is chosen at random; it is open with probability p and closed with probability $1-p$. If bond is determined to be closed then the walker stays at the occupied site. But if the bond is open, the walker crosses it and occupies the chosen nearest neighbor. Once the state of a bond has been chosen, it remains in that state for all time.

As expected, the critical phenomenon in the percolation process determines different qualitative regimes for the random walk. The walk is, in effect, a walk on the open cluster at the origin. For $p < p_c$, the cluster at the origin is finite with probability one, and the cluster size distribution decays rapidly (equation 2.7), so that the mean square displacement of the walker cannot increase without bound. For $p = p_c$, there is no infinite cluster at the origin, but almost; the distribution of finite clusters has an algebraically decaying tail. Furthermore, as discussed above, there is no scale on which a large cluster is homogeneous. As the walker wanders farther from the origin, it encounters ever larger blobs to get lost on and ever larger holes to go around. One can think of the lattice as having different densities on different length scales, and thus a diffusivity that varies with the length scale. Thus asymptotically, the mean square displacement is not proportional to the time n, but is proportional to n to some power less than 1. Or, in the case of the Bethe lattice, $\langle S^2 \rangle$ grows logarithmically. A simulation on the Bethe lattice for $z = 3$ is shown in Fig. 2.4.

When $p > p_c$, there are two possibilities for a realization of the walk; the walker begins either on the infinite cluster or on a finite cluster. The distribution of the largest clusters decays rapidly so that realizations of the walk on these clusters do not contribute to the asymptotic mean square displacement. Only the paths on the infinite cluster contribute. When the walker has traveled a distance much farther

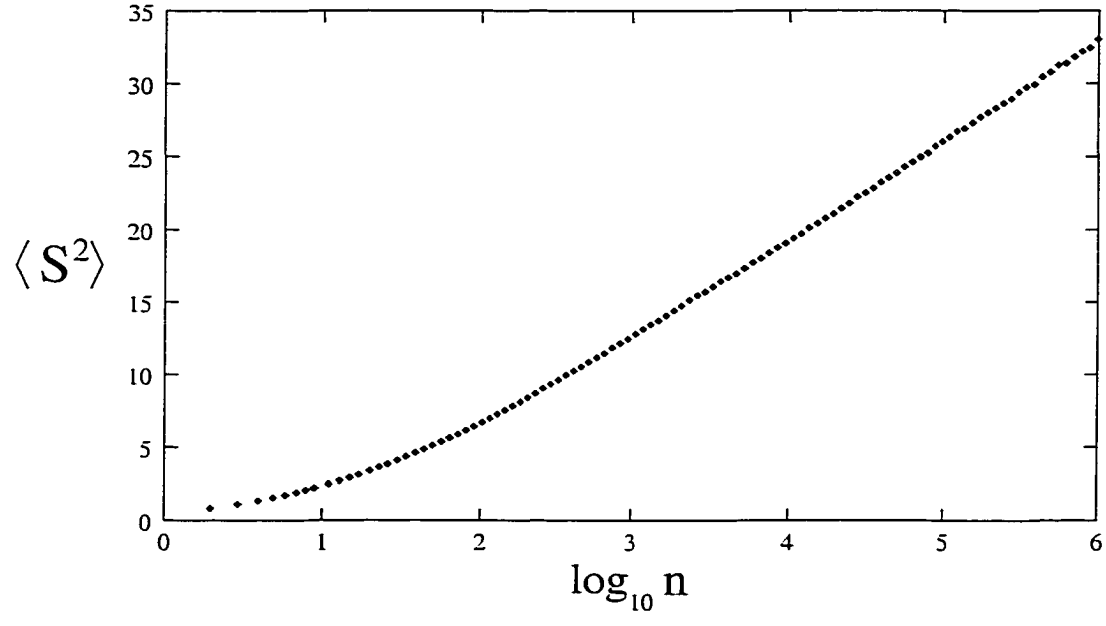

Figure 2.4: Mean square displacement on the static lattice at the percolation threshold $p = p_c$. The data is from Monte Carlo simulations on the Bethe Lattice with $z = 3$. Although, it is well known that no infinite cluster exists at $p = p_c = 1/2$, the figure shows that the mean square displacement increases logarithmically with time. The average is over 10^5 trials. The metric used is given by (2.44).

than ξ, the infinite lattice appears homogeneous, so we expect normal diffusion, but with a reduced diffusivity. Below, we consider each of these cases and note the relevant critical exponents.

When $p < p_c$ and the bonds are static ($\nu = 1$), the mean square displacement approaches a limit as the time $n \to \infty$. The interesting quantity in this case is the asymptotic mean square displacement. When $n = \infty$ the walker occupies each site on the cluster at the origin C with equal probability. So the limiting mean square displacement on C is a kind of mean square radius

$$R^2(C) = \sum_{x \in C} \frac{\|x\|^2}{|C|}, \tag{2.14}$$

where $\|x\|$ is the distance of the site x from the origin. Note that this radius depends on the position of the cluster relative to the origin. The mean square displacement is then $R^2(C)$ averaged over all clusters

$$\langle S_\infty^2 \rangle = \langle R^2(C) \rangle = \sum_c P(C = c) R^2(c), \tag{2.15}$$

where c is a particular realization of the cluster at the origin, and the sum is over all possible clusters. Equation 2.15 gives the asymptotic mean square displacement of the random walk on a sub-critical percolation process. We write $\langle S_\infty^2 \rangle$ in a form convenient for calculations by defining a mean square radius averaged over all clusters of size $|C| = s$,

$$R_s^2 = \frac{\sum_{\{c:|c|=s\}} P(C = c) R^2(c)}{P(|C| = s)}, \tag{2.16}$$

so that (2.15) becomes

$$\langle S_\infty^2 \rangle = \sum_s R_s^2 \, P(|C| = s). \tag{2.17}$$

Now we assume that, for the range of s that we are interested in, R_s^2 obeys a single power law

$$R_s^2 \approx s^{2\epsilon}. \tag{2.18}$$

In the sums we consider, such as (2.17), we will see that the main contribution comes from large s, but s smaller than the crossover mass $(p_c - p)^{1/\sigma}$. Thus s is in the regime where the clusters have a fractal structure. So we expect $\epsilon \neq 1/d$, even if the dominant clusters are roughly spherical.

We find the critical exponent of $\langle S_\infty^2 \rangle$, using the scaling ansatz for the cluster mass (2.11). Furthermore, we express the exponent ϵ in terms of the other critical exponents. To do this, we use R_s^2 in an expression for the correlation length that involves (2.11). Thus, we can express ϵ as a function of σ, θ, and ϕ. Under reasonable assumptions the definition of correlation length (2.9) is equivalent to

$$\xi^2 = \frac{\sum_{x \in \mathbb{Z}^d} \|x\|^2 P(x \in C)}{\sum_{x \in \mathbb{Z}^d} P(x \in C)}. \tag{2.19}$$

In order to rewrite this equation in terms of cluster mass, we use the indicator function. Letting ω be a particular realization of the percolation process, and letting A be a (measurable) event, we define

$$1_A(\omega) = \begin{cases} 1 & \text{if event } A \text{ occurs for configuration } \omega, \\ 0 & \text{otherwise .} \end{cases} \tag{2.20}$$

It is easy to see that $\langle 1_A \rangle = P(A)$. Then we have

$$\sum_{x \in \mathbb{Z}^d} \|x\|^2 P(x \in C) = \sum_{x \in \mathbb{Z}^d} \|x\|^2 \langle 1_{x \in C} \rangle \tag{2.21}$$

$$= \left\langle \sum_{x \in \mathbb{Z}^d} \|x\|^2 1_{x \in C} \right\rangle \tag{2.22}$$

$$= \left\langle \sum_{x \in C} \|x\|^2 \right\rangle \tag{2.23}$$

$$= \sum_s sP(|C| = s) \frac{\sum_{\{c:|c|=s\}} P(C = c) \sum_{x \in C} \frac{\|x\|^2}{|C|}}{P(|C| = s)} \tag{2.24}$$

$$= \sum_s sP(|C| = s) R_s^2 \, . \tag{2.25}$$

In a similar manner, we have that

$$\sum_{x \in \mathbb{Z}^d} P(x \in C) = \sum_s sP(|C| = s) = \langle |C| \rangle \, . \tag{2.26}$$

So we rewrite (2.19) as

$$\xi^2 = \frac{\sum_s sP(|C| = s) R_s^2}{\sum_s sP(|C| = s)}. \tag{2.27}$$

Because we assume that $R_s^2 \approx s^{2\epsilon}$, both the numerator and the denominator are moments of $P(|C| = s)$. We use the scaling ansatz (2.11) to compute the kth moment of $P(|C| = s)$ as

$$\begin{aligned} \sum_s s^k P(|C| = s) &= \sum_s s^{k-\theta} f\left[(p_c - p)s^\sigma\right] \\ &\approx \sigma^{-1} |p - p_c|^{\frac{-k+\theta-1+\sigma}{\sigma}} \int_0^\infty dz \; z^{\frac{+k-\theta+1-\sigma}{\sigma}} f(z), \end{aligned} \tag{2.28}$$

where $z = (p_c - p)s^\sigma$ if $p < p_c$ and $z = (p - p_c)s^\sigma$ if $p > p_c$. Here, we assume that $k - \theta \geq -1$ so that the sum diverges until the rapid decay of $f(z)$ begins. Thus, as p approaches p_c the major contribution of the sum occurs for large s and we are justified in replacing the sum with an integral. Then the critical exponent of the kth moment of $P(|C| = s)$ is $(-k + \theta - 1 + \sigma)/\sigma$. Now we evaluate the critical exponent

in (2.27). The numerator has $k = 2\epsilon + 1$, while the denominator has $k = 1$. So ξ^2 diverges with the power $-2\epsilon/\sigma$. Because we defined ϕ via $\xi \approx |p - p_c|^{-\phi}$, we have that $-2\phi = -2\epsilon/\sigma$, or $\epsilon = \sigma\phi$.

The expression for $\langle S_\infty^2 \rangle$ given in (2.17) is the kth moment of $P(|C| = s)$, with $k = 2\epsilon$. Thus, the critical exponent for this moment is $-2\phi + (\theta - 1 + \sigma)/\sigma$. A similar exercise shows that the critical exponent for the strength of the infinite cluster (2.12) is $\beta = (\theta - 1 + \sigma)/\sigma$. So, for $p < p_c$, we have

$$\langle S_\infty^2 \rangle \approx (p_c - p)^{\beta - 2\phi}. \tag{2.29}$$

The asymptotic mean square displacement $\langle S_\infty^2 \rangle$ can be calculated exactly in one dimension and on the Bethe lattice. In one dimension one has

$$\langle S_\infty^2 \rangle = \frac{p}{(1-p)^2}. \tag{2.30}$$

Straley (29) has calculated that on the Bethe lattice with $z = 3$

$$\langle S_\infty^2 \rangle = \frac{3}{2p}\left(3p^2 - 4p + 4(1-p)^2 \ln\frac{1-p}{1-2p}\right). \tag{2.31}$$

We performed Monte Carlo simulations that agree with (2.30) and (2.31).

Now we turn our attention to the walk on the static disordered lattice when $p \geq p_c$. As in the sub-critical case, scaling arguments and numerous Monte Carlo studies provide a rather solid picture of the phenomenology as p approaches p_c from above. When $p = 1$ all bonds are open and we have an ordinary random walk with $D = 1$. When p is only a bit less than 1, there are only a few holes of size ξ, which is rather small. After a few time steps, when the distribution of the position has spread over a length scale greater than ξ, we find that the walk is again diffusive with a slightly reduced diffusivity. In the discussion above we saw that $D = 0$

for $p < p_c$. If we believe that there is only one critical point p_c, we expect that $D(p)$ is continuous for $p > p_c$. Furthermore, because at $p = p_c$ there is no infinite cluster and the large clusters have a fractal structure, it seems likely that $D(p_c) = 0$. Indeed, simulations show that $D(p)$ is continuous for $0 \leq p \leq 1$. In particular, $D(p)$ appears to obey a power law,

$$D(p) \approx (p - p_c)^{\mu} \quad \text{as } p \downarrow p_c. \tag{2.32}$$

The critical exponent μ is sometimes called a dynamic critical exponent. This is because μ arises when a dynamic process is added to the percolation process and attempts to derive μ by considering only percolation have failed. It is widely believed that μ is also the critical exponent for conductivity on the percolation process. Finally, we ask for the behavior of the walk at the critical point. At the critical point $p = p_c$ it appears that the cluster size distribution decays slowly enough that the expectation of the mean square displacement $\langle S_n^2 \rangle$ is not bounded. However, the walk exhibits anomalous diffusion, that is $\langle S_n^2 \rangle$ grows as t to a power less than one. See, for example, Fig. 2.4.

We relate the behavior in all three regimes via a scaling assumption. The new scaling exponents will be expressed as functions of the static exponents and the dynamic exponent μ. We noted above that, on scales smaller than ξ, the percolation process near p_c is indistinguishable from the process at p_c. Only on scales greater than ξ can one distinguish, for instance, on which side of the percolation threshold p lies. So if the time n is large, but small enough that the walker has not wandered farther than ξ, we should see anomalous diffusion, as on the critical process. For much larger times, we expect to see the diffusive behavior if $p > p_c$, or a bounded mean square displacement if $p < p_c$. It is believed that the correlation function

$P(x \in C)$ obeys a scaling assumption similar to (2.11), with the displacement of x as the independent variable. Because time varies as distance to a power, with the power taking different values in different regimes, it is reasonable that the mean square displacement should also satisfy a scaling assumption,

$$\langle S_n^2 \rangle^{1/2} \sim n^k r[(p - p_c)n^x], \tag{2.33}$$

where $r(z)$ is a scaling function, and n is the time. In the scaling assumptions that we have encountered, a crossover scale separates regions of algebraic and exponential decay. The situation is somewhat different here, in that we require $r(z)$ to behave like a power of z for large z. If z is large and positive, the walker is diffusing on the super-critical lattice over distances greater than ξ. In this case, $\langle S_n^2 \rangle^{1/2} \propto (p-p_c)^{\mu/2}$, according to (2.32), so we must have $r(z) \propto (p - p_c)^{\mu/2}$. Then $\langle S_n^2 \rangle^{1/2} \approx n^{k+\mu x/2}$. Because the walk is diffusive in this regime, we must have $k + \mu x/2 = 1/2$, which gives one equation relating k and x. Similarly, when $p < p_c$, we must have $r(z) \propto (-z)^{-k/x}$ for $-z \gg 1$ in order that $\langle S_n^2 \rangle^{1/2}$ be independent of the time n. Then, in order that the dependence on p agrees with the static limit (2.29), we require $k/x = \phi - \beta/2$. Solving the two equations for k and x, we find that

$$x = \frac{1}{2\phi + \mu - \beta}, \tag{2.34}$$

and

$$k = \frac{\phi - \beta/2}{2\phi + \mu - \beta}. \tag{2.35}$$

At the critical point, we have $\langle S_n^2 \rangle^{1/2} \approx n^k$. The time scale separating the two types of motion is $|p - p_c|^{-1/x}$. For times that are long, but shorter than this time scale, anomalous diffusion with exponent k is observed. At longer times, the motion either becomes bounded for $p < p_c$, or diffusive for $p > p_c$.

2.6 Scaling behavior of D in the FBRW

In this section, we look for scaling behavior near the critical point $(p, \nu) = (p_c, 1)$ in the FBRW. While the material in the preceding section is well known, this section relates an original contribution. We have already mentioned that the diffusivity D decays as $1/\tau$ when $p < p_c$, while it approaches a constant for large τ when $p > p_c$. In Fig. 2.3 on page 31 we saw that, when $p = p_c$, D decays to zero more slowly than it does below the critical bond density. For instance, on the Bethe lattice at $p = p_c$, we find $D \propto \tau^{-\alpha}$ with $\alpha \approx 0.66$. We make a scaling ansatz that connects these three observations.

A scaling ansatz for the FBRW makes sense if we believe the story of critical behavior on the static lattice given in the previous section. We saw that D decays as $\tau^{-\alpha}$ when $p = p_c$. For a given value of τ, the diffusive behavior is observed after a finite time, during which the walker has explored only a finite portion of the lattice. If $p - p_c$ is small enough, then the walker does not reach distances larger than the correlation length before fluctuations destroy the clusters. It follows that, if $|p - p_c|$ is small enough, the statistics of this walk should be indistinguishable from a walk with $p = p_c$. Thus, we expect a crossover phenomenon. When $|p - p_c|$ is small, there is a range of τ for which D decays as $\tau^{-\alpha}$. For larger τ, D tends to a constant if $p > p_c$ or decays as $1/\tau$ if $p < p_c$. We make an ansatz similar to (2.11) and (2.33), namely that

$$D \sim \tau^{-\alpha} g[(p - p_c)\tau^{\kappa}]. \tag{2.36}$$

We note that because this ansatz assumes that τ is large, we expect that is is valid for other models, such as the HZ model. Now we determine the asymptotic behavior of $g(z)$. When $z \gg 1$, we must recover (2.32), $D \approx \tau^0 (p - p_c)^{\mu}$. Thus $g(z) \approx z^{\mu}$ for

$z \gg 1$. In order to get the factor τ^0, we must have

$$-\alpha + \kappa\mu = 0. \tag{2.37}$$

When $-z \gg 1$, we must have

$$D \approx \frac{1}{\tau}(p - p_c)^{-a}, \tag{2.38}$$

where a is some undetermined critical exponent. To satisfy (2.38) we must have $g(z) \approx z^{-a}$ when $-z \gg 1$ and

$$-\alpha - \kappa a = -1. \tag{2.39}$$

Taking α and μ to be known and using (2.37) and (2.39), we find that

$$a = \frac{\mu(1-\alpha)}{\alpha}, \tag{2.40}$$

and that

$$\kappa = \frac{\alpha}{\mu}. \tag{2.41}$$

Using the known value on the Bethe lattice $\mu = 3$, and the value from our Monte Carlo data $\alpha \approx 0.66$ (See Fig. 2.3 on page 31.), we find that $a \approx 1.5$, and $\kappa \approx 2/9$. We can test the scaling assumption by making a log-log plot of a Monte Carlo determination of D as a function of p. Fig. 2.5 provides a direct determination of a using (2.38) which gives $a \approx 1.5$ in agreement with the value obtained from (2.40). It is important to note that in one case, a was determined from the dependence of D on τ, while in the other case, it was determined from the dependence of D on $p - p_c$.

There is still the question of relating the exponents in the ansatz (2.36) to the known exponents from scaling laws on the static lattice. We have one unknown

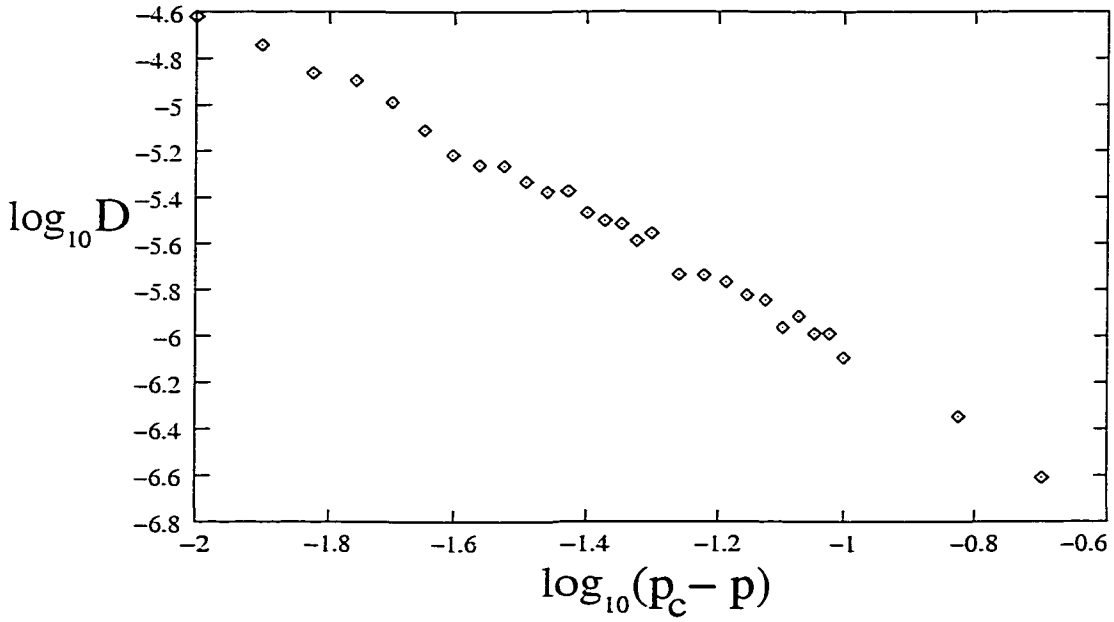

Figure 2.5: Diffusivity D determined from Monte Carlo simulations on the Bethe lattice near the critical point. For all points $\tau = 10^7$. The data supports the conjecture $D \propto (p_c - p)^a$. The slope of the best linear fit gives $a = 1.5 \pm 0.03$. The error assumes only statistical error. In fact, there may be other small errors present. Points towards the right of the plot contain increasing errors from corrections to scaling because $p_c - p$ is too large. Points toward the left may begin to leave the scaling regime because z in $g(z)$ in (2.36) becomes too small. Each point is computed from walks of 10^5 steps and 10^5 trials. More points to the left cannot be included without longer Monte Carlo runs because the walks fail to converge to diffusive motion.

parameter, which we can take for instance to be a. At present we have no conjecture relating a to known exponents. It would be interesting to study a scaling ansatz for intermediate times on the FBRW similar to that given in (2.33). This may also provide an equation expressing a as a function of other exponents.

2.7 Random Walks on the Bethe Lattice

We now address the choice of metric for the random walk on the Bethe lattice. For the simple random walk on Euclidean lattices in d dimensions, we have $\langle S_{n+1}^2 \rangle - \langle S_n^2 \rangle = 1$ for all n, while the first moment vanishes because of the symmetry of the walk. We want to find a distance function on the Bethe lattice with this simple property. First, we remind the reader of the structure of the Bethe lattice. To construct the lattice, we begin with a site at the origin and then make a bond from the origin to each of z new sites. The origin is called generation 0, while the z new sites are called generation 1. Then, for each site x in generation 1, we create $z-1$ sites and join each of these new sites to x with a bond. All of these $z(z-1)$ new sites form generation 2. Then we repeat this process indefinitely. A picture of the first four generations of a Bethe lattice with $z = 3$ is shown in Fig. 2.6.

One may choose the difference in generation number as the distance function on the Bethe lattice. However in this case, not only does the first moment not vanish, but it is only asymptotically linear in time. In particular, it can be shown that, if i is the generation, then for the simple random walk

$$\langle i_n \rangle = \frac{2}{z} \sum_{j=0}^{n-1} P_j(0) + n \frac{z-2}{z}, \tag{2.42}$$

where $P_i(0)$ is the probability to be at the origin at the j^{th} step. Often the square

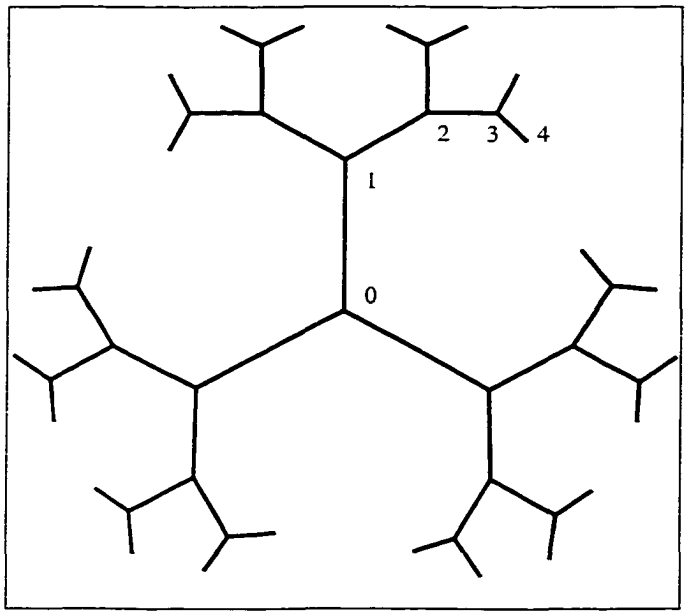

Figure 2.6: Bethe lattice with $z = 3$. The first 4 generations of sites are shown.

root of the difference between generations is taken as distance on the Bethe lattice, in which case, the second moment of the distance behaves asymptotically as it does on $\mathbb{Z}^d$. But our expansions and RG methods are computed using only a few steps near the origin, in which case the anomaly in (2.42) is important. Thus, we choose a distance function that produces diffusive behavior in the simple random walk at every time step. That is, we want to find a distance function d_i such that

$$\sum_{i=1}^{n} d_i^2 P_n(i) = n, \tag{2.43}$$

where $P_n(i)$ is the probability to be on the ith generation at time n. The function that satisfies this equation for all n for the simple random walk is

$$d_i^2 = i + 2\sum_{j=1}^{i-1} \frac{i-j}{(z-1)^j}, \tag{2.44}$$

which for large j becomes

$$d_i^2 \approx i\frac{z}{z-2} - 2\frac{z-1}{(z-2)^2}\,. \tag{2.45}$$

In the next chapter, we will take $z = 3$ and use the distance function (2.44) to compute the coefficients in the expansion of D. (The results of doing this calculation with a computer are shown in Table 3.1 on page 63.) The Monte-Carlo data for the FBRW are also computed using (2.44), and we find that the asymptotic mean square displacement is linear in time. Using the more complicated distance function adds little complexity when computing coefficients by machine, and the Monte-Carlo calculations are far more efficient on the Bethe lattice than they are in two and three Euclidean dimensions. Also, as noted above, we have the advantage of estimating the equilibration time on the static lattice τ_p numerically on the Bethe lattice.

CHAPTER 3

Expansions in Model Parameters

In this chapter, we present expansions of the diffusivity $D(p,\nu)$ for the fluctuating bond random walk. We assume that an expansion of the form

$$D(p,\nu) = \sum_{i=0}^{\infty} f_i(p)\nu^i, \tag{3.1}$$

exists and seek to compute the coefficients $f_i(p)$. We find that the coefficients $f_i(p)$ are polynomials in p with rational coefficients. We first give the details of obtaining the first few coefficients $f_i(p)$ for arbitrary d. We also tabulate about ten of the exact expansion coefficients obtained from a computer program for manipulating polynomials written specifically for this task (Tables 1–4). We then make a simple conjecture about the form of the terms in the expansion in ν based on the first several $f_i(p)$. Using this conjecture, we compute the first few terms in an expansion about $p = 0$.

3.1 Expansion of $D(p,\nu)$ About $\nu = 0$

In this section we calculate the diffusivity $D(p,\nu) = \lim_{n\to\infty} D_n^I(p,\nu)$ to third order in ν for for walks on $\mathbb{Z}^d$ with d arbitrary. We use the definition of $D_n^I(p,\nu)$ given by (2.5) on page 27. We shall see that the expansion in ν to n^{th} order can be calculated by considering all paths of n or fewer steps. The n^{th}-order expansion

predicts the diffusivity accurately to the extent that the walk has converged to asymptotic behavior at time n. Thus the expansion is better not only for smaller ν, but also for larger values of $|p - p_c|$. To derive the expansion, we study the incremental approximations to the diffusivity $D_n^I(p,\nu)$, given in (2.3). For the case $\nu = 0$, which is not essentially different from the simple random walk, it is easy to show that $D_n^I(0,p) = p$ for all n. For $\nu > 0$, the calculations below suggest that for all n greater than m, the coefficients of all powers of ν of order less than or equal to m in $D_n^I(p,\nu)$ are independent of n, and that these coefficients are polynomials in p with a finite number of non-vanishing terms (when m is finite). This is demonstrated below to third order for arbitrary dimension, and by manipulating polynomials on a computer[1], to approximately 10^{th} order on several lattices. In this chapter we assume that $D_n^I(p,\nu)$ converges. Notice that $D_n^I(p,\nu)$ is an approximation to the slope of the mean square displacement (Fig. 2.1). Because the second derivative of the mean square displacement appears to be always negative, $D_n^I(p,\nu)$ always overestimates the true value of D. The approximation $D_n^I(p,\nu)$ consists of the terms in the expansion to order n, plus some higher order terms. In fact $D_n^I(p,\nu)$ is a slightly better estimate of D, when compared with MC, than is the n^{th}-order expansion.

We express the diffusivity in a form convenient for deriving the expansions in ν and p. We begin by writing an expression for the probability that the walker executes a particular sequence of steps, given that it begins at the origin. The formulation presented here is for walks on $\mathbb{Z}^d$. We introduce paths and the

[1]Because these computations involve manipulating large numbers of polynomials with 10^3 or more terms, general purpose symbolic languages are not appropriate tools, as they are inefficient and lack fine grained memory management. We wrote simple C++ libraries with a naive implementation. One might improve the calculations by using optimized libraries for manipulating polynomials symbolically.

probability measure on the set of paths. A path σ is a sequence of steps (including both successful and failed attempts) beginning at the origin. Let $\mathcal{P}_n$ be the set of all paths of n steps. For $\sigma \in \mathcal{P}_n$, we write $\sigma = (\sigma_1, \ldots, \sigma_n)$, where $\sigma_i \in \{r_\alpha, l_\alpha, R_\alpha, L_\alpha : \alpha = 1 \ldots d\}$ are the steps. r_α and l_α represent failed steps along the positive and negative α^{th} coordinate axis, respectively. R_α and L_α represent successful steps along the positive and negative α^{th} coordinate axis, respectively. A successful step is one that traverses an open bond, and a failed step is one that attempts to cross a bond, but finds the bond closed and so leaves the position of the walker unchanged. We denote the set of successful steps and the set of failed steps by, respectively, $\mathcal{S}_s = \{R_\alpha, L_\alpha : \alpha = 1 \ldots d\}$ and $\mathcal{S}_f = \{r_\alpha, l_\alpha : \alpha = 1 \ldots d\}$. The set of all possible steps is $\mathcal{S} = \mathcal{S}_s \cup \mathcal{S}_f$. The expression $\lambda = \sigma\gamma$, where $\sigma \in \mathcal{P}_n$ and $\gamma \in \mathcal{P}_m$, means $\lambda = (\sigma_1, \ldots, \sigma_n, \gamma_1, \ldots, \gamma_m)$. Similarly, we write $\sigma s_1 s_2 \ldots$ for the concatenation of a path and single steps. We define the displacement vector $S(\sigma) = (S_1, \ldots, S_d)$, where S_α is equal to the number of elements of σ equal to R_α minus the number equal to L_α. Thus, $S(\sigma)$ is the displacement of the end vertex of σ from the origin.

We denote by $b(\sigma, i)$ the bond attempted at time i, that is, by the step σ_i. We define the interval between the time i and the earlier time when the bond $b(\sigma, i)$ was most recently attempted by

$$\begin{aligned} \gamma(\sigma, i) \; &= i - j \quad \text{if} \quad b(\sigma, i) = b(\sigma, j) \quad \text{for some} \quad j < i \;, \\ &\qquad \text{and} \quad b(\sigma, i) \neq b(\sigma, k) \quad \text{for all} \quad k, \;\; j < k < i \;. \end{aligned}$$

Note that if $\gamma(\sigma, i)$ is not defined then the bond $b(\sigma, i)$ is attempted for the first time at time i. Because the bond fluctuations and the direction of the attempted step

are independent, the single step transition probability can be written as the product of the probability that the attempt is in a particular direction and the probability that the attempted bond is in the state corresponding to σ_i. The probability that the ith step σ_i occurs, conditioned on the previous steps can be written

$$\pi(\sigma_i|\sigma_1,\ldots,\sigma_{i-1}) = \frac{1}{2d}\big[\psi(\sigma_i) + \phi(\sigma,i)\big] ,$$

where

$$\psi(\sigma_i) = \begin{cases} p & \text{if } \sigma_i \in \mathcal{S}_s, \\ q & \text{otherwise} , \end{cases}$$

$$\phi(\sigma,i) = \begin{cases} p\nu^t & \text{if } \sigma_i \in \mathcal{S}_f \text{ and } \sigma_{i-t} \in \mathcal{S}_f, \\ -p\nu^t & \text{if } \sigma_i \in \mathcal{S}_s \text{ and } \sigma_{i-t} \in \mathcal{S}_f, \\ q\nu^t & \text{if } \sigma_i \in \mathcal{S}_s \text{ and } \sigma_{i-t} \in \mathcal{S}_s, \\ -q\nu^t & \text{if } \sigma_i \in \mathcal{S}_f \text{ and } \sigma_{i-t} \in \mathcal{S}_s, \\ 0 & \text{if } \gamma(\sigma,i) \text{ is undefined}, \end{cases} \tag{3.2}$$

and $t = \gamma(\sigma,i)$. Note that there are values of i, $1 \le i \le n$ for which $\gamma(\sigma,i)$ is undefined. These correspond to steps that are attempting a bond for the first time. In this case, we let the bond probabilities assume their stationary values. We then define a probability measure π [which agrees with the bond state transition matrix (2.1) on page 25] on the set of paths via

$$\pi(\sigma) = \prod_{i=1}^{n} \frac{1}{2d}\big[\psi(\sigma_i) + \phi(\sigma,i)\big] . \tag{3.3}$$

The ith factor in the product in (3.3) is the ith single step transition probability; that is, the probability that the ith step takes the value σ_i.

We are usually concerned with the final step in a path, so when writing ϕ, we will often suppress the second argument, with the understanding that its value

is equal to the number of steps in σ. Likewise, if $\sigma \in \mathcal{P}_n$, then we write $\psi(\sigma)$ for $\psi(\sigma_n)$.

We note some symmetries, which we will refer to when performing the calculations below. The following applies in all dimensions, but we suppress indices denoting coordinate axes. We define three operations, $\mathcal{I}, \mathcal{R}, \mathcal{H}$, from $\mathcal{P}_n$ onto $\mathcal{P}_n$. We denote the spatial inverse of σ by $\mathcal{I}\sigma$, that is, in $\mathcal{I}\sigma$ all of the L's and R's are interchanged and all of the r's and l's are interchanged. We denote a partial spatial inversion of σ by $\mathcal{H}\sigma$. In $\mathcal{H}\sigma$, only the successful steps are inverted, that is, the L's and R's are interchanged, but the r's and l's remain unchanged. We denote a reversal of σ by $\mathcal{R}\sigma$, in which the order of the steps is reversed, that is, $\mathcal{R}\sigma = (\sigma_n, \sigma_{n-1}, \ldots, \sigma_1)$. Applying any of these operations twice, we see that

$$\mathcal{I}^2 = \mathcal{H}^2 = \mathcal{R}^2 = I\,.$$

The following symmetries are obvious,

$$S(\sigma) = S(\mathcal{R}\sigma) = -S(\mathcal{I}\sigma) = -S(\mathcal{H}\sigma)\,. \tag{3.4}$$

The symmetries of the probability are

$$\pi(\sigma) = \pi(\mathcal{I}\sigma) = \pi(\mathcal{R}\mathcal{H}\sigma)\,. \tag{3.5}$$

Note that applying $\mathcal{R}\mathcal{H}$ is equivalent to reversing time. The final equality may be less than obvious, but it can be proved by writing the single-step transition probabilities explicitly.

In order to compute $\langle S^2\rangle_n - \langle S^2\rangle_{n-1}$, we begin by writing explicitly the

mean square displacement for arbitrary dimension at time n,

$$\begin{aligned}
\langle S^2\rangle_n &= \sum_{\sigma\in\mathcal{P}_n} \pi(\sigma)S(\sigma)^2 \\
&= 2\sum_{i=1}^{d} \sum_{\substack{\sigma\in\mathcal{P}_{n-1} \\ \sigma_n\in\{R_i,r_i\}}} \pi(\sigma\sigma_n)S(\sigma\sigma_n)^2 \\
&= 2\sum_{\sigma\in\mathcal{P}_{n-1}} \sum_{i=1}^{d} \Big\{\pi(\sigma R_i)\big[S(\sigma)+e_i\big]^2 + \pi(\sigma r_i)S(\sigma)^2\Big\} \\
&= 2\sum_{\sigma\in\mathcal{P}_{n-1}} \sum_{i=1}^{d} \big\{\pi(\sigma R_i)\big[S(\sigma)^2 + 2S_i(\sigma) + 1\big] + \pi(\sigma r_i)S(\sigma)^2\big\} \\
&= \sum_{\sigma\in\mathcal{P}_{n-1}} \pi(\sigma)S(\sigma)^2 + 2\sum_{i=1}^{d} \sum_{\sigma\in\mathcal{P}_{n-1}} \pi(\sigma R_i)\big[2S_i(\sigma)+1\big] \\
&= \langle S^2\rangle_{n-1} + 2\sum_{i=1}^{d} \sum_{\sigma\in\mathcal{P}_{n-1}} \pi(\sigma R_i)\big[2S_i(\sigma)+1\big] \ .
\end{aligned} \tag{3.6}$$

In the second line, we wrote the final step of the walk explicitly and used the symmetry of the walk under exchange of L and R. In the second to the last line we used the identity

$$\sum_{i=1}^{d} \big[\pi(\sigma R_i) + \pi(\sigma r_i)\big] = \frac{1}{2}\pi(\sigma) \ .$$

We simplify (3.6) by noting that $p/(2d)$ is the probability that the n^{th} step is R_i if we place no conditions on the previous steps. We see this as well by using the symmetry property (3.5) to write

$$\sum_{\sigma\in\mathcal{P}_{n-1}} \pi(\sigma R_i) = \sum_{\sigma\in\mathcal{P}_{n-1}} \pi(L_i\sigma) = \frac{1}{2d}p \, .$$

Then we have

$$\langle S^2\rangle_n - \langle S^2\rangle_{n-1} = p + 4\sum_{i=1}^{d} \sum_{\sigma\in\mathcal{P}_{n-1}} \pi(\sigma R_i)S_i(\sigma) \ .$$

Using (3.3), we begin to write the final single-step transition probability explicitly,

$$\begin{aligned}\langle S^2\rangle_n - \langle S^2\rangle_{n-1} &= p + \frac{2}{d}\sum_{i=1}^{d}\sum_{\sigma\in\mathcal{P}_{n-1}} \pi(\sigma)\big[p+\phi(\sigma R_i)\big]S_i(\sigma) \\ &= p + \frac{2}{d}\sum_{i=1}^{d}\sum_{\sigma\in\mathcal{P}_{n-1}} \pi(\sigma)\phi(\sigma R_i)S_i(\sigma)\ .\end{aligned} \tag{3.7}$$

The sum involving the factor of p vanished due to symmetry [see (3.4)]. In (3.7) we have separated the difference in successive values of $\langle S^2\rangle$ into a part independent of ν and a part dependent on ν. We now separate the first-order term in ν. Let us call the sum in the final line S, and write out the factor for one more step explicitly,

$$S = \frac{1}{d^2}\sum_{i=1}^{d}\sum_{\sigma\in\mathcal{P}_{n-2}}\sum_{s\in\mathcal{S}} \pi(\sigma)\big[\psi(\sigma s)+\phi(\sigma s)\big]\phi(\sigma s R_i)S_i(\sigma s)\ .$$

Let us look for the term of order 1 in ν. In general, for any σ [see (3.2)], $\phi(\sigma)$ is of order 1 or greater in ν, or else vanishes. (The case in which $\phi(\sigma)$ vanishes may be thought of as "order infinity".) So $\phi(\sigma s)\phi(\sigma s R_i)$ must be order 2 or greater. Therefore, any order-1 terms must come from terms with the factor $\psi(\sigma s)\phi(\sigma s R_i)$. If $\phi(\sigma s R_i)$ is $O(\nu^1)$, then the sequence sR_i must attempt the same bond twice. For if sR_i were to attempt two different bonds, then the step R_i would be returning to a bond after more than one time unit and $\phi(\sigma s R_i)$ would be of order 2 or greater. So contributing terms must have $s \in \{r_i, L_i\}$. However, for $s = r_i$, $S(\sigma s) = S(\sigma)$, so the sum over σ vanishes by symmetry [see (3.4)]. This leaves only $s = L_i$ for which we have $\psi(L_i) = p$ and $\phi(\sigma L_i R_i) = q\nu$. Using $S_i(\sigma L_i) = S_i(\sigma) - 1$, we write just the terms contributing to first order in ν,

$$\frac{1}{d^2}\sum_{i=1}^{d}\sum_{\sigma\in\mathcal{P}_{n-2}} \pi(\sigma)pq\nu\big[S_i(\sigma)-1\big] = -\frac{1}{d}\sum_{\sigma\in\mathcal{P}_{n-2}} \pi(\sigma)pq\nu = -\frac{1}{d}pq\nu\ .$$

Writing this together with the remaining terms in S, we have

$$\begin{aligned}\langle S^2\rangle_n - \langle S^2\rangle_{n-1} =& p - \frac{1}{d}pq\nu \\ &+ \frac{1}{d^2}\sum_{i=1}^{d}\sum_{\sigma\in\mathcal{P}_{n-2}}\sum_{s\in\mathcal{S}}\pi(\sigma)\phi(\sigma s)\phi(\sigma s R_i)S_i(\sigma s) \\ &+ \frac{1}{d^2}\sum_{i=1}^{d}\sum_{\sigma\in\mathcal{P}_{n-2}}\sum_{s\in\mathcal{S}\setminus\{r_i,L_i\}}\pi(\sigma)\psi(s)\phi(\sigma s R_i)S_i(\sigma s)\ .\end{aligned}$$

In the last line, each explicit factor of ϕ must be $O(\nu^2)$. In the previous line, each explicit factor of ϕ must be $O(\nu^1)$. Therefore, we have determined the change in the mean square displacement through order 1 in ν. Note that we assume that the motion is diffusive and that the expansion exists. We have not demonstrated here that the residual terms are summable as $n \to \infty$. However, as noted above, Monte-Carlo evidence strongly suggests that the motion is, in fact, asymptotically diffusive.

This procedure can be continued to compute higher orders in ν. At each stage, one collects factors that depend only on some fixed number of final steps in the walk and then integrates over previous steps. Let us compute the coefficient of ν^2. We write the single-step transition probability for σ_{n-2} explicitly,

$$\begin{aligned}\langle S^2\rangle_n - \langle S^2\rangle_{n-1} =& p - \frac{1}{d}pq\nu \\ &+ \frac{1}{2d^3}\sum_{i=1}^{d}\sum_{\sigma\in\mathcal{P}_{n-3}}\sum_{s's\in\mathcal{S}^2}\pi(\sigma)\big[\psi(s') + \phi(\sigma s')\big]\phi(\sigma s' s)\phi(\sigma s' s R_i)S_i(\sigma s' s) \\ &+ \frac{1}{2d^3}\sum_{i=1}^{d}\sum_{\sigma\in\mathcal{P}_{n-3}}\sum_{s'\in\mathcal{S}}\sum_{s\in\mathcal{S}\setminus\{r_i,L_i\}}\pi(\sigma)\big[\psi(s') + \phi(\sigma s')\big]\psi(s)\phi(\sigma s' s R_i)S_i(\sigma s' s)\ .\end{aligned}$$

All terms with factors of $\phi(\sigma s')$ will be at least $O(\nu^3)$, so we ignore them at this

step. The integrands that we need to consider are

$$s's \in \mathcal{S}^2 \;:\; \psi(s')\phi(\sigma s's)\phi(\sigma s'sR_i)S_i(\sigma s's) \tag{3.8}$$

$$s' \in \mathcal{S}, s \in \mathcal{S} \setminus \{r_i, L_i\} \;:\; \psi(s')\psi(s)\phi(\sigma s'sR_i)S_i(\sigma s's)\ . \tag{3.9}$$

The lowest-order terms in (3.8) must have $s'sR_i$ attempt a single bond 3 times. The possible paths are, $R_iL_iR_i$, $r_ir_iR_i$, $L_ir_iR_i$, and $l_iL_iR_i$. As in the the calculation of lower orders, we must have $S_i(s's) \neq 0$ in order to have a non-vanishing contribution. The two paths satisfying this condition are $L_ir_iR_i$ and $l_iL_iR_i$. For $L_ir_iR_i$ the factors in (3.8) are $\psi(L_i) = p$, $\phi(\sigma L_ir_i) = q\nu$, $\phi(\sigma L_ir_iR_i) = p\nu$, and $S_i(L_ir_i) = -1$. Summing over i, the contribution is $-\frac{1}{2d^2}qp^2\nu^2$. For $l_iL_iR_i$, the factors are, $\psi(l_i) = q$, $\phi(\sigma l_iL_i) = -p\nu$, $\phi(\sigma l_iL_iR_i) = q\nu$, and $S_i(l_iL_i) = -1$. Summing over i, the contribution is $\frac{1}{2d^2}q^2p\nu^2$.

The lowest order terms in (3.9) must have $s'sR_i$ attempt two bonds, b_1 and b_2 in the sequence $b_1b_2b_1$. We also must check that paths following this sequence do not conflict with the restriction on s and s' given in (3.9). Contributing paths that remain on a single axis are of the form $L_il_iR_i$, which, when summed over i, contribute $-\frac{1}{2d^2}q^2p\nu^2$. There are also paths of the form L_isR_i, where $s \in \{r_j, l_j\}$ for all $j \neq i$. Summing the contribution from these paths over i and j gives $-\frac{d-1}{d^2}q^2p\nu^2$. We now have counted all of the terms through second order in ν.

We rewrite (3.7) again, but show the second order terms explicitly,

$$\begin{aligned}\langle S^2\rangle_n - \langle S^2\rangle_{n-1} =& p - \frac{1}{d}pq\nu - \Big(\frac{1}{2d^2}p^2q + \frac{d-1}{d^2}q^2p\Big)\nu^2 \\ &+ \frac{1}{2d^3}\sum_{i=1}^{d}\sum_{\sigma\in\mathcal{P}_{n-3}}\sum_{s's\in\mathcal{S}^2}\pi(\sigma)\phi(\sigma s')\phi(\sigma s's)\phi(\sigma s'sR_i)S_i(\sigma s's) \\ &+ \frac{1}{2d^3}\sum_{i=1}^{d}\sum_{\sigma\in\mathcal{P}_{n-3}}\sum_{s's\in\mathcal{T}_{3,1}}\pi(\sigma)\psi(s')\phi(\sigma s's)\phi(\sigma s'sR_i)S_i(\sigma s's) \\ &+ \frac{1}{2d^3}\sum_{i=1}^{d}\sum_{\sigma\in\mathcal{P}_{n-3}}\sum_{s's\in\mathcal{T}_{3,2}}\pi(\sigma)\phi(\sigma s')\psi(s)\phi(\sigma s'sR_i)S_i(\sigma s's) \\ &+ \frac{1}{2d^3}\sum_{i=1}^{d}\sum_{\sigma\in\mathcal{P}_{n-3}}\sum_{s's\in\mathcal{T}_{3,3}}\pi(\sigma)\psi(s')\psi(s)\phi(\sigma s'sR_i)S_i(\sigma s's),\end{aligned} \tag{3.10}$$

where,

$$\mathcal{T}_{3,1} = \mathcal{S}^2 \setminus \{R_iL_i, r_ir_i, L_ir_i, l_iL_i\},$$

$$\mathcal{T}_{3,2} = \mathcal{S}\times\{l_i, R_i\},$$

$$\mathcal{T}_{3,3} = \Big\{s's : s's\in\mathcal{S}^2, \text{ except omit } L_is \text{ for } s\in\{r_j,l_j\}j\neq i, \text{ and omit } s'r_i, s'L_i, L_il_i\Big\}.$$

The sums in (3.10) that are not evaluated explicitly consist of terms that are of order 3 in ν. The next term in the expansion is computed easily in the same way, although we omit the details here. We have finally (for $n > 3$)

$$\begin{aligned}\langle S^2\rangle_n - \langle S^2\rangle_{n-1} =& p - \frac{1}{d}pq\nu - \Big(\frac{1}{2d^2}p^2q + \frac{d-1}{d^2}pq^2\Big)\nu^2 \\ &- \Big(\frac{(d-1)^2}{d^3}pq^3 + \frac{d-1}{d^3}p^2q^2 + \frac{(d-1)+1}{2d^3}p^3q\Big)\nu^3 + O(\nu^4).\end{aligned} \tag{3.11}$$

As stated above, the RHS of (3.11) is independent of n for $n > 3$.

The dependence on dimension of the approximation for $D(p,\nu)$ given by (3.11) is shown in Fig. 3.1 for $\tau \approx 3$. The dependence is strongest away from the

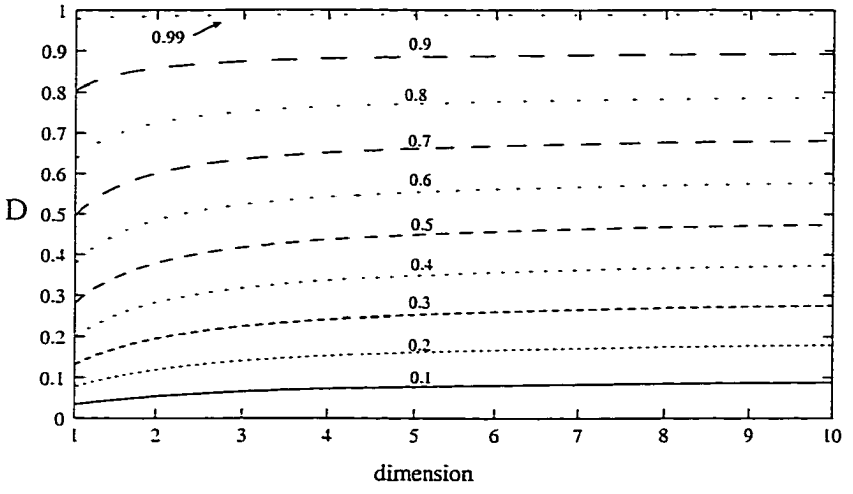

Figure 3.1: Expansion of D in ν for arbitrary dimension, taking $\nu = 0.7$ ($\tau \approx 3$). There are several curves for values of p from 0.1 to 0.99.

trivial value of $p = 1$, and $D(p, \nu)$ becomes more trivial with increasing dimension. Of course, the behavior will vary more strongly if more terms are present, and ν is near 1. In particular, p_c is a decreasing function of d.

We also have computed the coefficients on a computer to tenth order in one dimension, to eighth order in two dimensions, to seventh order in three dimensions, and to ninth order on the Bethe lattice with coordination number 3. Tables 1–4 show these coefficients as functions of p. We also have produced tables of coefficients as functions of both p and q that are organized in the same way as those in the manual calculation presented above. The latter tables are useful, for instance, for checking the manual calculations, but we do not present these tables here.

3.2 Expansion of $D(p, \nu)$ About $p = 0$

In this section, we compute one or two terms (depending on d) in expansions in p about $p = 0$. These expansions are obtained by looking at the coefficients of p (or

	Order in p									
	1	2	3	4	5	6	7	8	9	10
Order in ν										
0	1									
1	$\frac{-2}{3}$	$\frac{2}{3}$								
2	$\frac{-2}{9}$	$\frac{2}{9}$								
3	$\frac{-2}{27}$	$\frac{2}{27}$	$\frac{-4}{27}$	$\frac{4}{27}$						
4	$\frac{-2}{81}$	$\frac{-16}{81}$	$\frac{16}{81}$	$\frac{14}{81}$	$\frac{-4}{27}$					
5	$\frac{-2}{243}$	$\frac{-34}{243}$	$\frac{4}{27}$	$\frac{20}{81}$	$\frac{-112}{243}$	$\frac{52}{243}$				
6	$\frac{-2}{729}$	$\frac{-106}{729}$	$\frac{146}{729}$	$\frac{58}{729}$	$\frac{-406}{729}$	$\frac{538}{729}$	$\frac{-76}{243}$			
7	$\frac{-2}{2187}$	$\frac{-178}{2187}$	$\frac{94}{2187}$	$\frac{326}{2187}$	$\frac{-394}{729}$	$\frac{310}{243}$	$\frac{-2900}{2187}$	$\frac{1052}{2187}$		
8	$\frac{-2}{6561}$	$\frac{-574}{6561}$	$\frac{284}{2187}$	$\frac{-34}{243}$	$\frac{-484}{6561}$	$\frac{8344}{6561}$	$\frac{-17732}{6561}$	$\frac{15518}{6561}$	$\frac{-556}{729}$	
9	$\frac{-2}{19683}$	$\frac{-970}{19683}$	$\frac{-658}{19683}$	$\frac{2302}{19683}$	$\frac{-958}{19683}$	$\frac{18130}{19683}$	$\frac{-69916}{19683}$	$\frac{111820}{19683}$	$\frac{-84136}{19683}$	$\frac{24388}{19683}$

Table 3.1: Coefficients in expansion of D about $\nu = 0$ for the Bethe lattice

	Order in p										
	1	2	3	4	5	6	7	8	9	10	11
Order in ν											
0	1										
1	-1	1									
2	0	$\frac{-1}{2}$	$\frac{1}{2}$								
3	0	0	$\frac{-1}{2}$	$\frac{1}{2}$							
4	0	$\frac{-1}{4}$	$\frac{1}{4}$	$\frac{-1}{8}$	$\frac{1}{8}$						
5	0	0	$\frac{-1}{4}$	$\frac{1}{2}$	$\frac{-5}{8}$	$\frac{3}{8}$					
6	0	$\frac{-1}{8}$	$\frac{1}{4}$	$\frac{-3}{8}$	0	$\frac{7}{16}$	$\frac{-3}{16}$				
7	0	0	$\frac{-1}{8}$	$\frac{1}{8}$	$\frac{-3}{8}$	$\frac{9}{8}$	$\frac{-21}{16}$	$\frac{9}{16}$			
8	0	$\frac{-1}{16}$	$\frac{3}{16}$	$\frac{-19}{32}$	$\frac{7}{8}$	$\frac{-11}{64}$	$\frac{-95}{64}$	$\frac{255}{128}$	$\frac{-95}{128}$		
9	0	0	$\frac{-3}{16}$	$\frac{3}{8}$	$\frac{-5}{32}$	$\frac{-7}{32}$	$\frac{-75}{64}$	$\frac{127}{32}$	$\frac{-509}{128}$	$\frac{175}{128}$	
10	0	$\frac{-1}{32}$	$\frac{1}{8}$	$\frac{-15}{32}$	$\frac{17}{16}$	$\frac{-273}{128}$	$\frac{17}{8}$	$\frac{273}{128}$	$\frac{-495}{64}$	$\frac{1837}{256}$	$\frac{-577}{256}$

Table 3.2: Coefficients in expansion of D about $\nu = 0$ for one dimension

	Order in p								
	1	2	3	4	5	6	7	8	9
Order in ν									
0	1								
1	$\frac{-1}{2}$	$\frac{1}{2}$							
2	$\frac{-1}{4}$	$\frac{3}{8}$	$\frac{-1}{8}$						
3	$\frac{-1}{8}$	$\frac{1}{4}$	$\frac{-1}{4}$	$\frac{1}{8}$					
4	$\frac{-1}{16}$	0	$\frac{-1}{64}$	$\frac{31}{128}$	$\frac{-21}{128}$				
5	$\frac{-1}{32}$	$\frac{-1}{16}$	$\frac{13}{128}$	$\frac{19}{64}$	$\frac{-35}{64}$	$\frac{31}{128}$			
6	$\frac{-1}{64}$	$\frac{-17}{128}$	$\frac{9}{32}$	$\frac{9}{64}$	$\frac{-467}{512}$	$\frac{261}{256}$	$\frac{-195}{512}$		
7	$\frac{-1}{128}$	$\frac{-15}{128}$	$\frac{33}{128}$	$\frac{21}{256}$	$\frac{-1151}{1024}$	$\frac{2249}{1024}$	$\frac{-489}{256}$	$\frac{319}{512}$	
8	$\frac{-1}{256}$	$\frac{-1}{8}$	$\frac{79}{256}$	$\frac{-257}{2048}$	$\frac{-3939}{4096}$	$\frac{13201}{4096}$	$\frac{-79937}{16384}$	$\frac{118327}{32768}$	$\frac{-34325}{32768}$

Table 3.3: Coefficients in expansion of D about $\nu = 0$ for two dimensions

	Order in p							
	1	2	3	4	5	6	7	
Order in ν								
0	1							
1	$\frac{-1}{3}$	$\frac{1}{3}$						
2	$\frac{-2}{9}$	$\frac{7}{18}$	$\frac{-1}{6}$					
3	$\frac{-4}{27}$	$\frac{10}{27}$	$\frac{-19}{54}$	$\frac{7}{54}$				
4	$\frac{-8}{81}$	$\frac{77}{324}$	$\frac{-107}{324}$	$\frac{215}{648}$	$\frac{-91}{648}$			
5	$\frac{-16}{243}$	$\frac{37}{243}$	$\frac{-83}{324}$	$\frac{235}{486}$	$\frac{-967}{1944}$	$\frac{119}{648}$		
6	$\frac{-32}{729}$	$\frac{271}{5832}$	$\frac{-145}{2916}$	$\frac{2549}{5832}$	$\frac{-1399}{1458}$	$\frac{9749}{11664}$	$\frac{-115}{432}$	
7	$\frac{-64}{2187}$	$\frac{-25}{4374}$	$\frac{1597}{17496}$	$\frac{5371}{17496}$	$\frac{-23987}{17496}$	$\frac{36071}{17496}$	$\frac{-17083}{11664}$	$\frac{14369}{34992}$

Table 3.4: Coefficients in expansion of D about $\nu = 0$ for three dimensions

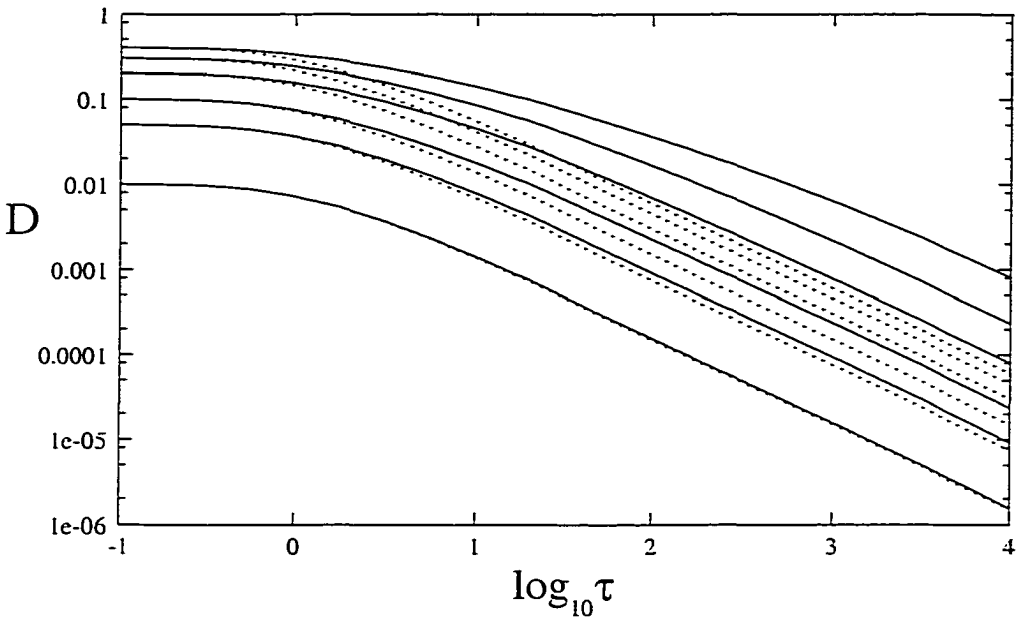

Figure 3.2: Diffusivity D on the Bethe lattice. Curves are for different values of p (all with $p < p_c$), which are found by following the curves to the left border. Solid lines are MC. Dotted lines are the expansion to first order in p. Both the expansion and the Monte Carlo give $D \propto 1/\tau$ for large τ. But, as p increases, the expansion predicts that the asymptotic behavior in τ begins too early.

p^2 for $d = 1$) in several of the terms in an expansion about $\nu = 0$. These coefficients are the first terms in a geometric series (see Tables 1–4). We postulate that this pattern continues— that is the coefficients of p or p^2, for those orders of ν that do not appear in the tables, are the higher-order terms in this series. We then sum the infinite series to obtain the small-p expansion. The resulting coefficients show the correct behavior at $\nu = 0$ and $\nu = 1$, and they agree with the Monte-Carlo results for small p (Figs. 3.2 and 3.3).

In one dimension the small-p result is

$$D(p,\nu) \approx p(1-\nu) + p^2\left(\nu - \frac{\nu^2/2}{1-\nu^2/2}\right) = p(1-\nu) + p^2\frac{\nu(2+\nu)(1-\nu)}{2-\nu^2} .$$

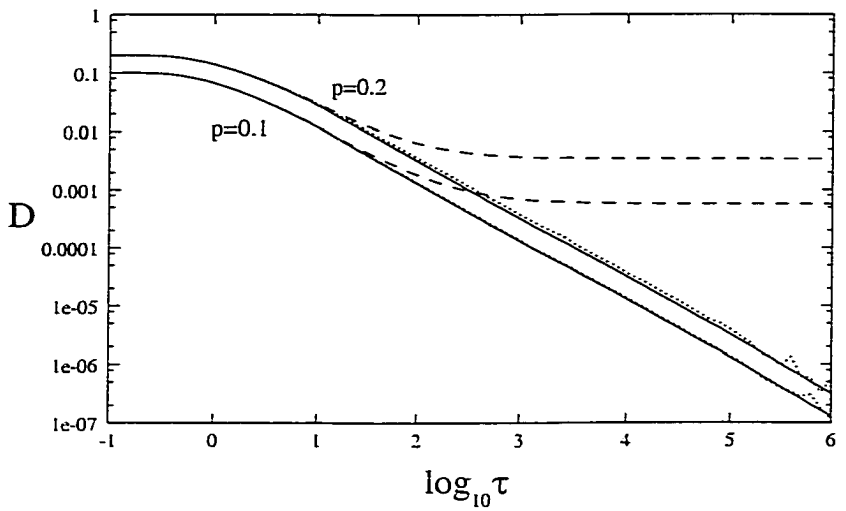

Figure 3.3: Diffusivity D in one dimension. Dotted lines are the MC data. Dashed lines are the expansion to 10th order in ν. Solid lines are the expansion to second order in p. Notice that $D \propto 1/\tau$ for large τ. Because the expansion in p is to second order, the agreement with Monte Carlo is better than in Fig. 3.2. The expansion in p is good for large τ. The expansion in ν begins to fail when $\tau = 10$, that is, when $\nu^{10} = e^{-1}$. For very large τ the Monte Carlo produces bond fluctuation events only rarely, so that statistical fluctuations are visible.

For small p and large τ (*i.e.* $\nu \approx 1 - \frac{1}{\tau}$) this expression becomes

$$D(p,\nu) \approx (p + 3p^2)\frac{1}{\tau} \ . \tag{3.12}$$

Figure 3.3 compares the expansion in p (through p^2), the expansion in ν (through ν^{10}) and the MC for one dimension for $p = 0.1$ and $p = 0.2$. Notice that the expansion to tenth order in ν begins to fail when $\tau = 10$. The predictions of the expansions in ν become constant for large τ, which is consistent with the discussion above, as they are actually giving the intermediate behavior, which is independent of τ when τ is large. The systematic error in the expansion in p is not clearly visible on this plot for $p = 0.1$, but is visible for large τ for $p = 0.2$.

On the Euclidean lattice in d dimensions, the terms in the expansion about $\nu = 0$ with a coefficient containing only one factor of p appear to have the form

$$-\frac{(d-1)^{n-1}}{d^n} p\nu^n \ .$$

This can be seen by examining the tables of coefficients for one, two, and three dimensions [and by examining (3.11)]. Summing over n, and adding the term p for $n = 0$, we see that on the Euclidean lattice in d dimensions the small-p result is

$$D(p,\nu) \approx p\left(1 - \frac{\nu}{d-(d-1)\nu}\right) \ .$$

For small p and large τ this expression becomes

$$D(p,\nu) \approx dp\frac{1}{\tau} \ .$$

On the Bethe lattice, with coordination number $z = 3$, the small-p result is

$$D(p,\nu) \approx p\left(1 - \frac{2}{3}\,\frac{\nu}{1-\nu/3}\right) \ . \tag{3.13}$$

For small p and large τ this expression becomes

$$D(p,\nu) \approx \frac{9}{4} p \frac{1}{\tau} \ . \tag{3.14}$$

We compare the expansion for small p in one dimension (3.12) with the exact expression for $\langle S_\infty^2 \rangle$, which is easily be shown to be (5)

$$\langle S_\infty^2 \rangle = \frac{p}{(1-p)^2} \ . \tag{3.15}$$

The first two terms in the expansion of (3.15) are $p + 2p^2$. Comparing these terms with (3.12) we find that, for small p and large τ, the relation $D = \langle S_\infty^2 \rangle / \tau$ (with the average taken at $\tau = \infty$) does not hold, as it does for the EMA of the HZ model (the continuous-time version of our model), as well as for DRN model. (See page 21). Our Monte-Carlo studies also show that, for large τ, $D \propto 1/\tau$, but that the coefficient is not $\langle S_\infty^2 \rangle$.

CHAPTER 4

The Renormalization Group Technique

In this chapter we present the renormalization group method that we used to calculate numerical approximations D_{RG} to the diffusivity. In the first section, we describe the technique. In the next section, we compare D_{RG} to estimates of the diffusivity obtained via Monte Carlo techniques D_{MC} and draw conclusions about the efficacy of the RG methods. Finally, we calculate the dependence of D_{RG} on τ for large τ.

4.1 The RG technique

Applications of renormalization group techniques in statistical physics rely on the assumption that the macroscopic behavior of a system is invariant under an appropriate rescaling of space and time, accompanied by a change in parameters of the system. For a simple random walk, the distribution of the displacement is asymptotically Gaussian, and is thus invariant under a rescaling of space by a factor b and of time by a factor b^2. In particular, the diffusivity does not change under this rescaling. However, with our model, a rescaling of time also entails a change in the rate of bond fluctuations, so that, if we begin with particular values for p and ν and rescale time by some factor $b > 1$ we will see an apparent increase in the rate of bond fluctuations, that is $\tau \to \tau/b$. How does the mean bond density change

under rescaling? We see from Fig. 2.2 on page 30, that we can hold the diffusivity constant by decreasing both p and ν by an appropriate amount. So in order to replace the process by a rescaled process with the same diffusivity, we need to decrease p. We know how ν changes under rescaling of time, as it is simply related to τ. Suppose we are able to make a good estimate of the apparent value of p under a modest rescaling of time and space. We may think of the process of rescaling the parameters as a map from the domain of (p, ν) onto itself. We may hope that after a process of repeated rescaling, the parameters will flow under the map to a fixed point for which we can approximate the diffusivity. For the map we choose below, it turns out that most initial points flow to a fixed point $(p^*, 0)$, where p^* depends on the initial values of the parameters. We know that $D(p, 0) = p$, so that p^* is our estimate of the diffusivity.

Now we give the details of the RG maps. We distinguish quantities on the rescaled lattice by a prime and refer to the rescaled lattice as the primed lattice. Let us consider replacing n time steps on the original lattice with m time steps on the primed lattice, where $m < n$. We are rescaling time by a factor of n/m. Thus, the physical bond fluctuation time changes according to

$$\tau' = \frac{m}{n}\tau, \quad \text{or} \tag{4.1}$$

$$\nu' = \nu^{n/m}. \tag{4.2}$$

We may use D_n^A (equation 2.2 on page 27) as an approximation of the diffusivity on each of two lattices. We then require that p' be chosen such that

$$D_m^A(p', \nu') = D_n^A(p, \nu), \tag{4.3}$$

where ν' is determined by (4.2). We call the RG map determined by (4.2) and

(4.3) RGA. In general, (4.3) is a polynomial equation in p' that must be solved numerically.

We may also choose D_n^I (equation 2.3 on page 27) as an approximation to the diffusivity. Thus, we define a map called RGB via (4.2) and

$$D_m^I(p', \nu') = D_n^I(p, \nu). \tag{4.4}$$

Regardless of whether we choose D_n or D_n^I as an approximation, the computation of the RG estimate proceeds as follows. We choose a pair (p, ν) for which we wish to compute an approximation of $D(p, \nu)$. We then solve (4.1) and (4.3) [or (4.4)] for ν' and p'. We take (4.3) and (4.4) to be polynomial equations in p', and find numerically that they each have only one root between 0 and 1. We then replace p with p' and ν with ν' and iterate the procedure. It turns out that the equation for p' becomes approximately $p' = p$, while ν' decreases exponentially in the iteration number (when $\nu \neq 1$). Thus, the pair (p, ν) flows to a fixed point $(p^*, 0)$, with the value p^* depending on the initial choice of p and ν. Because $D(p, 0) = p$, we take p^* to be the estimate D_{RG}. In order to solve for p' numerically, we must compute D_n^A as a polynomial in p and ν. (An example is given in Appendix A.) Although this computation is rather expensive, iterating the maps is relatively easy.

The first step in understanding a particular RG map is to characterize the fixed points and basins of attraction of the flow. In our case, the important aspects of these features are generic to both RGA and RGB for all values of m and n that we studied. A particular example of the flow for RGA is given in Fig. 4.1. The flow of ν, given by (4.2), is independent of p. Considered as a one-dimensional map, $\nu = 0$ is a stable fixed point, $\nu = 1$ is an unstable fixed point, and all points ν with $0 < \nu < 1$ flow to 0. In general, the flow of p depends on ν. But, because

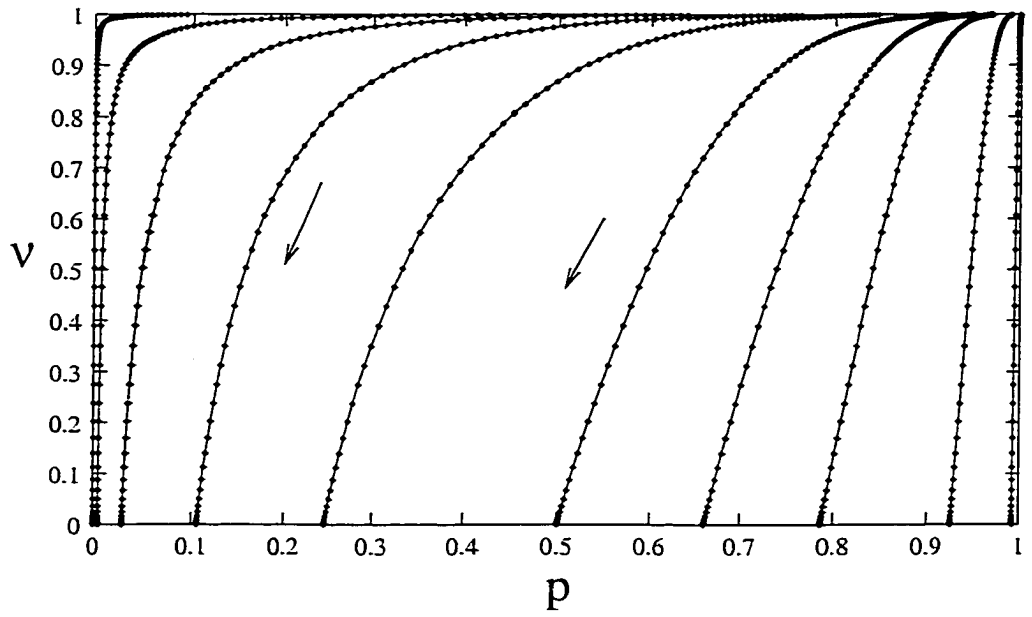

Figure 4.1: RG flow on the Bethe Lattice ($z = 3$, $p_c = 1/2$) for $\mathrm{RGA}_{9,10}$. The flow diminishes both p and ν. Each curve begins with $\nu = 0.999$ and a different value of p, and represents a sequence of iterations of the RG map that converges to a different point on the line $\nu = 0$. For larger initial values of ν the flow stays closer to the top and left edges of the plot.

$D_n^A(0,\nu) = D_n^I(0,\nu) = 0$ and $D_n^A(1,\nu) = D_n^I(1,\nu) = 1$ for any ν, we see that $p = 0$ and $p = 1$ are fixed points for any ν when the flow of p is considered to be one-dimensional. Furthermore, by expanding D^A about $p = 0$ and $p = 1$, we can show that the point $p = 1$ is unstable for all ν, while $p = 0$ stable for all ν. Finally, all p are fixed points of the map for p when $\nu = 0$. Putting these observations together, we find the fixed points for the two-dimensional map. $(p,\nu) = (0,1)$ is a fixed point stable in the p direction and unstable in the ν direction. $(p,\nu) = (1,1)$ is a fixed point unstable in both the p and ν directions. The points $(p,0)$ for $0 \leq p \leq 1$ are stable fixed points. When ν is small, we may consider only the terms proportional to ν in the equations determining the flow of p. On the Bethe lattice with $z = 3$, these terms are proportional to $p^2 - p$ and thus have a maximum at $p = 1/2$. (This can be checked for $n = 1$ to $n = 10$ by referring to Appendix A. If our expansion in ν is correct, this behavior persists for all n.) This maximum is evident in Fig. 4.1, as the change in p is most rapid for p near $1/2$. We find that the coefficients for higher orders of ν have maxima in p at different points. These points tend to move toward p_c, but our limited data do not indicate clearly whether they converge to p_c. For instance, in one dimension, the maxima for large powers of ν are near $p = 0.8$. In three dimensions, they are near 0.3. Finally, we note the flow of points with ν very close to 1. If p is not near 1, then p will decrease to nearly zero before ν has changed appreciably. Then, as p approaches zero asymptotically, ν will eventually leave the region near 1 and move quickly to zero. This behavior is shown more clearly in Fig. 4.2. We will analyze this asymptotic behavior in more detail in section 4.3.

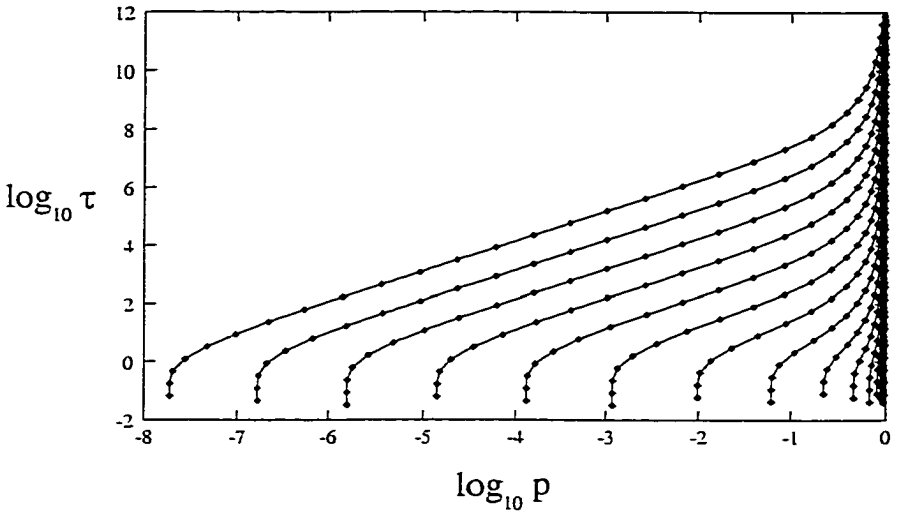

Figure 4.2: RG flow on the Bethe Lattice ($z = 3$) for $\mathrm{RGA}_{3,8}$. The curves are for initial values of $p = 0.99$ and $\tau = 10^n$, with $n = 1, \ldots 14$. When τ is large, the curves can be made to coincide by a shift along the vertical axis. For small p, they can be made to coincide by a shift in the horizontal axis.

4.2 Results of the RG Technique

In this section we evaluate the utility of the RG methods in estimating the diffusivity. We will make a quantitative comparison of the RG estimates and Monte Carlo estimates D_{MC} on the Bethe lattice below. We will refer frequently to the relative error of D_{RG} with respect to D_{MC}, by which we mean $(D_{\mathrm{RG}} - D_{\mathrm{MC}})/D_{\mathrm{MC}}$. (For example, see Figs. 4.4, 4.5, and 4.6.) But first we explain the results in a qualitative way by examining the fixed points. We compare our RG to the flow that would result if we were to construct our map with perfect estimates of D. Such a flow would follow contours of a plot of the true value of D as a function of p and ν, which we approximate with Monte Carlo estimates in Fig. 4.3. Our previous discussion suggests that the fixed points of an RG flow correspond to parameters for which the macroscopic view of the model is invariant under a change of scale. (See for instance

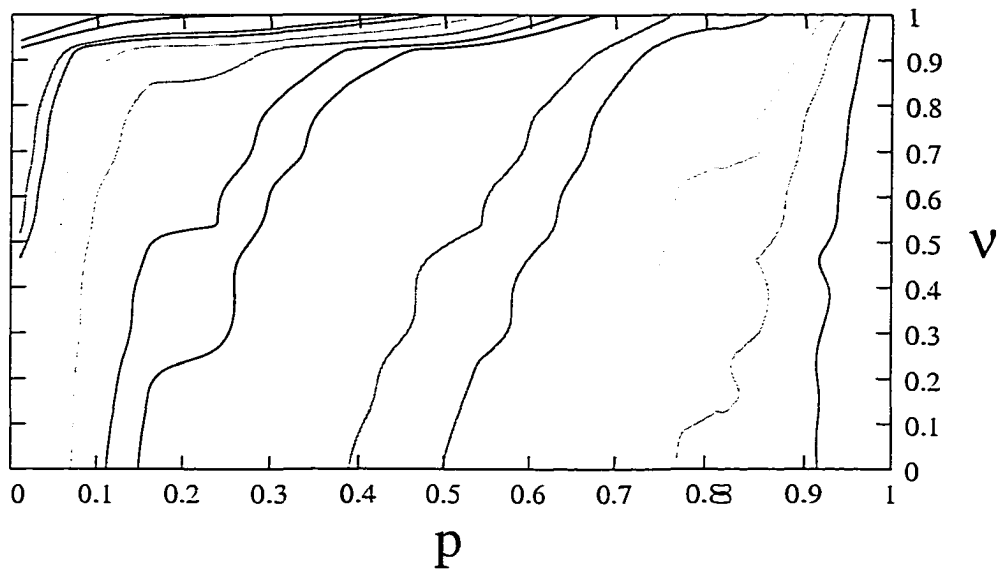

Figure 4.3: Contour plot of Monte Carlo estimates D_{MC} for the Bethe lattice with $z = 3$. The irregularities in the lines are artifacts from discrete sampling of parameter space. The value of D for a contour is equal to the value of p at which the line crosses the line $\nu = 0$. The effect of the critical point $(p, \nu) = (1/2, 1)$ is visible. Some of the curves shown touch the line $\nu = 1$ at values of p with $p > p_c$. All points on the line $\nu = 1$ with $p < p_c$ are on the contour $D = 0$.

(9).) For instance, when applying RG methods to the static percolation problem, one typically finds a one-dimensional map with three fixed points; $p = 0, 1,$ and p^*. (See (26).) In this case, it is the correlation length ξ that we want to hold invariant under iteration of the map. At the points $p = 0$ and $p = 1$, ξ is 0. The point p^* is an approximation of the critical point, for which $\xi = \infty$. Only at these three points is ξ invariant under a change of length scale. The fixed points of the RG for the FBRW occur for parameter values for which the true behavior of the system is invariant under a rescaling of time and space. At the point $(p, \nu) = (1, 1)$, the temporal correlation is infinite and the correlation length $\xi = 0$. (If we include the infinite cluster in the computation of the correlation length, then ξ is infinite.) At this point both temporal and spatial correlations are invariant under a change of scale. The point $(p, \nu) = (0, 1)$ is invariant for the same reason. When $\tau > 0$, we expect spatial correlations to persist over short enough time scales. But for points $(p, 0)$ with $0 < p < 1$, the fluctuations are infinitely rapid so that effects of spatial correlations are destroyed on any finite time scale. Thus, these points are invariant in the actual system as well. However, the maps RGA and RGB are deficient in that there is no fixed point representing the critical point $(p_c, 1)$, except in the case $d = 1$. This feature limits the utility of these maps in the vicinity of the critical point when $d \neq 1$. When $d = 1$, the fixed points $(1, 1)$ and $(p_c, 1)$ coincide. Furthermore, we will see below that RGA for $d = 1$ also predicts the asymptotic behavior in τ correctly. Thus, the 1–d map captures the important features of the true flow and so produces excellent numerical predictions. $\mathrm{RGA}_{m,n}$ does well in this case even for relatively small m and n. For instance, it was the success of $\mathrm{RGA}_{1,4}$ in the work by LNS (19) that prompted the present study.

This leaves us with the question of how the absence of a critical point in

the RG maps affects the predictions of the approximations D_{RG} when $d > 1$ and on the Bethe Lattice. As we mentioned before, the approximations D^A and D^I, are quite accurate as long as ν is not near 1. So we expect the RG maps to do well in this region. But for ν near 1, we expect the absence of a critical point to be manifest. It turns out that the maps in higher dimensions behave qualitatively as they do in one dimension. That is, the flow as $\nu \to 1$ looks roughly as it should in the sub-critical phase. In particular, we will see below that D_{RG} decays algebraically in τ to zero for all values of p. In the actual model, D decays to a non-zero constant for $p > p_c$. Furthermore, we will see that D_{RGA} decays as $\tau^{-\alpha}$, where α approaches 1 as m and n increase. Thus, unless τ is very large, RGA gives a decay that is close to the true behavior of the model when $p < p_c$, as seen in Figs. 4.5 and 4.6 . This decay, together with an accurate flow away from $\nu = 1$ results in good numerical predictions D_{RGA} when ν is near 1 and $p < p_c$. Seen this way, the point $(p, \nu) = (1, 1)$ can indeed be viewed as representing the critical point $(p_c, 1)$. It is numerically inaccurate, but the flow away from this point represents qualitatively (and even somewhat numerically) the flow away from $(p_c, 1)$ in the actual system. Because RGB is based on much more accurate estimates of D than is RGA, we will find that RGB does much better when ν is not close to 1. However, $\mathrm{RGB}_{m,n}$ for large m and n predicts a decay in τ with an exponent much larger than 1, so it makes poor predictions when ν is close to 1. These observations are illustrated in Figs. 4.4 and 4.5 .

Details of the performance of the various RG methods depend in a complicated way on the model parameters and m and n and the dimension of the lattice. Now that we have desribed the broad features of the flow, we will attempt to fill in some details. In general, we get the best results from the RG maps when m and n

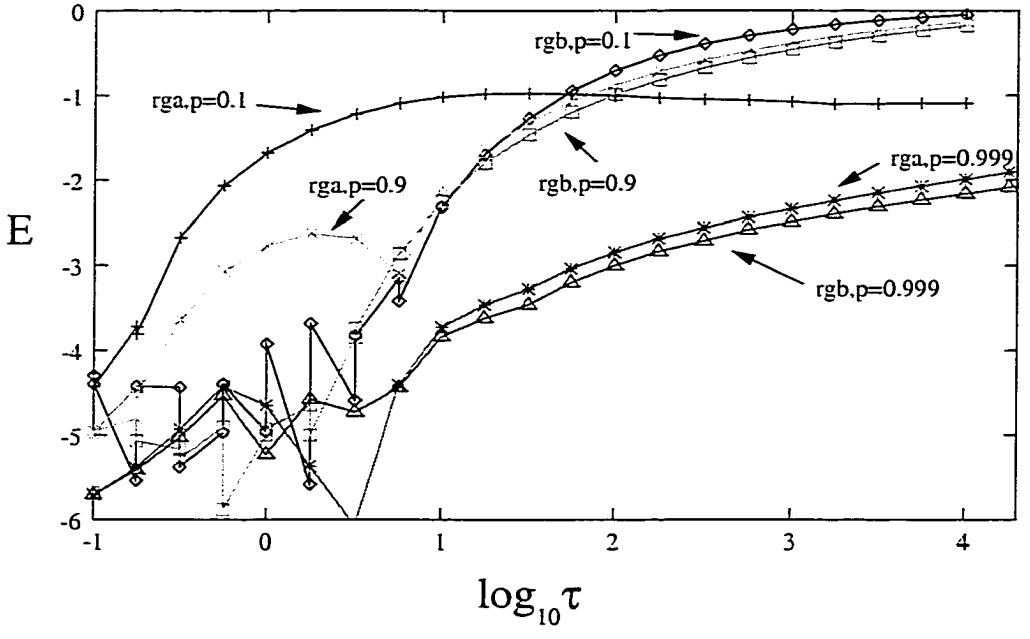

Figure 4.4: Relative error of D_{RG} compared to D_{MC} for the Bethe lattice. Here, $E = \log_{10}(|D_{\mathrm{RG}} - D_{\mathrm{MC}}|/D_{\mathrm{MC}})$. The curves are computed for several values of p, using $\mathrm{RGA}_{9,10}$ and $\mathrm{RGB}_{9,10}$. All maps do best when τ is small, but RGB is much better than RGA here. For the RGA shown here $\alpha =$, so that for p well below p_c the estimate of D is good even for large values of τ. For $p > p_c$ (*eg.* $p = 0.9$), the RG maps predict an algebraic decay to zero, while the Monte Carlo result predicts decay to a constant. Notice the statistical fluctuations in D_{MC}, which are of order 10^{-5}–10^{-6} times the value of D_{MC}.

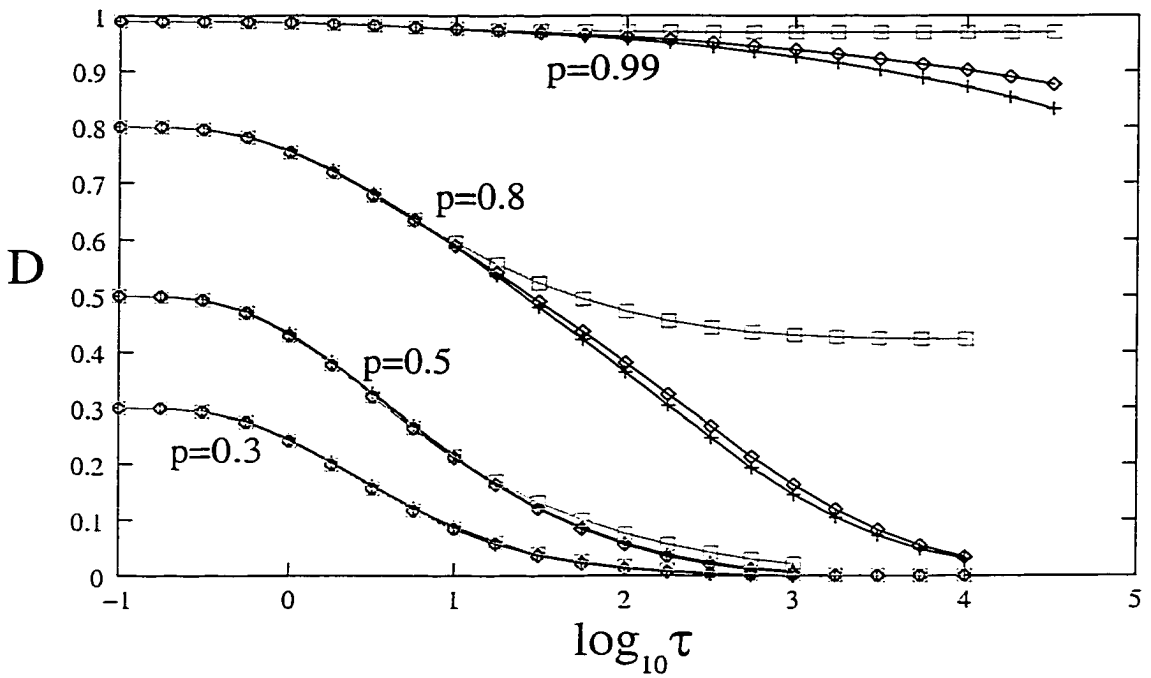

Figure 4.5: Comparison of Monte Carlo estimates D_{MC} to RG estimates D_{RG} for $\mathrm{RGA}_{9,10}$ and $\mathrm{RGB}_{9,10}$ on the Bethe lattice, for which $p_c = 0.5$. Squares are D_{MC}, pluses are for $\mathrm{RGA}_{9,10}$, and diamonds are for $\mathrm{RGB}_{9,10}$. For $p < p_c$, the diffusivity D_{MC} decays to 0. For $p > p_c$, it tends to a constant. The RG estimates decay to 0 both above and below p_c. As p increases, the onset of the algebraic decay in the RG estimates begins for larger values of τ.

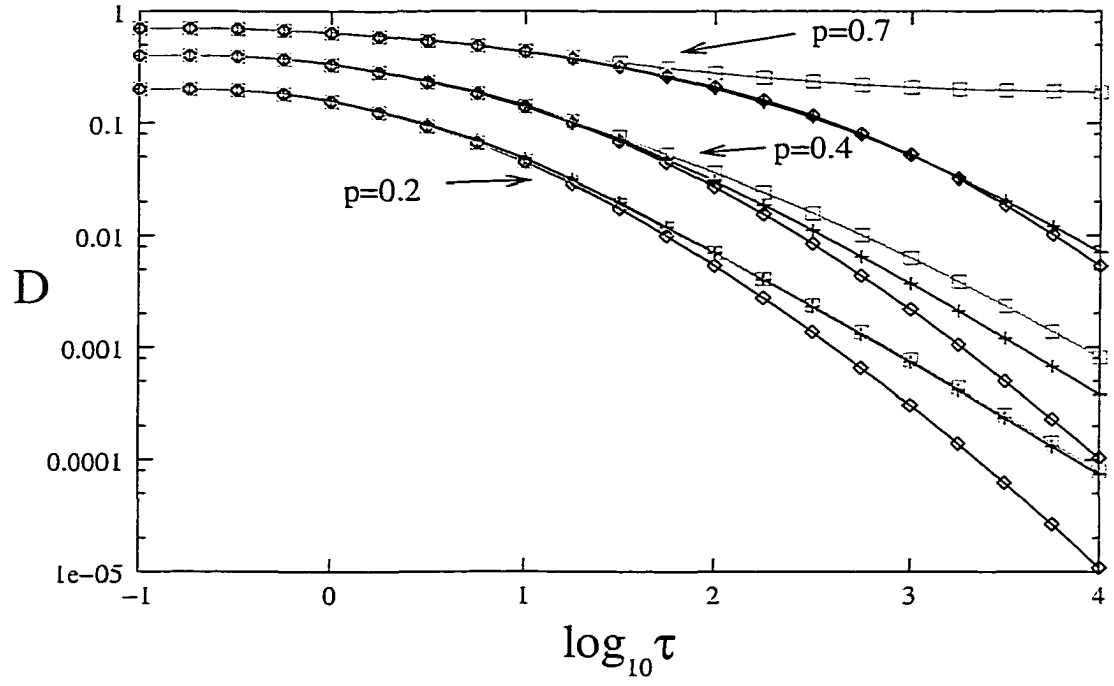

Figure 4.6: Comparison of Monte Carlo estimates D_{MC} to RG estimates D_{RG} for $\mathrm{RGA}_{9,10}$ and $\mathrm{RGB}_{9,10}$ on the Bethe lattice, for which $p_c = 0.5$. Squares are D_{MC}, pluses are for $\mathrm{RGA}_{9,10}$, and diamonds are for $\mathrm{RGB}_{9,10}$. For $p < p_c$, all three estimates show algebraic decay; *i.e.* $D \propto \tau^{-\alpha}$. For D_{MC}, $\alpha \approx 1$. For the RGs, α is known exactly. For $\mathrm{RGA}_{9,10}$, $\alpha \approx 0.9997$. For $\mathrm{RGB}_{9,10}$, $\alpha \approx 10$. For small p, $\mathrm{RGA}_{9,10}$ is close to D_{MC} when they both begin to decay at nearly the same rate, resulting in a good numerical estimate for rather large τ. For $p > p_c$, the RG predictions continue to decay algebraically, while D_{MC} tends to a constant.

in (4.2), (4.3), and (4.4) are as large as possible (with $m < n$). Typical values are $m = 9$ and $n = 10$. The relative error generally decreases both with increasing m and increasing n. However, for RGA, the error changes sign as a function of the parameters. So this rule is violated for many values of τ and p. RGB does much better than RGA when τ is not too large. When τ is large enough (much greater than m and n), RGA does much better than RGB if $p < p_c$ although RGA fails eventually for large enough τ. If $p > p_c$ and τ increases past n, both RGA and RGB begin to fail, with RGB performing slightly better. However, as p becomes larger, both maps fail less rapidly with increasing τ. Both RGA and RGB fail to capture even the qualitative behavior for $p > p_c$ and τ very large. In particular, RGA and RGB both predict that $D_{\mathrm{RG}} \to 0$ as τ increases, while D_{MC} and previous studies show that the diffusivity actually decays to a non-zero constant. In general, the relative error of all RG maps increases without bound with increasing τ. We see evidence of this behavior in the Monte Carlo data (Fig. 4.4) as well as in the asymptotic analysis discussed below. (We will also discuss some exceptional cases in which the relative error approaches a limit. Also, there is a brief dip in the error for RGA as the sign of the error changes.) The relative error in RGA decreases with increasing p when τ is not too large. When τ is large enough, the error first decreases then begins to increase when p is still less than p_c, then begins to decrease again when $p > p_c$. The relative error in RGB decreases as p moves away from the critical point in either direction and toward 0 and 1. Except when p is very near 1, $\mathrm{RGB}_{m,n}$ has a much lower relative error than $\mathrm{RGA}_{m,n}$ for τ small enough. If m is not much smaller than n, then this regime includes values of $\tau \lessapprox n$.

We need to ask whether the RG maps give estimates that improve on the approximations D_n^A and D_n^I, that is, the approximations on which the maps are

based. The short answer is yes, when τ is not too large, as illustrated in Fig. 4.7. It is appropriate to compare the relative error in $\mathrm{RGA}_{9,10}$ to that in D^A_{10}, and the relative error in $\mathrm{RGB}_{9,10}$ to that in D^I_{10}. (One could argue that we should use D^A_9 and D^I_9, but the results are quite similar.) We see that, for $p < p_c$, $\mathrm{RGA}_{m,n}$ improves on D^A_n for all τ. For values of τ that are larger than those plotted, we expect this behavior to continue, because $\mathrm{RGA}_{m,n}$ decays algebraically in τ, as does the true value of D, while D^A_n approaches a non-zero limit. For $p > p_c$ RGA is not an improvement for large τ. We expect this because the true value of D decays to a non-zero limit in this case. Comparing $\mathrm{RGB}_{m,n}$ and D^I_n we see much the same behavior, except that $\mathrm{RGB}_{m,n}$ does not give as great an improvement as $\mathrm{RGA}_{m,n}$ does for large τ and $p < p_c$. Also, when τ is not too large, both $\mathrm{RGB}_{m,n}$ and D^I_n have much smaller relative error than do $\mathrm{RGA}_{m,n}$ and D^A_n, as is expected. The general features of the performance of the RG maps relative to the approximate diffusivities, which are discussed above, do not depend m and n. Similar curves are also obtained for different values of p, with the same qualitative behavior depending on whether p is greater than or less than p_c. Particularly large and small values of p were chosen for Fig. 4.7 in order that the curves be well separated.

4.3 Behavior of the RG for large τ

We present asymptotic expressions for D_{RG} in the limit that τ is large. Although the expressions are derived non-rigorously, we show by comparison with numerical evaluation of the RG maps that they are obeyed to within machine precision. When τ is large and $p < p_c$, we believe that $D \propto 1/\tau$. Monte Carlo studies in one and two dimensions and on the Bethe lattice show this behavior clearly. The conjectured expansion about $p = 0$ shows this behavior in all dimensions. (See Figs. 3.2 and

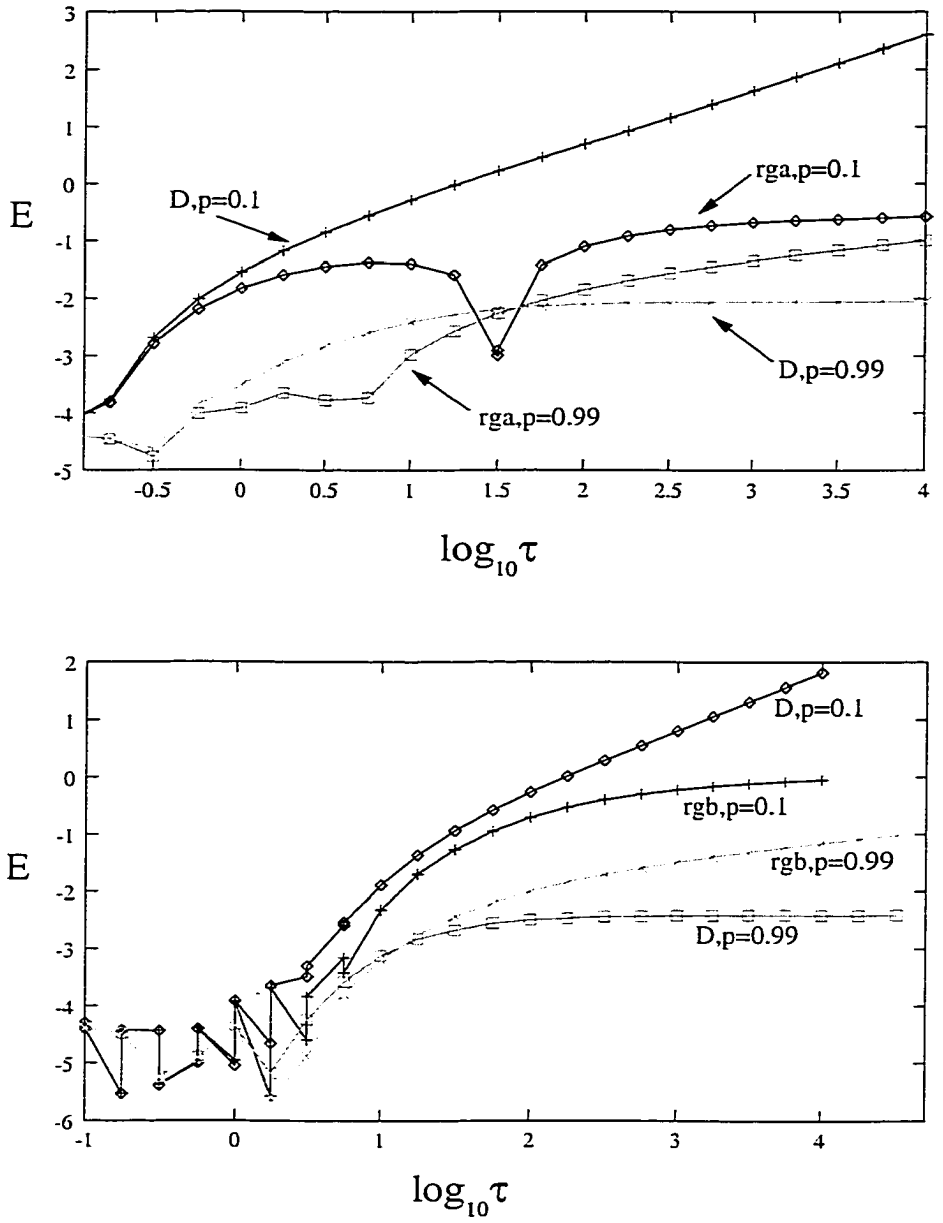

Figure 4.7: Comparison of relative error in D_{RG} to relative error in D^A and D^I on the Bethe lattice for various values of p. For all curves, $E = \log_{10}(|D_x - D_{\mathrm{MC}}|/D_{\mathrm{MC}})$, where D_x is one of $\mathrm{RGA}_{9,10}$, $\mathrm{RGB}_{9,10}$, D^A_{10} or D^I_{10}. Upper plot: curves marked D are for D^A_{10}; curves marked rga are for $\mathrm{RGA}_{9,10}$. Lower plot: curves marked D are for D^I_{10}; curves marked rgb are for $\mathrm{RGB}_{9,10}$. When τ is less than about 10 or 100, the RG maps improve on the estimates D^A and D^I. The RG maps, generally perform worse for larger τ. An exception is RGA when $p < p_c$, in which case RGA predicts algebraic decay in τ with nearly the correct exponent, while the estimate D^A incorrectly decays rapidly to a constant. Notice that the statistical noise in the Monte Carlo data when both τ and the error are small obscures the relative position of the curves.

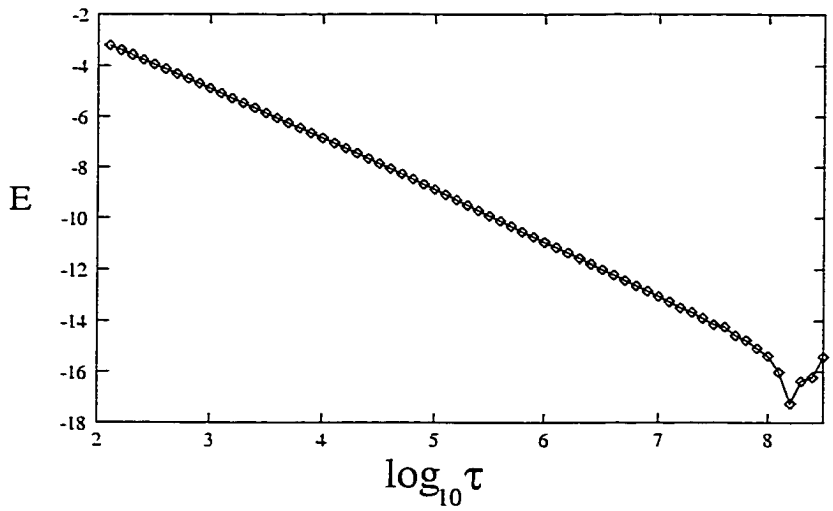

Figure 4.8: Approach of $\mathrm{RGA}_{4,5}$ on the Bethe lattice to asymptotic behavior. Here, $E = \ln(d(\ln D)/d(\ln \tau) + \alpha_A)$, where the derivative is evaluated numerically, and $\alpha_A \approx 0.963$ is computed according to equation (4.8). The plot shows that the derivative approaches $-\alpha_A$ roughly exponentially. (The irregularities at very large τ are due to the finite precision of computer calculations.

3.3 .) As we saw in the introduction, related models also show this behavior. We are interested in the extent to which the RG methods capture this behavior. As $\tau \to \infty$ we find the methods $\mathrm{RGA}_{m,n}$ and $\mathrm{RGB}_{m,n}$ give estimates of D that obey

$$D_{\mathrm{RG}} \propto \tau^{-\alpha}, \tag{4.5}$$

where the proportionality constant depends on p. We will show below how to calculate α. The difference between (4.5) and the exact numerical evaluation of D_{RG} given in section 4.1 decays roughly exponentially with increasing τ. But when n/m is large enough, small oscillations are superimposed on this decay (Figs. 4.8 and 4.9)

The exponent α depends m and n, whether we use RGA or RGB, and the dimension of lattice, but not on p. In most cases, we can write a simple expression for α in terms of the coefficients of the linear terms in the maps. We find that $\mathrm{RGA}_{m,n}$ gives $\alpha = 1$ for all m and n in one dimension, while $\alpha < 1$ on the other

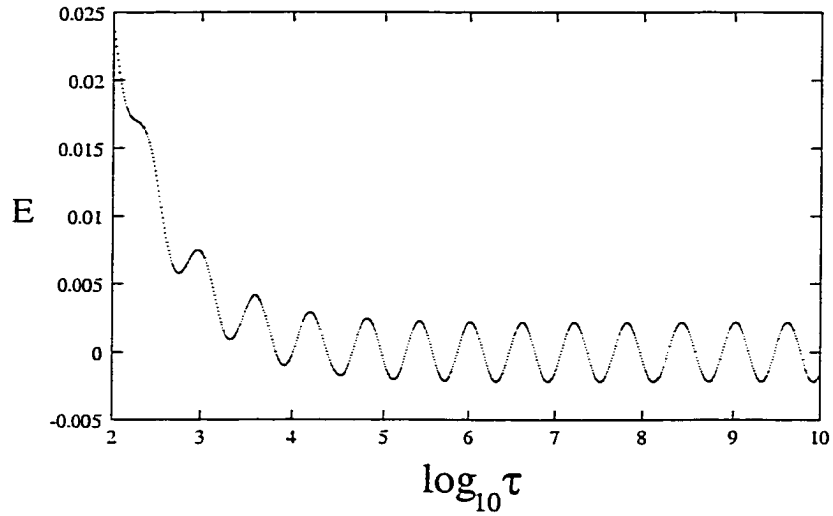

Figure 4.9: Approach of $\mathrm{RGA}_{1,4}$ on the Bethe lattice to asymptotic behavior. Here, $E = d(\ln D)/d(\ln \tau) + \alpha_A$, where the derivative is evaluated numerically, and $\alpha_A \approx 0.716$ is computed according to equation (4.8). The plot shows that the derivative approaches, but oscillates about, $-\alpha_A$.

lattices, but $\alpha \to 1$ monotonically in both m and n. For $\mathrm{RGB}_{m,n}$, we find that α increases without bound and monotonically with m and n, but that, on the Euclidean lattices, $\alpha = 1$ for special choices of m and n. Thus, while increasing m and n makes $\mathrm{RGB}_{m,n}$ more accurate for smaller values of τ, it becomes less accurate when τ is large enough.

The exponent α is determined by the coefficients of the leading terms in the map for p. We find that $D^A_n(p,\nu)$ and $D^I{}_n(p,\nu)$ for values of n from 1 to about 10, in 1,2, and 3 dimensions and on the Bethe Lattice, are given by

$$D^I_n(p,1) = a^{n-1}p + O(p^2) \quad \text{and} \tag{4.6}$$

$$D^A_n(p,1) = \frac{1}{n}\frac{1-a^n}{1-a}p + O(p^2), \tag{4.7}$$

where $a = (d-1)/d$ in d-dimensions and $a = 1/3$ on the Bethe lattice, for $z = 3$. Although we have not calculated these coefficients for larger values of n, we assume

that these formulas hold with the same values of a for all n. [(4.6) holds if and only if (4.7) holds, but we have demonstrated neither equation for n larger than 10.] We will show below that for $\mathrm{RGA}_{m,n}$, $\alpha = \alpha_A$, which is given by

$$\alpha_A = \frac{\ln \frac{m(1-a^n)}{n(1-a^m)}}{\ln \frac{m}{n}}. \tag{4.8}$$

In one dimension, $a = 0$, so that $\alpha_{m,n} = 1$ for all m and n. Thus, even for $m = 1$ and $n = 4$ as in LNS (19), the correct asymptotic behavior is observed and the relative error tends to a limit. However, in higher dimensions and on the Bethe lattice, $\alpha_{m,n} < 1$, and tends rapidly to 1 as m and n increase. Thus, for $p < p_c$, increasing m and n greatly improves the performance of RGA for large τ.

For $\mathrm{RGB}_{m,n}$ (except in one dimension) we find that, $\alpha = \alpha_B$, which is given by

$$\alpha_B = \frac{(n-m)\ln a}{\ln \frac{m}{n}}. \tag{4.9}$$

We now show that α_A increases monotonically in both m and n and approaches 1. We also show that α_B increases without bound and monotonically in m and n, so that $\alpha_B = 1$ for at most one pair of values of m and n. We make the substitution $x = a^m$ and $y = a^n$. So we have that $0 < x < 1$ and $0 < y < 1$. In the following discussion we assume that x and y are restricted to this interval. Notice that, as m and n increase, x and y approach zero. Substituting for a, m, and n, we rewrite (4.8) as

$$\alpha_A = 1 - \frac{\ln \frac{1-x}{1-y}}{\ln \frac{\ln x}{\ln y}}. \tag{4.10}$$

Similarly, the expression for α_B is

$$\alpha_B = -\frac{\ln \frac{x}{y}}{\ln \frac{\ln x}{\ln y}}. \tag{4.11}$$

By expanding the logarithms, it is easy to see that $\alpha_A \geq 0$, $\alpha_B \geq 0$, $\lim_{x\to y} \alpha_A = 1 - y\ln(y)/(y-1)$, $\lim_{x\to 0} \alpha_A = 1$, $\lim_{x\to y} \alpha_B = -ln(y)$, and $\lim_{x\to 0} \alpha_B = \infty$. Because α_A and α_B are symmetric in x and y, the limits obtained by exchanging x and y are the same. Because we are mostly concerned with how these exponents change for small m and n, we would like to show that these limits are approached monotonically. That is, we need to show that $\partial\alpha_A/\partial x < 0$ and $\partial\alpha_B/\partial x < 0$.

These statements of the monotonicity of (4.10) and (4.11) are particular cases of the following proposition, which we prove below.

Restrict x and y to an interval (a, b) and suppose

$$\beta(x,y) = \beta(y,x) = \frac{f(x)-f(y)}{g(x)-g(y)}, \tag{4.12}$$

with $f'(x)/g'(x)$ monotonic. Then $\Delta = f'(x)g''(x) - g'(x)f''(x)$ is either negative or positive on the entire interval. If $\Delta > 0$ then $\partial\beta/\partial x < 0$ and $\partial\beta/\partial y < 0$. If $\Delta < 0$ then $\partial\beta/\partial x > 0$ and $\partial\beta/\partial y > 0$.

We apply this proposition for $\beta = \alpha_A - 1$, because the constant term does not affect the monotonicity. In this case, we have $f(x) = -\ln(1-x)$ and $g(x) = \ln(-\ln(x))$. Thus $f'(x)/g'(x) = x\ln(x)/(1-x)$ and $(f'(x)/g'(x))' = (1 - x + \ln x)/(1-x)^2 < 0$ so that $f'(x)/g'(x)$ is monotonic. To show this last inequality, we note that $\ln x$ and $x-1$ are equal at $x = 1$ and their first derivatives are equal at $x = 1$. But $(\ln x)'' = -1/x^2 < 0$, while $(x-1)'' = 0$. Now we evaluate Δ.

$$f'(x)g''(x) - g'(x)f''(x) = \frac{-(1+\ln x)}{x^2(1-x)(\ln x)^2} - \frac{1}{x(1-x)^2\ln x} = -\frac{\ln x + 1 - x}{x^2(1-x)^2(\ln x)^2}, \tag{4.13}$$

which is positive, by the same argument given above. Thus $\partial\alpha_A/\partial x < 0$.

Now we apply the proposition for $\beta = \alpha_B$. In this case, $f(x) = -\ln(x)$

and $g(x) = \ln(-\ln(x))$. We have $f'(x)/g'(x) = -\ln(x)$, which is monotonic. And $\Delta = x^{-3}[\ln(x)]^{-2} > 0$, so that $\partial\alpha_B/\partial x < 0$. Because α_B increases monotonically in m and in n, it can only assume the value 1 for at most one pair of values of m and n.

We now prove the proposition stated above. From the symmetry in (4.12), we see that if $\partial\beta/\partial x < 0$ for all x and y, then $\partial\beta/\partial y < 0$. So we need only show $\partial\beta/\partial x < 0$. We calculate

$$\frac{\partial\beta}{\partial x} = [g(x) - g(y)]^{-2}\,[f'(x)g(x) - g'(x)f(x) - f'(x)g(y) + g'(x)f(y)]\,. \qquad (4.14)$$

We define $\gamma(x,y) = f'(x)g(y) - g'(x)f(y)$. If γ has only one maximum γ_{max} in y and it occurs at $y = x$, then the second factor in (4.14) is $\gamma_{max} - \gamma$ so that $\partial\beta/\partial x > 0$. Likewise, if γ has only one minimum at $y = x$, then $\partial\beta/\partial x < 0$. We now show that indeed γ has only one extremum in y and that it occurs at $y = x$. We have $\partial\gamma/\partial y = f'(x)g'(y) - g'(x)f'(y)$. Because $\partial\gamma/\partial y = 0$ only if $f'(x)/g'(x) = f'(y)/g'(y)$, and $f'(x)/g'(x)$ is monotonic by hypothesis, the only extremum in y of γ occurs at $y = x$. From the sign of $\Delta = \partial^2\gamma/\partial y^2|_{y=x} = f'(x)g''(x) - g'(x)f''(x)$, we determine if the extremum is a maximum or a minimum. This demonstrates the proposition.

We understand why (4.8) and (4.9) are correct with the help of Figs. 4.1 and 4.2 . Let us choose an initial pair (p,τ) with p not too near 1., but $1/\tau$ small (i.e., ν near 1). We see in Fig. 4.1 that the flow takes p to a value near zero, while τ remains large, and then takes τ to zero while p becomes even smaller. Thus, the map is always in an asymptotic region for which one or both of p and $1/\tau$ is small. The behavior of the flow in these regimes is seen more clearly on a logarithmic scale in Fig. 4.2. It turns out that for RGA on all lattices the map for p [equation 4.3] is independent of τ as $\tau \to \infty$. The same is true for RGB on the Bethe lattice,

and for $d > 1$. The independence of p' from τ, together with the fact that τ varies exponentially with the number of iterations, explains the observed invariance of the curves in Fig. 4.2 under translation along the $\log\tau$ axis when τ is large. When the map has been iterated until p is small, but τ is still large, then p' is linear in p (equation 4.6). Because τ' is always linear in τ, we have in this region that both τ and p vary exponentially with the number of iterations, with an exponent that is independent of τ and p and is given by (4.8) or (4.9). In this region, the curves are linear on a log-log plot (Fig. 4.2). Finally, when p is small, but τ is of order 1 or smaller, p' has a complicated dependence on τ, but is linear in p so that the composition of several iterations is still linear in p. Thus the curves in this region are invariant under a shift in $\log p$. So, asymptotically, the curves are similar except that with increasing τ, they take a longer path in the linear (on the log-log scale) regime. The resulting decrease in $\log p$ is determined by the slope of the line in the linear regime.

Because the map is actually discrete, the points do not move tangentially to the flow, and the curves are not perfectly translationally invariant in the small p region. So one expects some small oscillating corrections to the asymptotic behavior. However, numerical results show these effects to be curiously small. They are only detectable numerically when n/m is rather large (greater than about 2). The presence and absence of oscillations depending on m and n is illustrated in Figs. 4.8 and 4.9 .

In one dimension, the analysis of RGB is more complicated. We cannot use a linearized map for the evolution of p, because the term of order one in p and order zero in $1/\tau$ vanishes. Using the non-vanishing terms of lowest order, the map

for p becomes

$$\frac{1}{2^{m-2}}p'^2 + \frac{p'}{\tau'} = \frac{1}{2^{n-2}}p^2 + \frac{p}{\tau} \tag{4.15}$$

When p is small, but $p > 1/\tau$, the quadratic term in p dominates, and the map is independent of τ. As the map is iterated, p becomes smaller and $1/\tau$ becomes larger, so that, eventually the term linear in p dominates. In this case, substituting $\tau' = (m/n)\tau$, we see that dependence on τ cancels and the map is again independent of τ. But in the crossover region, when $p \approx 1/\tau$, the quadratic equation must be solved, and the map is, in general, not independent of τ. However, for the special case that $m = 2$ and $n = 4$, the map reduces to $p' = p/2$ in all regions for which (4.15) is appropriate, including the crossover region. In this case, $\tau' = \tau/2$, so that $\alpha_{2,4} = 1$ for $\mathrm{RGB}_{2,4}$ in one dimension.

CHAPTER 5

Asymptotic Distribution

The present model, and related models, have already received some study (13; 19) that suggests that the probability distribution is is Gaussian at long times. The evidence suggest that the distribution is Gaussian for all $\nu < 1$ (and there is no reason to believe otherwise). In this chapter, we prove that the distribution function of the normalized position of the walker is asymptotically normal on a restricted domain in parameter space.

For the discussion in this chapter, we will generalize the model slightly by making the bond process discrete in time. If the bond is blocked at time n then, with probability α, it will be open at time $n+1$. Likewise, if it is open at time n, then with probability β, it will be blocked at time $n+1$. There is a pair (α, β) corresponding to each pair (p, ν) from the previous chapters. But the converse is not true. There are, for instance, pairs (α, β) for which the bond-state correlation oscillates as it decays in time.

To prove the central limit theorem, we analyze the dependence of the future and the past. If they are sufficiently independent then the distribution converges to a normal distribution. We begin by showing that the process is stationary. We can then make use of powerful results from the well-developed theory of stationary processes. In particular we show that our process is uniformly mixing with an exponentially decaying mixing coefficient. (The mixing coefficient is a number

that measures the dependence of future and past.) This is a rather strong statement, which satisfies the hypotheses of a number of limit theorems designed for applications.

5.1 The Process

In this section we present the notation that we will use in the remainder of the chapter. The walker occupies the vertices of the Euclidean lattice, which we take to be $\mathbb{Z}^d$ together with the bonds (edges) connecting all pairs of vertices for which one vertex differs from the other by one of the unit vectors $\{\pm\mathbf{e}_j\}$. The walker attempts a step at each time $n \in \{1, 2, \dots\}$ with equal probability to one of the $2d$ possible neighbors. The states of the bonds are represented by of a set of random variables, the **bond states** B_n^y— one for each bond y in the lattice at each time n. Thus, we can describe the state of the entire system via a sequence of vector-valued random variables

$$(A_n, \{B_n^y; y \in \mathcal{B}\}), \tag{5.1}$$

where n labels time, $\mathcal{B}$ is the set of all bonds, and the sequence of **attempts** $A_n \in \{\pm\mathbf{e}_j\}$ are independent, identically distributed random variables with $\mathbf{P}(A_n = \mathbf{e}_j) = \mathbf{P}(A_n = -\mathbf{e}_j) = 1/(2d)$. For a fixed bond y, we have a random vector or sequence of bond states $B^y = (B_1^y, B_2^y, \dots)$. We let the collection of all B^y and all A_n be independent. We let the collection of B^y be identically distributed. A cumbersome, but precise, statement of the independence is

$$\begin{aligned}\mathbf{P}(A_{x_i} \in a_i, B^{y_j}_{z_{j,k}} \in b_{j,k};\ i = 1, \dots, N_1;\ j = 1, \dots, N_2;\ k = 1, \dots, M_j) \\ = \prod_i \mathbf{P}(A_{x_i} \in a_i) \prod_j \mathbf{P}(B^{y_j}_{z_{j,k}} \in b_{j,k}; k = 1, \dots, M_j),\end{aligned} \tag{5.2}$$

where the equality holds for arbitrary sets satisfying the following conditions. a_i and $b_{j,k}$ are subsets of the ranges of the increments and bond variables, respectively. The x_i and $z_{j,l}$ are positive integers and $\{y_j\}$ is a set of distinct bond variables.

For each fixed bond y we take the sequence B^y to be the two state Markov chain, which entails two free parameters. The two states are 0 (blocked) and 1 (open). If the walker attempts to cross a bond in the open state, the step is successful. If the walker attempts to cross a bond in the blocked state, the step fails and he remains on the same vertex until the next time, when another attempt to cross a bond is made. For each y, we denote the bond-state transition probabilities by

$$p_{i,j} = \mathbf{P}(B^y_{n+1} = j | B^y_n = i) \ . \tag{5.3}$$

The transition matrix has the general form

$$\mathbf{p} = \begin{pmatrix} 1-\alpha & \alpha \\ \beta & 1-\beta \end{pmatrix} . \tag{5.4}$$

We assume $\alpha, \beta > 0$. Computing the nth power of this matrix, one obtains the probabilities for moving from state i to state j in n time steps

$$\mathbf{p^{(n)}} = \begin{pmatrix} p^{(n)}_{0,0} & p^{(n)}_{0,1} \\ p^{(n)}_{1,0} & p^{(n)}_{1,1} \end{pmatrix} = \begin{pmatrix} q + p\nu^n & p - p\nu^n \\ q - q\nu^n & p + q\nu^n \end{pmatrix} , \tag{5.5}$$

where $p = \alpha/(\alpha+\beta)$, $q = 1-p$, and $\nu = 1-\beta-\alpha$. We allow p to take values on $(0,1]$ and ν to take values on $(-1,1)$. As is evident from (5.5), the numbers $p^{(n)}_{i,j}$ converge exponentially to numbers p_j, independently of i. We have $p_1 = p$ and $p_0 = 1-p = q$. If we complete the specification of the distribution of the bond variables by letting $\mathbf{P}(B^y_0 = i) = p_i$, then for each y, B^y_n is a stationary sequence.

We define three random sequences— the **increment** X_n, the **displacement** S_n, and the **bond attempted** at time n, Y_n,

$$
\begin{aligned}
X_n =& A_n B_n^{Y_n} = \begin{cases} \mathbf{e}_k & \text{if } A_n = \mathbf{e}_k \text{ and } B_n^{Y_n} = 1, \quad k = 1, \ldots, d \\ -\mathbf{e}_k & \text{if } A_n = -\mathbf{e}_k \text{ and } B_n^{Y_n} = 1, \quad k = 1, \ldots, d \\ 0 & \text{otherwise ,} \end{cases} \\
S_n =& \sum_{i=1}^{n} X_n, \quad S_0 = 0, \\
Y_n =& \text{ the bond extending in the direction } A_n \\
& \text{from the vertex given by } S_{n-1}.
\end{aligned}
\tag{5.6}
$$

Here, S_n is considered to be a vector with its tail at the origin. In the following sections we will study X_n and S_n. We will show that X_n is a stationary process, and that the limiting distribution of $S_n/\sqrt{n}$ is the normal distribution.

We define the nth **step** by $C_n = (A_n, B_n^{Y_n})$. Notice that C_n, unlike X_n, carries complete information about the attempted direction and whether it was successful. We define the **path** $C = (C_1, \ldots, C_n)$, and let $\Omega_1 = \{\pm\mathbf{e}_k, k = 1 \ldots d\} \times \{0, 1\}$ and $\Omega_n = \Omega_1^{(n)}$. Consider the event

$$S = \{C_1 = \omega_1, \ldots, C_n = \omega_n\}, \tag{5.7}$$

where the non-random quantity $\omega = (\omega_1, \ldots, \omega_n) \in \Omega_n$. On the event S, each of the Y_i, takes a constant value. To see this, begin with $S_0 = 0$ and note that fixing $C_1 = \omega_1$ also determines Y_1 and S_1. If S_{i-1} is determined and $C_i = \omega_i$, then Y_{i+1} and S_i are determined. Therefore, the event can also be expressed

$$S = \{A_i = a_i, B_i^{y_i} = b_i; i = 1, \ldots, n\}, \tag{5.8}$$

where the constants a_i, b_i, and y_i are determined via (5.6). It follows from this observation that we can take Ω_n to be the space of elementary events and $A_i, B_i^{Y_i}, Y_i, C_i, X_i$, and S_i to be functions of ω. In the following we will use the probability space $(\Omega_n, \mathcal{F}_n, \mathbf{P}_n)$, where $\mathcal{F}_n$ is the set of all subsets of Ω_n, and $\mathbf{P}_n$ is constructed below. Because $C(\omega) = \omega$ and $C_i(\omega) = \omega_i$, we will also refer to ω as a path and ω_i as a step. For $\omega \in \Omega_n$, we use the notation $\pi_n(\omega)$ for $\mathbf{P}(C_1 = \omega_1, \ldots, C_n = \omega_n)$. For $\lim_{n\to\infty}(\Omega_n, \mathcal{F}_n, \mathbf{P}_n)$, we use the notation $(\Omega, \mathcal{F}, \mathbf{P})$. (Kolmogorov's extension theorem ensures that $\mathbf{P}$ exists and is unique. See, for example, reference (7), pg 428.) For concatenations of paths, we write $\omega\tau = (\omega_1, \ldots, \omega_n, \tau_1, \ldots, \tau_m)$, where $\omega \in \Omega_n$, $\tau \in \Omega_m$, and $\omega\tau \in \Omega_{m+n}$.

We will need the following definition.

Definition 1. A path ω is i,j-**returning** if $j > i$, $Y_j(\omega) = Y_i(\omega)$ and $Y_j(\omega) \neq Y_i(\omega)$, for all k, $i < k < j$. In other words, the path attempts a bond at time i, and attempts it again for the first time at time j.

We can construct $\pi_n(\omega)$ iteratively. If ω is (m,n)-returning, then, using (5.2) and the Markov property of the bond variables,

$$\begin{aligned} \pi_n(\omega) &= \mathbf{P}(\omega_n|\omega_1, \ldots, \omega_{n-1})\pi_{n-1}(\omega_1, \ldots, \omega_{n-1}) \\ &= \frac{1}{2d}\mathbf{P}(B_n^y = b_n|B_m^y = b_m)\pi_{n-1}(\omega_1, \ldots, \omega_{n-1}). \end{aligned} \tag{5.9}$$

Because the entire history is known in the conditional probability, the bond $Y_n = y$ and the time m are known. If the bond y has not been attempted before time n, then the factor in (5.9) assumes the stationary value $\mathbf{P}(B_n^y = b_n)$. When ω is (i,j)-returning and y is the bond attempted at time i, we will use the notation

$$\mathbf{P}(B_i^y = b_i|B_j^y = b_j) = \psi_i(\omega) + \phi_i(\omega), \tag{5.10}$$

where $\psi_i(\cdot)$ is the term in the bond-transition probability (5.5) that is independent of ν, and $\phi_i(\cdot)$ is the term that depends on ν. If, for a fixed j, there is no i for which ω is (i,j)-returning, then $\phi_j(\omega) = 0$. Thus, $\psi_i(\cdot) \in \{p, q\}$ and $\phi_i(\cdot) \in \{0, \pm p\nu^{i-j}, \pm q\nu^{i-j}\}$. In this way, $\pi_n(\omega)$ can be decomposed,

$$\pi_n(\omega) = \prod_{i=1}^{n} \frac{1}{2d} \left[\psi_i(\omega) + \phi_i(\omega)\right]. \tag{5.11}$$

If $\omega \in \Omega_k$ and $m, n \leq k$, we define

$$\pi_{m,n}(\omega) = \prod_{i=m}^{n} \frac{1}{2d} \left[\psi_i(\omega) + \phi_i(\omega)\right]. \tag{5.12}$$

Thus, $\pi_{m,n}(\omega) = \mathbf{P}(C_m = \omega_m, \ldots, C_n = \omega_n | C_1 = \omega_1, \ldots, C_{m-1} = \omega_{m-1})$. Let $\mathcal{A}_m$ be the set of all m-tuples whose elements take values on $\{0, 1\}$. We define, for $i \leq m$,

$$f_i(\cdot, \alpha) = \begin{cases} \psi_i(\cdot) & \text{if } \alpha_i = 0, \\ \phi_i(\cdot) & \text{if } \alpha_i = 1. \end{cases} \tag{5.13}$$

We expand the product in (5.11) and write

$$\pi_n(\omega) = \frac{1}{(2d)^n} \sum_{\alpha \in \mathcal{A}_n} \left[f_1 \cdots f_n\right](\omega, \alpha). \tag{5.14}$$

In the remainder of this section, we present some definitions that will be useful in analyzing terms in sums such as those in (5.14). We define $\mathcal{T} = \Omega_n \times \mathcal{A}_m$, with $m \geq n$.

Definition 2. We say that a pair $(\omega, \alpha) \in \mathcal{T}$ is i,j-**returning** if ω is (i,j)-returning and $f_j(\cdot, \alpha) = \phi_j(\cdot)$.

Remark. Definition 2 gives a necessary and sufficient condition that $f_j(\cdot, \alpha) = c\nu^{j-i}$, where $c \in \{\pm p, \pm q\}$.

Definition 3. We say that a pair $(\omega, \alpha) \in \mathcal{T}$ is i,j-**finished** if i is the greatest integer, with $i \leq j$, for which the following condition holds.

For each $k \geq i$, such that $f_k(\cdot, \alpha) = \phi_k(\cdot)$, there is an $l \geq i$ such that (ω, α) is (l,k)-returning.

Remark. Two immediate consequences of Definition 3 are that $f_i(\cdot, \alpha) = \psi_i(\cdot)$ (that is, $\alpha_i = 0$), and that $[f_i \cdots f_n](\omega, \alpha)$ is independent of ω_k and α_k for $k < i$.

Lemma 1. *Consider a fixed $j \in \{1, \ldots, n\}$ and $(\omega, \alpha) \in \mathcal{T}$. If there is no $k \in \{1, \ldots, n\}$ for which $f_k(\omega, \alpha) = 0$, then there is an i such that (ω, α) is (i,j)-finished. Furthermore, if (ω, α) is (i,j)-finished, then i is unique.*

Remark. Lemma 1 means that any contributing term in sums such as (5.14) corresponds to a pair (ω, α) that is (i,j)-finished for a unique i.

Proof. Because i is the maximum of a finite set of integers, it is unique. To show existence, we assume that (ω, α) is not (i,j)-finished for any i. Then there is no i for which the condition in Definition 3 holds. This means that there is some $k \geq j$ with with $f_k(\cdot, \alpha) = \phi_k(\cdot)$, but (ω, α) is not (l,k)-returning. This implies that $f_k(\omega, \alpha) = 0$. □

5.2 Stationarity of X_n

Theorem 2. *The sequences C_n and X_n are stationary. That is, for each n, the distributions of*

$$(C_k, \ldots, C_{k+n}) \text{ and } (X_k, \ldots, X_{k+n}) \tag{5.15}$$

are independent of k.

Proof. The events $\{(C_k, \ldots, C_{k+n}) \in \tilde{A}\}$ and $\{(X_k, \ldots, X_{k+n}) \in \tilde{B}\}$ can be written as disjoint unions of elementary events ω of the type in (5.7). But we argued that

these events can be expressed by the event given in (5.8), with the advantage that the random bond Y_i no longer appears. Because (5.2) holds for the event in (5.8), and, for each y, $(B_1^y, B_2^y, \dots)$ is a stationary sequence, then the probability of the event in (5.8) can be written as the product of probabilities of events, each of which involves only one stationary sequence. Because the probability of the union of disjoint events is the sum of the probabilities of the events, each of which is independent of k, the statement of the theorem follows. □

5.3 Central Limit Theorem

We want to measure the dependence between two events that are separated by n time steps. Let $\tau^A \in \Omega_r$, and $\tau^B \in \Omega_s$ be arbitrary paths of length r and s. We define the events $A = \{C_1 = \tau_1^A, \dots, C_r = \tau_r^A\}$ and $B = \{C_{r+n+1} = \tau_1^B, \dots, C_r = \tau_{r+n+s}^B\}$. Because C_i is a stationary sequence, $\mathbf{P}(B) = \mathbf{P}(C_1 = \tau_1^B, \dots, C_r = \tau_s^B)$. We define $z = \max\{p, q\}$.

Lemma 3.

$$\frac{|\mathbf{P}(AB) - \mathbf{P}(A)\mathbf{P}(B)|}{\mathbf{P}(A)} \leq (2^{d+1} z\nu)^n. \tag{5.16}$$

Proof. Because $\mathbf{P}(AB) - \mathbf{P}(A)\mathbf{P}(B) = [\mathbf{P}(B|A) - \mathbf{P}(B)]\mathbf{P}(A)$, we need only analyze $\mathbf{P}(B|A) - \mathbf{P}(B)$. For $\omega' \in \Omega_n$, let $M(\omega') = \{C_{r+1} = \omega_1', \dots, C_{r+n} = \omega_n'\}$. Then

$$\begin{aligned} \mathbf{P}(B|A) - \mathbf{P}(B) &= \sum_{\omega' \in \Omega_n} \mathbf{P}(M|A) \left\{\mathbf{P}(B|A \cap M) - \mathbf{P}(B)\right\} \\ &= \sum_{\omega' \in \Omega_n} \pi_{r+1,r+n}(\tau^A \omega') \left[\pi_{r+n+1,r+n+s}(\tau^A \omega' \tau^B) - \pi_{1,s}(\tau^B)\right]. \end{aligned} \tag{5.17}$$

Let $\mathcal{A}_{n+r+s}^*$ be the set of all $\alpha \in \mathcal{A}_{n+r+s}$ such that $\alpha_i = 1$ for $i \leq r$. (The value 1 is not important, but we do not want to sum over α_i for $i \leq r$.) We define

$\alpha' = (\alpha_{r+n+1}, \ldots, \alpha_{r+n+s})$, and write

$$\mathbf{P}(B|A) - \mathbf{P}(B) = \frac{1}{(2d)^{n+s}} \sum_{\omega' \in \Omega_n} \sum_{\alpha \in \mathcal{A}^*_{n+r+s}} [f_{r+1} \cdots f_{r+n}]\,(\tau^A \omega', \alpha) \;\times$$
$$\left\{ [f_{r+n+1} \cdots f_{r+n+s}]\,(\tau^A \omega' \tau^B, \alpha) - [f_1 \cdots f_s]\,(\tau^B, \alpha') \right\}. \quad (5.18)$$

Suppose $(\tau^A \omega' \tau^B, \alpha)$ is $(r+n+1, r+n+1)$-finished. It follows immediately that $[f_{r+n+1} \cdots f_{r+n+s}]\,(\tau^A \omega' \tau^B, \alpha)$ is independent of $\tau^A \omega'$ and thus is equal to $[f_1 \cdots f_s]\,(\tau^B, \alpha')$. On the other hand, if $(\tau^A \omega' \tau^B, \alpha)$ is $(a, r+n+1)$-finished for some $a < r+n+1$, then there must be some $i < r+n+1$ and $j \geq r+n+1$ such that $(\tau^A \omega' \tau^B, \alpha)$ is (i,j)-returning. In other words, $f_j(\cdot, \alpha) = \phi_j(\cdot)$, and $\tau^A \omega' \tau^B$ is (i,j)-returning. But this means that $f_{j-(r+n)}(\tau^B, \alpha') = \phi_{j-(r+n)}(\tau^B) = 0$, because the bond attempted by $\tau^B_{j-(r+n)}$ was not visited by any previous step in τ^B. It follows from Lemma 1 that some of the terms in $\mathbf{P}(B)$ cancel terms in $\mathbf{P}(B|A \cap M)$, while the remaining terms in $\mathbf{P}(B)$ vanish. We can now write

$$\mathbf{P}(B|A) - \mathbf{P}(B) = \frac{1}{(2d)^{n+s}} \sum_{(\omega,\alpha) \in \mathcal{T}} [f_{r+1} \cdots f_{r+n+s}]\,(\omega, \alpha), \quad (5.19)$$

where $\mathcal{T}$ consists of all pairs with the restrictions $\omega = \tau^A \omega' \tau^B$, and that (ω, α) is $(a, r+n+1)$-finished for some $a < r+n+1$. [Stated more simply, (ω, α) is $(a, r+n)$-finished for some a.]

Before continuing, we introduce two lemmas that refer to the set $\mathcal{T}$ used in (5.19).

Lemma 4. *If $(\omega, \alpha) \in \mathcal{T}$ is $(a, r+n)$-finished, then*

$$[f_a \cdots f_{r+n+s}]\,(\omega, \alpha) = c\nu^{r+n-a}, \quad (5.20)$$

where $|c| \leq 1$.

Proof. For some $l_1 > r+n$ and $k_1 \leq r+n$, (ω, α) must be (k_1, l_1)-returning; otherwise (ω, α) would be $(r+n+1, r+n+1)$-finished, but $\mathcal{T}$ excludes such pairs. We make the following proposition.

If (ω, α) is (k_i, l_i)-returning, with $k_i > a$, then (ω, α) must be (k_{i+1}, l_{i+1})-returning, with $a \leq k_{i+1} < k_i \leq l_{i+1}$.

To demonstrate this proposition, we consider the two cases $f_{k_i}(\cdot, \alpha) = \psi_{k_i}(\cdot)$ and $f_{k_i}(\cdot, \alpha) = \phi_{k_i}(\cdot)$ separately. If $f_{k_i}(\cdot, \alpha) = \phi_{k_i}(\cdot)$, then, by Definition 3, (ω, α) must be (m, k_i)-returning for some m with $a \leq m < k_i$. But in this case, we can take $k_{i+1} = m$ and $l_{i+1} = k_i$, satisfying the proposition. Now consider the second case, $f_{k_i}(\cdot, \alpha) = \psi_{k_i}(\cdot)$. Assume that the proposition does not not hold. In particular, assume (ω, α) is (k_i, l_i)-returning with $k_i > a$, but that (ω, α) is not (k_{i+1}, l_{i+1})-returning for any k_{i+1}, l_{i+1} with $a \leq k_{i+1} < k_i < l_{i+1}$. Then, for every $j > k_i$ for which $f_j(\cdot, \alpha) = \phi_j(\cdot)$, ω is (m, j)-returning for some $m > k_i$. But this implies that (ω, α) is (k_i, l_i)-finished, and thus contradicts the hypothesis that a is the largest integer for which the condition in Definition 3 holds. So the proposition is proved.

Because $n + r + s - a$ is finite, and $k_{i+1} < k_i$, there must be an M for which $k_M = a$. For each pair k_i, l_i, there is a factor of $\nu^{l_i - k_i}$ in the left hand side of (5.20). Multiplying these factors, we obtain a factor of ν raised to an exponent.

This exponent can be written

$$\sum_{i=1}^{M}(l_i - k_i) = l_1 - a + \sum_{i=2}^{M} l_i - \sum_{i=1}^{M-1} k_i \tag{5.21a}$$

$$= l_1 - a + \sum_{i=2}^{M}(l_i - k_{i-1}) \tag{5.21b}$$

$$\geq l_1 - a \tag{5.21c}$$

$$> r + n - a, \tag{5.21d}$$

where we used the fact that $l_i > k_{i-1}$ in (5.21c). The remaining factors in the L.H.S. of (5.20) take values p, q and $\pm p\nu^x, \pm q\nu^x$, for positive integers x. And the coefficients of the factors $\nu^{l_i - k_i}$ are $\pm p, \pm q$. So $|c| \leq 1$. This completes the proof of Lemma 4. □

Lemma 5. *If $(\omega, \alpha) \in \mathcal{T}$ is $(a, r+n)$-finished for some $a > r$, then ω stands in a one-to-one relation with an ω' such that $(\omega', \alpha) \in \mathcal{T}$ and $[f_{r+1} \cdots f_{r+n}](\omega, \alpha) - [f_{r+1} \cdots f_{r+n}](\omega', \alpha) = 0$.*

Proof. (ω, α) must be (a, b)-returning for some b. We define ω' by $\omega_i = \omega'_i$ for all $i \neq a$, and ω'_a as follows. Let $\omega'_a = (-\mathbf{e}_x, 1)$ if $\omega_a = (\mathbf{e}_x, 0)$; $\omega'_a = (\mathbf{e}_x, 0)$ if $\omega_a = (-\mathbf{e}_x, 1)$; $\omega'_a = (-\mathbf{e}_x, 0)$ if $\omega_a = (\mathbf{e}_x, 1)$; and $\omega'_a = (\mathbf{e}_x, 1)$ if $\omega_a = (-\mathbf{e}_x, 0)$, where x is one of the coordinate axes. Let y_i be the bond attempted by ω_i and y'_i be the bond attempted by ω'_i. Clearly, for $i < a$, we have $y_i = y'_i$. But for $i \geq a$, y'_i is translated by $-\mathbf{e}_x$ or $\mathbf{e}_x$ relative to y_i. Still, for $i, j \geq a$, $y_i = y_j$ if and only if $y'_i = y'_j$. Notice that we defined ω'_a in such a way that this statement holds for $i = a$. It follows that, for $i \geq a$, ω' is (i, j)-returning if and only if ω is (i, j)-returning, so that (ω', α) is $(a, r+n)$-finished. Consider some $j > a$, but $j \neq b$. If $\alpha_j = 1$, then, because (ω, α) is (i, j)-returning with $i \geq a$ and $\omega_i = \omega'_i$ and $\omega_j = \omega'_j$, it follows that $\phi_j(\omega) = \phi_j(\omega')$. On the other hand, if $\alpha_j = 0$, then $f_j(\cdot, \alpha) = \psi_j(\cdot)$, which depends

only on ω_j and not on ω_i, so that $\psi_j(\omega) = \psi_j(\omega')$. Now $\alpha_a = 0$, otherwise neither (ω, α) nor (ω', α) would be $(a, r+n)$-finished. Referring to (5.5), we see that, for any ω_b,

$$\psi_a(\omega)\phi_b(\omega) = -\psi_a(\omega')\phi_b(\omega') = pq\nu^{b-a}. \tag{5.22}$$

Thus terms for which (ω, α) is $(a, r+n)$-finished for some $a > r$ cancel pairwise. This completes the proof of Lemma 5. □

Now we can finish the proof of lemma 3. In Lemma 5 we showed that terms in the sum in (5.19) vanish if (ω, α) is $(a, r+n)$-finished for $a > r$. The remaining terms are $(a, r+n)$-finished for $a \leq r$. But, by Lemma 4, these terms each contain a factor of ν^x, where $x \geq n$. The remaining factors are less than 1 in magnitude. Now suppose each term in the sum contributes the the upper bound just computed. There are 2^{d+1} terms in the sum, so we have shown the statement in Lemma 3. □

Lemma 6. *The sequence X_n is uniformly mixing, with a mixing coefficient $|\gamma(n)| < (2^{d+1}z\nu)^n$. The uniform mixing condition is (see (14), page 308)*

$$\sup_{A \in \mathcal{M}_1^r, B \in \mathcal{M}_{r+n}^\infty} \frac{|\mathbf{P}(AB) - \mathbf{P}(A)\mathbf{P}(B)|}{\mathbf{P}(A)} = \gamma(n) \to 0, \tag{5.23}$$

where $\mathcal{M}_i^j$ is the σ-algebra generated by $(X_i, X_{i+1}, \ldots, X_j)$.

Proof. We demonstrate that $\gamma(n)$ is bounded by $(2^{d+1}z\nu)^n$ uniformly in A and B as follows. The events A and B can be written as disjoint unions of events of the

type in the statement of Lemma 3. We take $A = \cup_i A_i$ and $B = \cup_i B_i$, and write

$$\begin{aligned}
&|\mathbf{P}([\cup_i A_i] \cap [\cup_j B_j]) - \mathbf{P}(\cup_i A_i)\mathbf{P}(\cup_j B_j)| \\
=&|\mathbf{P}(\cup_{i,j} A_i \cap B_j) - \mathbf{P}(\cup_i A_i)\mathbf{P}(\cup_j B_j)| \\
=&\left|\sum_{i,j} \mathbf{P}(A_i \cap B_j) - \mathbf{P}(A_i)\mathbf{P}(B_j)\right| \\
=&\left|\sum_i \mathbf{P}(A_i) \sum_j [\mathbf{P}(B_j|A_i) - \mathbf{P}(B_j)]\right| \\
=&\mathbf{P}(A)\left|\sum_j [\mathbf{P}(B_j|A_i) - \mathbf{P}(B_j)]\right| \\
<&\mathbf{P}(A)(2^{d+1} z\nu)^n
\end{aligned} \tag{5.24}$$

□

We state the central limit theorem.

Theorem 7. *Let $z = \max\{p, q\}$. If $8(2^d)z\nu < p$, then the following statements hold for the sequence X_n.*

$$\sigma^2 = \mathbf{E}(X_1^2) + 2\sum_{j=2}^{\infty} \mathbf{E}(X_1 X_j) < \infty. \tag{5.25}$$

and

$$\lim_{n\to\infty} \mathbf{P}\left\{\sigma^{-1} n^{-\frac{1}{2}} \sum_{j=1}^{\infty} X_j < z\right\} = (2\pi)^{-\frac{1}{2}} \int_{-\infty}^{x} e^{-\frac{1}{2}u^2} du \tag{5.26}$$

Remark. There are many limit theorems designed to be easily applied to specific processes such as X_n. The relatively strong condition that the mixing coefficient decays exponentially (and that X_n is bounded) allow us to choose from several such theorems. We choose one that is easy to state. We note that statements about mixing and limits are usually made about sequences with index $n \in \mathbb{Z}$. However, any stationary sequence $\{X_n : n > 0\}$ can be embedded in a stationary sequence $\{Y_n : n \in \mathbb{Z}\}$. See, for example reference (7) pg 293.

Proof. The conclusion follows from a theorem by Ibragimov and Linnick (reference (14), theorem 18.5.2, pg 344). For a stationary, uniformly mixing sequence, (5.25) follows if $\sum_{n=1}^{\infty}[\gamma(n)]^{(1/2)} \leq \infty$, and we have shown that this is true if $2(2^d)z\nu < 1$. Equation (5.26) follows if $\sigma \neq 0$. Because $\mathbf{E}(X_1^2) = p$, we must show that the sum in (5.25) is greater than $-p$. The negative contribution to $\mathbf{E}(X_1X_j)$ is $-2P(X_1 = 1, X_j = -1)$. So we must require $8(2^d)z\nu < p$. □

CHAPTER 6

Conclusions

In this chapter, we summarize our work and note some interesting open questions. We analyzed a model of diffusion on a fluctuating, disordered lattice (the fluctuating bond random walk) using a variety of analytic and numerical techniques in order to compute the diffusion constant D. We obtained accurate numerical results for a wide range of model parameters and verified the scaling behavior that one expects on the basis of the theory of critical phenomena.

We introduced lattice fluctuations by assuming that the bonds connecting lattice sites appear and disappear randomly in time, with p denoting the mean density of open bonds and τ denoting the correlation time in the state of a single bond. We computed the diffusivity as a function of p and τ. The motion is asymptotically diffusive (the mean square displacement is proportional to time) except on a critical manifold defined by $\tau = \infty$ and $p \geq p_c$, where p_c is the critical probability for bond percolation.

We performed Monte Carlo simulations of the fluctuating bond random walk (FBRW) on the Bethe lattice with $z = 3$ for several values of p and $\nu = \exp(-1/\tau)$. We found that the motion approaches asymptotic behavior on a time scale that diverges as $(p, \nu) \to (p_c, 1)$. (Note that this distinguishes $(p_c, 1)$ from other points on the critical manifold mentioned above.) Thus, we were able to extract accurate estimates of D from the Monte Carlo data for values of (p, ν) that

are not too close to $(p_c, 1)$. The Monte Carlo data also confirmed our intuitive expectation that D increases with increasing p and decreases with increasing ν.

We predicted the scaling behavior of D near the critical point $(p_c, 1)$. We confirmed this behavior and measured the critical exponents using the Monte Carlo data for the Bethe lattice. It remains to understand how the exponents in our scaling formulas are related to known scaling exponents. Our hypothesis should be tested via Monte Carlo studies on Euclidean lattices as well. We expect that the scaling behavior will exhibit universality— in particular the critical exponents will depend on the dimension but not on the details of the structure of the lattice. The scaling should be found in both discrete and continuous time models, as they have the same behavior for large τ.

We computed exact expansions for D in the limit that the number of steps $n \to \infty$. We computed terms in an expansion about $\nu = 0$ to several orders for several lattices. We found that coefficients in this expansion are polynomials in p, each with a number of terms that increases with the power of ν. With some plausible assumptions, we obtained one or two terms in an expansion about $p = 0$ for the same lattices. The coefficients in this expansion are more complicated and are not in general polynomials in ν. Both expansions agree well with the Monte Carlo results. It would be interesting to better characterize the terms in the expansions in order to compute more of them and also to improve our lower bound on the radius of convergence of the series in ν.

We computed estimates of D using a renormalization group (RG) scheme and compared the results to the estimates of D that we obtained through the methods mentioned above. The RG scheme used here is based on a scheme used by

Levermore, *et. al.* (19) to study the FBRW in one-dimension. Here we mention the two most important extensions to their method that we made in this study. First, we replaced a diagramatic method for computing approximates to the diffusivity by a special purpose computer algebra program. Second, we applied the method to higher dimensions and to the Bethe lattice. While the calculation of the approximate diffusivities used in the RG scheme is computationally expensive, once these calculations are done, the RG method can be quickly applied to obtain an estimate of the diffusivity for any pair of parameter values.

We provided some answers to the question of how well the RG flow describes the actual FBRW. We found that the critical point in our model is represented by the unstable fixed point $(p, \nu) = (1, 1)$ in the RG flow. In one dimension the unstable fixed point is numerically equal to the critical point in the exact model. Indeed, it has been seen (19) that the RG in one dimension gives excellent numerical predictions of D. However, we showed that effects of the super-critical phase of the percolation problem are present in the FBRW when ν is near one (*e.g.* in the scaling laws). The RG has no basin of attraction corresponding to the super-critical phase, and thus predicts the behavior of D poorly in this region. However, if ν is not near 1, or if $p < p_c$, the RG reproduces the correct qualitative behavior, and gives good numerical results, even for $d > 1$. It would be interesting to find an RG scheme that makes a better prediction of the critical point— one that captures some of the super-critical behavior.

Finally, we proved that the distribution of the walker's position converges to a normal distribution (when suitably normalized) for certain model parameters. The restriction on the parameters is computed from a lower bound on the radius of

convergence of a particular series. There are many interesting possible extensions to this work. *i*) All other evidence (*e.g.* Monte Carlo evidence) supports the claim that the series in fact converges on the entire parameter space. A proof that this is the case would be interesting to obtain, as it may shed light on the nature of the model, in particular on the question of how to compute the diffusivity. *ii*) Although calculating the variance is in general difficult, it appears that the variance is less than p for $\nu > 0$. Understanding this in a rigorous way may not be too difficult. *iii*) We mentioned the HZ model, which replaces the steps at discrete times with steps occurring at exponentially distributed random times with mean separation 1 (13). There is evidence that this model also obeys a central limit theorem. But a proof might look much different than the present proof, because the time between steps may be arbitrarily large or small and the easy expression of relevant quantities as power series in ν is no longer possible. *iv*) Another physically relevant generalization is to allow more than two bond states. A two state Markov process in a stationary state necessarily satisfies detailed balance, and thus the stationary measure is reversible. It would be interesting to see what effects an irreversible measure might have on the distribution.

APPENDIX A

Average Approximates D^A for the Bethe Lattice

We tabulate the average approximates D_n^A to the diffusivity for the Bethe lattice with $z = 3$. We list D_n^A for n from 1 to 10. The approximates are computed by machine according to

$$D_n^A(p,\nu) = \frac{1}{n}\langle S_n^2\rangle, \tag{A.1}$$

as on page 27.

$$D_1^A(p,\nu) = p. \tag{A.2}$$

$$D_2^A(p,\nu) = p\left(1 - \frac{1}{3}\nu\right) + p^2\left(\frac{1}{3}\nu\right). \tag{A.3}$$

$$D_3^A(p,\nu) = p\left(1 - \frac{4}{9}\nu - \frac{2}{27}\nu^2\right) + p^2\left(\frac{4}{9}\nu + \frac{2}{27}\nu^2\right). \tag{A.4}$$

$$\begin{aligned} D_4^A(p,\nu) = {} & \\ & p\left(1 - \frac{1}{2}\nu - \frac{1}{9}\nu^2 - \frac{1}{54}\nu^3\right) + p^2\left(\frac{1}{2}\nu + \frac{1}{9}\nu^2 + \frac{1}{54}\nu^3 - \frac{1}{18}\nu^4\right) \\ & + p^3\left(-\frac{1}{27}\nu^3 + \frac{1}{9}\nu^4\right) + p^4\left(\frac{1}{27}\nu^3 - \frac{1}{18}\nu^4\right). \end{aligned} \tag{A.5}$$

$$
\begin{aligned}
D_5^A(p,\nu) = \\
&p\left(1-\frac{8}{15}\nu-\frac{2}{15}\nu^2-\frac{4}{135}\nu^3-\frac{2}{405}\nu^4\right)\\
&+p^2\left(\frac{8}{15}\nu+\frac{2}{15}\nu^2+\frac{4}{135}\nu^3-\frac{34}{405}\nu^4-\frac{4}{135}\nu^5-\frac{2}{135}\nu^6\right)\\
&+p^3\left(-\frac{8}{135}\nu^3+\frac{52}{405}\nu^4+\frac{4}{45}\nu^5+\frac{2}{81}\nu^6\right)\\
&+p^4\left(\frac{8}{135}\nu^3-\frac{4}{405}\nu^4-\frac{4}{45}\nu^5-\frac{2}{405}\nu^6\right)\\
&+p^5\left(-\frac{4}{135}\nu^4+\frac{4}{135}\nu^5-\frac{2}{405}\nu^6\right).
\end{aligned}
\tag{A.6}
$$

$$
\begin{aligned}
D_6^A(p,\nu) = \\
&p\left(1-\frac{5}{9}\nu-\frac{4}{27}\nu^2-\frac{1}{27}\nu^3-\frac{2}{243}\nu^4-\frac{1}{729}\nu^5\right)\\
&+p^2\left(\frac{5}{9}\nu+\frac{4}{27}\nu^2+\frac{1}{27}\nu^3-\frac{25}{243}\nu^4-\frac{35}{729}\nu^5-\frac{1}{27}\nu^6-\frac{2}{243}\nu^7-\frac{2}{243}\nu^8\right)\\
&+p^3\left(-\frac{2}{27}\nu^3+\frac{34}{243}\nu^4+\frac{8}{81}\nu^5+\frac{26}{243}\nu^6+\frac{1}{729}\nu^7+\frac{2}{81}\nu^8-\frac{1}{81}\nu^9\right)\\
&+p^4\left(\frac{2}{27}\nu^3+\frac{5}{243}\nu^4-\frac{8}{243}\nu^5-\frac{116}{729}\nu^6+\frac{11}{243}\nu^7-\frac{29}{729}\nu^8+\frac{1}{27}\nu^9\right)\\
&+p^5\left(-\frac{4}{81}\nu^4-\frac{38}{729}\nu^5+\frac{106}{729}\nu^6-\frac{5}{81}\nu^7+\frac{28}{729}\nu^8-\frac{1}{27}\nu^9\right)\\
&+p^6\left(\frac{26}{729}\nu^5-\frac{41}{729}\nu^6+\frac{17}{729}\nu^7-\frac{11}{729}\nu^8+\frac{1}{81}\nu^9\right).
\end{aligned}
\tag{A.7}
$$

$$
\begin{aligned}
D_7^{\mathrm{A}}(p,\nu) = \\
&p\left(1-\frac{4}{7}\nu-\frac{10}{63}\nu^2-\frac{8}{189}\nu^3-\frac{2}{189}\nu^4-\frac{4}{1701}\nu^5-\frac{2}{5103}\nu^6\right)\\
&+p^2\left(\frac{4}{7}\nu+\frac{10}{63}\nu^2+\frac{8}{189}\nu^3-\frac{22}{189}\nu^4-\frac{104}{1701}\nu^5\right.\\
&\qquad\left.-\frac{268}{5103}\nu^6-\frac{32}{1701}\nu^7-\frac{10}{567}\nu^8-\frac{8}{1701}\nu^9-\frac{8}{1701}\nu^{10}\right)\\
&+p^3\left(-\frac{16}{189}\nu^3+\frac{4}{27}\nu^4+\frac{20}{189}\nu^5+\frac{614}{5103}\nu^6+\frac{92}{1701}\nu^7+\frac{64}{1701}\nu^8-\frac{20}{1701}\nu^9+\frac{16}{1701}\nu^{10}\right.\\
&\qquad\left.-\frac{16}{1701}\nu^{11}-\frac{10}{5103}\nu^{12}\right)\\
&+p^4\left(\frac{16}{189}\nu^3+\frac{8}{189}\nu^4+\frac{4}{567}\nu^5-\frac{638}{5103}\nu^6-\frac{668}{5103}\nu^7-\frac{2}{729}\nu^8+\frac{244}{5103}\nu^9-\frac{2}{1701}\nu^{10}\right.\\
&\qquad\left.+\frac{188}{5103}\nu^{11}+\frac{2}{729}\nu^{12}\right)\\
&+p^5\left(-\frac{4}{63}\nu^4-\frac{188}{1701}\nu^5+\frac{230}{5103}\nu^6+\frac{436}{1701}\nu^7-\frac{388}{5103}\nu^8-\frac{44}{1701}\nu^9-\frac{74}{5103}\nu^{10}\right.\\
&\qquad\left.-\frac{92}{1701}\nu^{11}+\frac{2}{567}\nu^{12}\right)\\
&+p^6\left(\frac{104}{1701}\nu^5+\frac{292}{5103}\nu^6-\frac{412}{1701}\nu^7+\frac{500}{5103}\nu^8-\frac{4}{189}\nu^9+\frac{94}{5103}\nu^{10}+\frac{20}{567}\nu^{11}-\frac{38}{5103}\nu^{12}\right)\\
&+p^7\left(-\frac{76}{1701}\nu^6+\frac{416}{5103}\nu^7-\frac{200}{5103}\nu^8+\frac{80}{5103}\nu^9-\frac{38}{5103}\nu^{10}-\frac{44}{5103}\nu^{11}+\frac{16}{5103}\nu^{12}\right).
\end{aligned}
\tag{A.8}
$$

$$
\begin{aligned}
D_8^A(p,\nu) = \\
&p\left(1-\frac{7}{12}\nu-\frac{1}{6}\nu^2-\frac{5}{108}\nu^3-\frac{1}{81}\nu^4-\frac{1}{324}\nu^5-\frac{1}{1458}\nu^6-\frac{1}{8748}\nu^7\right)\\
&+p^2\left(\frac{7}{12}\nu+\frac{1}{6}\nu^2+\frac{5}{108}\nu^3-\frac{41}{324}\nu^4-\frac{23}{324}\nu^5-\frac{187}{2916}\nu^6-\frac{233}{8748}\nu^7\right.\\
&\quad\left.-\frac{77}{2916}\nu^8-\frac{7}{729}\nu^9-\frac{5}{486}\nu^{10}-\frac{2}{729}\nu^{11}-\frac{2}{729}\nu^{12}\right)\\
&+p^3\left(-\frac{5}{54}\nu^3+\frac{25}{162}\nu^4+\frac{1}{9}\nu^5+\frac{95}{729}\nu^6+\frac{461}{8748}\nu^7+\frac{22}{243}\nu^8-\frac{133}{8748}\nu^9+\frac{29}{1458}\nu^{10}\right.\\
&\quad\left.-\frac{7}{486}\nu^{11}+\frac{1}{486}\nu^{12}-\frac{41}{4374}\nu^{13}-\frac{1}{1458}\nu^{14}-\frac{1}{729}\nu^{15}\right)\\
&+p^4\left(\frac{5}{54}\nu^3+\frac{19}{324}\nu^4+\frac{1}{27}\nu^5-\frac{145}{1458}\nu^6-\frac{839}{8748}\nu^7-\frac{37}{162}\nu^8+\frac{1135}{8748}\nu^9-\frac{137}{8748}\nu^{10}\right.\\
&\quad\left.+\frac{64}{729}\nu^{11}-\frac{11}{1458}\nu^{12}+\frac{205}{4374}\nu^{13}-\frac{35}{4374}\nu^{14}+\frac{13}{2187}\nu^{15}-\frac{8}{2187}\nu^{16}\right)\\
&+p^5\left(-\frac{2}{27}\nu^4-\frac{25}{162}\nu^5-\frac{22}{729}\nu^6+\frac{457}{2916}\nu^7+\frac{1028}{2187}\nu^8-\frac{2503}{8748}\nu^9+\frac{100}{2187}\nu^{10}-\frac{803}{4374}\nu^{11}\right.\\
&\quad\left.+\frac{199}{4374}\nu^{12}-\frac{859}{8748}\nu^{13}+\frac{169}{4374}\nu^{14}-\frac{41}{2916}\nu^{15}+\frac{32}{2187}\nu^{16}\right)\\
&+p^6\left(\frac{13}{162}\nu^5+\frac{415}{2916}\nu^6-\frac{17}{324}\nu^7-\frac{2689}{4374}\nu^8+\frac{3289}{8748}\nu^9-\frac{161}{1458}\nu^{10}+\frac{305}{1458}\nu^{11}-\frac{679}{8748}\nu^{12}\right.\\
&\quad\left.+\frac{937}{8748}\nu^{13}-\frac{89}{1458}\nu^{14}+\frac{59}{2916}\nu^{15}-\frac{16}{729}\nu^{16}\right)\\
&+p^7\left(-\frac{19}{243}\nu^6-\frac{413}{4374}\nu^7+\frac{1919}{4374}\nu^8-\frac{610}{2187}\nu^9+\frac{475}{4374}\nu^{10}-\frac{95}{729}\nu^{11}+\frac{241}{4374}\nu^{12}-\frac{527}{8748}\nu^{13}\right.\\
&\quad\left.+\frac{91}{2187}\nu^{14}-\frac{133}{8748}\nu^{15}+\frac{32}{2187}\nu^{16}\right)\\
&+p^8\left(\frac{263}{4374}\nu^7-\frac{1135}{8748}\nu^8+\frac{184}{2187}\nu^9-\frac{331}{8748}\nu^{10}+\frac{149}{4374}\nu^{11}-\frac{43}{2916}\nu^{12}+\frac{121}{8748}\nu^{13}-\frac{23}{2187}\nu^{14}\right.\\
&\quad\left.+\frac{13}{2916}\nu^{15}-\frac{8}{2187}\nu^{16}\right).
\end{aligned}
\tag{A.9}
$$

$$
\begin{aligned}
D_9^A(p,\nu) = \\
&p\Big(1-\frac{16}{27}\nu-\frac{14}{81}\nu^2-\frac{4}{81}\nu^3-\frac{10}{729}\nu^4-\frac{8}{2187}\nu^5-\frac{2}{2187}\nu^6-\frac{4}{19683}\nu^7-\frac{2}{59049}\nu^8\Big)\\
&+p^2\Big(\frac{16}{27}\nu+\frac{14}{81}\nu^2+\frac{4}{81}\nu^3-\frac{98}{729}\nu^4-\frac{172}{2187}\nu^5-\frac{160}{2187}\nu^6-\frac{644}{19683}\nu^7-\frac{1960}{59049}\nu^8\\
&\quad-\frac{92}{6561}\nu^9-\frac{298}{19683}\nu^{10}-\frac{112}{19683}\nu^{11}-\frac{40}{6561}\nu^{12}-\frac{32}{19683}\nu^{13}-\frac{32}{19683}\nu^{14}\Big)\\
&+p^3\Big(-\frac{8}{81}\nu^3+\frac{116}{729}\nu^4+\frac{28}{243}\nu^5+\frac{302}{2187}\nu^6+\frac{1016}{19683}\nu^7+\frac{1868}{19683}\nu^8+\frac{388}{19683}\nu^9+\frac{1526}{59049}\nu^{10}\\
&\quad-\frac{104}{6561}\nu^{11}+\frac{92}{19683}\nu^{12}-\frac{320}{19683}\nu^{13}\\
&\quad+\frac{14}{19683}\nu^{14}-\frac{184}{19683}\nu^{15}-\frac{26}{19683}\nu^{16}-\frac{16}{19683}\nu^{17}-\frac{14}{19683}\nu^{18}\Big)\\
&+p^4\Big(\frac{8}{81}\nu^3+\frac{52}{729}\nu^4+\frac{44}{729}\nu^5-\frac{58}{729}\nu^6-\frac{1352}{19683}\nu^7-\frac{478}{2187}\nu^8-\frac{5548}{59049}\nu^9+\frac{1040}{19683}\nu^{10}\\
&\quad+\frac{2180}{19683}\nu^{11}+\frac{698}{59049}\nu^{12}+\frac{5356}{59049}\nu^{13}-\frac{1150}{59049}\nu^{14}+\frac{964}{19683}\nu^{15}-\frac{748}{59049}\nu^{16}\\
&\quad+\frac{32}{19683}\nu^{17}+\frac{8}{59049}\nu^{18}-\frac{28}{19683}\nu^{19}+\frac{4}{59049}\nu^{20}\Big)\\
&+p^5\Big(-\frac{20}{243}\nu^4-\frac{412}{2187}\nu^5-\frac{194}{2187}\nu^6+\frac{520}{6561}\nu^7+\frac{24188}{59049}\nu^8+\frac{26900}{59049}\nu^9-\frac{20012}{59049}\nu^{10}-\frac{3496}{19683}\nu^{11}\\
&\quad-\frac{3130}{59049}\nu^{12}-\frac{10348}{59049}\nu^{13}+\frac{6056}{59049}\nu^{14}-\frac{7348}{59049}\nu^{15}+\frac{4538}{59049}\nu^{16}-\frac{244}{59049}\nu^{17}\\
&\quad+\frac{158}{19683}\nu^{18}+\frac{124}{19683}\nu^{19}-\frac{136}{59049}\nu^{20}\Big)\\
&+p^6\Big(\frac{208}{2187}\nu^5+\frac{152}{729}\nu^6+\frac{208}{2187}\nu^7-\frac{23924}{59049}\nu^8-\frac{19684}{19683}\nu^9+\frac{15688}{19683}\nu^{10}+\frac{664}{19683}\nu^{11}\\
&\quad+\frac{10526}{59049}\nu^{12}+\frac{8884}{59049}\nu^{13}-\frac{11162}{59049}\nu^{14}+\frac{1228}{6561}\nu^{15}-\frac{1018}{6561}\nu^{16}+\frac{964}{59049}\nu^{17}-\frac{1282}{59049}\nu^{18}\\
&\quad-\frac{8}{729}\nu^{19}+\frac{56}{6561}\nu^{20}\Big)\\
&+p^7\Big(-\frac{76}{729}\nu^6-\frac{4552}{19683}\nu^7+\frac{5296}{59049}\nu^8+\frac{71164}{59049}\nu^9-\frac{58720}{59049}\nu^{10}+\frac{4216}{19683}\nu^{11}-\frac{17342}{59049}\nu^{12}\\
&\quad-\frac{1708}{59049}\nu^{13}+\frac{9764}{59049}\nu^{14}-\frac{3236}{19683}\nu^{15}+\frac{8908}{59049}\nu^{16}-\frac{556}{19683}\nu^{17}+\frac{1552}{59049}\nu^{18}\\
&\quad+\frac{184}{19683}\nu^{19}-\frac{736}{59049}\nu^{20}\Big)\\
&+p^8\Big(\frac{2104}{19683}\nu^7+\frac{8708}{59049}\nu^8-\frac{46220}{59049}\nu^9+\frac{37798}{59049}\nu^{10}-\frac{4684}{19683}\nu^{11}+\frac{13000}{59049}\nu^{12}\\
&\quad-\frac{2192}{59049}\nu^{13}-\frac{4096}{59049}\nu^{14}+\frac{4504}{59049}\nu^{15}-\frac{4274}{59049}\nu^{16}+\frac{1228}{59049}\nu^{17}-\frac{314}{19683}\nu^{18}\\
&\quad-\frac{76}{19683}\nu^{19}+\frac{484}{59049}\nu^{20}\Big)\\
&+p^9\Big(-\frac{556}{6561}\nu^8+\frac{460}{2187}\nu^9-\frac{122}{729}\nu^{10}+\frac{1544}{19683}\nu^{11}-\frac{3668}{59049}\nu^{12}+\frac{1064}{59049}\nu^{13}\\
&\quad+\frac{214}{19683}\nu^{14}-\frac{280}{19683}\nu^{15}+\frac{272}{19683}\nu^{16}-\frac{328}{59049}\nu^{17}+\frac{232}{59049}\nu^{18}+\frac{4}{6561}\nu^{19}\\
&\quad-\frac{40}{19683}\nu^{20}\Big).
\end{aligned}
\tag{A.10}
$$

$$
\begin{aligned}
D_{10}^{A}(p,\nu) = {} & p\Big(1-\frac{3}{5}\nu-\frac{8}{45}\nu^2-\frac{7}{135}\nu^3-\frac{2}{135}\nu^4-\frac{1}{243}\nu^5-\frac{4}{3645}\nu^6-\frac{1}{3645}\nu^7-\frac{2}{32805}\nu^8-\frac{1}{98415}\nu^9\Big)\\
& +p^2\Big(\frac{3}{5}\nu+\frac{8}{45}\nu^2+\frac{7}{135}\nu^3-\frac{19}{135}\nu^4-\frac{103}{1215}\nu^5-\frac{293}{3645}\nu^6-\frac{137}{3645}\nu^7-\frac{1267}{32805}\nu^8-\frac{1727}{98415}\nu^9-\frac{631}{32805}\nu^{10}\\
& \quad -\frac{2}{243}\nu^{11}-\frac{298}{32805}\nu^{12}-\frac{112}{32805}\nu^{13}-\frac{8}{2187}\nu^{14}-\frac{32}{32805}\nu^{15}-\frac{32}{32805}\nu^{16}\Big)\\
& +p^3\Big(-\frac{14}{135}\nu^3+\frac{22}{135}\nu^4+\frac{16}{135}\nu^5+\frac{526}{3645}\nu^6+\frac{37}{729}\nu^7+\frac{1076}{10935}\nu^8+\frac{1417}{98415}\nu^9+\frac{2104}{32805}\nu^{10}\\
& \quad -\frac{593}{32805}\nu^{11}+\frac{308}{32805}\nu^{12}-\frac{727}{32805}\nu^{13}+\frac{16}{32805}\nu^{14}-\frac{1628}{98415}\nu^{15}-\frac{52}{32805}\nu^{16}-\frac{46}{6561}\nu^{17}\\
& \quad -\frac{14}{6561}\nu^{18}-\frac{38}{32805}\nu^{19}-\frac{14}{32805}\nu^{20}-\frac{44}{98415}\nu^{21}\Big)\\
& +p^4\Big(\frac{14}{135}\nu^3+\frac{11}{135}\nu^4+\frac{32}{405}\nu^5-\frac{232}{3645}\nu^6-\frac{19}{405}\nu^7-\frac{256}{1215}\nu^8-\frac{7171}{98415}\nu^9-\frac{4055}{19683}\nu^{10}+\frac{21107}{98415}\nu^{11}\\
& \quad +\frac{839}{98415}\nu^{12}+\frac{14903}{98415}\nu^{13}-\frac{1519}{98415}\nu^{14}+\frac{596}{6561}\nu^{15}-\frac{2968}{98415}\nu^{16}+\frac{268}{6561}\nu^{17}\\
& \quad -\frac{1144}{98415}\nu^{18}+\frac{98}{32805}\nu^{19}-\frac{16}{6561}\nu^{20}+\frac{172}{98415}\nu^{21}-\frac{124}{98415}\nu^{22}-\frac{8}{32805}\nu^{23}-\frac{13}{32805}\nu^{24}\Big)\\
& +p^5\Big(-\frac{4}{45}\nu^4-\frac{262}{1215}\nu^5-\frac{494}{3645}\nu^6+\frac{7}{405}\nu^7+\frac{11852}{32805}\nu^8+\frac{39871}{98415}\nu^9\\
& \quad +\frac{20972}{32805}\nu^{10}-\frac{77789}{98415}\nu^{11}+\frac{758}{98415}\nu^{12}-\frac{1481}{3645}\nu^{13}+\frac{14326}{98415}\nu^{14}-\frac{21802}{98415}\nu^{15}\\
& \quad +\frac{20198}{98415}\nu^{16}-\frac{14584}{98415}\nu^{17}+\frac{10934}{98415}\nu^{18}-\frac{124}{6561}\nu^{19}+\frac{1976}{98415}\nu^{20}-\frac{44}{3645}\nu^{21}\\
& \quad +\frac{82}{10935}\nu^{22}-\frac{26}{19683}\nu^{23}+\frac{94}{32805}\nu^{24}-\frac{86}{98415}\nu^{25}\Big)\\
& +p^6\Big(\frac{26}{243}\nu^5+\frac{953}{3645}\nu^6+\frac{259}{1215}\nu^7-\frac{1558}{6561}\nu^8-\frac{79513}{98415}\nu^9-\frac{48296}{32805}\nu^{10}\\
& \quad +\frac{180163}{98415}\nu^{11}-\frac{18301}{98415}\nu^{12}+\frac{24023}{32805}\nu^{13}-\frac{39109}{98415}\nu^{14}+\frac{32324}{98415}\nu^{15}-\frac{48659}{98415}\nu^{16}\\
& \quad +\frac{3938}{10935}\nu^{17}-\frac{6430}{19683}\nu^{18}+\frac{8812}{98415}\nu^{19}-\frac{6169}{98415}\nu^{20}+\frac{1618}{32805}\nu^{21}-\frac{134}{6561}\nu^{22}\\
& \quad +\frac{106}{10935}\nu^{23}-\frac{989}{98415}\nu^{24}+\frac{86}{19683}\nu^{25}\Big)\\
& +p^7\Big(-\frac{152}{1215}\nu^6-\frac{46}{135}\nu^7-\frac{6218}{32805}\nu^8+\frac{71788}{98415}\nu^9+\frac{46642}{19683}\nu^{10}-\frac{273811}{98415}\nu^{11}+\frac{28}{45}\nu^{12}-\frac{98516}{98415}\nu^{13}\\
& \quad +\frac{58766}{98415}\nu^{14}-\frac{30518}{98415}\nu^{15}+\frac{20584}{32805}\nu^{16}-\frac{17627}{32805}\nu^{17}+\frac{9808}{19683}\nu^{18}-\frac{6209}{32805}\nu^{19}+\frac{11176}{98415}\nu^{20}\\
& \quad -\frac{1927}{19683}\nu^{21}+\frac{628}{19683}\nu^{22}-\frac{2036}{98415}\nu^{23}+\frac{1916}{98415}\nu^{24}-\frac{172}{19683}\nu^{25}\Big)\\
& +p^8\Big(\frac{526}{3645}\nu^7+\frac{12113}{32805}\nu^8-\frac{2684}{19683}\nu^9-\frac{80321}{32805}\nu^{10}+\frac{261779}{98415}\nu^{11}-\frac{18257}{19683}\nu^{12}+\frac{31556}{32805}\nu^{13}\\
& \quad -\frac{54221}{98415}\nu^{14}+\frac{18406}{98415}\nu^{15}-\frac{15059}{32805}\nu^{16}+\frac{46021}{98415}\nu^{17}-\frac{8398}{19683}\nu^{18}+\frac{2177}{10935}\nu^{19}-\frac{11792}{98415}\nu^{20}+\frac{667}{6561}\nu^{21}\\
& \quad -\frac{64}{2187}\nu^{22}+\frac{2044}{98415}\nu^{23}-\frac{683}{32805}\nu^{24}+\frac{172}{19683}\nu^{25}\Big)\\
& +p^9\Big(-\frac{556}{3645}\nu^8-\frac{23438}{98415}\nu^9+\frac{15542}{10935}\nu^{10}-\frac{141541}{98415}\nu^{11}+\frac{63926}{98415}\nu^{12}-\frac{17864}{32805}\nu^{13}+\frac{9536}{32805}\nu^{14}\\
& \quad -\frac{52}{729}\nu^{15}+\frac{18412}{98415}\nu^{16}-\frac{2393}{10935}\nu^{17}+\frac{19124}{98415}\nu^{18}-\frac{10219}{98415}\nu^{19}+\frac{6586}{98415}\nu^{20}-\frac{1061}{19683}\nu^{21}\\
& \quad +\frac{478}{32805}\nu^{22}-\frac{334}{32805}\nu^{23}+\frac{226}{19683}\nu^{24}-\frac{86}{19683}\nu^{25}\Big)\\
& +p^{10}\Big(\frac{12194}{98415}\nu^9-\frac{34297}{98415}\nu^{10}+\frac{32681}{98415}\nu^{11}-\frac{17203}{98415}\nu^{12}+\frac{4324}{32805}\nu^{13}-\frac{6539}{98415}\nu^{14}\\
& \quad +\frac{1394}{98415}\nu^{15}-\frac{1102}{32805}\nu^{16}+\frac{1403}{32805}\nu^{17}-\frac{3604}{98415}\nu^{18}+\frac{707}{32805}\nu^{19}-\frac{299}{19683}\nu^{20}+\frac{1141}{98415}\nu^{21}\\
& \quad -\frac{298}{98415}\nu^{22}+\frac{194}{98415}\nu^{23}-\frac{251}{98415}\nu^{24}+\frac{86}{98415}\nu^{25}\Big).
\end{aligned}
\tag{A.11}
$$

REFERENCES

[1] R. H. Austin, K. W. Beeson, L. Eisenstein, and H. Frauenfelder. Dynamics of ligand binding to myoglobin. *Bioch.*, 14:5355–5373, 1975.

[2] J. Bricmont and A. Kupiainen. Renormalization group for diffusion in a random medium. *Phys. Rev. Lett.*, 66:1689–1692, 1991.

[3] S. R. Broadbent and J. M. Hammersley. Percolation processes. *Proc. Camb. Philos. Soc.*, 53:629–645, 1957.

[4] P. G. de Gennes. La percolation: un concept unificateur. *La Recherche*, 7:919–927, 1976.

[5] S. D. Druger, M. A. Ratner, and A. Nitzan. Dynamic bond percolation theory: A microscopic model for diffusion in dynamically disordered systems. i. definition and one-dimensional case. *J. Chem. Phys.*, 79:3133, 1983.

[6] S. D. Druger, M. A. Ratner, and A. Nitzan. Generalized hopping model for frequency-dependent transport in a dynamically disordered medium, with applications to polymer solid electrolytes. *Phys. Rev. B*, 31:3939–3947, 1985.

[7] R. Durrett. *Probability: Theory and Examples.* Wadsworth & Brooks/Cole, Pacific Grove, California, 1991.

[8] P. J. Flory. *J. Am. Chem. Soc.*, 63:3091, 1941.

[9] N. Goldenfeld. *Phase Transitions and the Renormalization Group.* Publisher, New York, 1821.

[10] R. Granek and A. Nitzan. Correlated dynamic percolation: Many bond effective-medium theory. *J. Chem. Phys.*, 90:3784–1989, 1989.

[11] G. Grimmett. *Percolation.* Springer-Verlag, New York, 1989.

[12] A. B. Harris, Y. Meir, and A. Aharony. Diffusion on percolating clusters. *Phys. Rev. B*, 36:8752–8764, 1987.

[13] A. K. Harrison and R. Zwanzig. Transport on a dynamically disordered lattice. *Phys. Rev. A*, 32:1072–1075, 1985.

[14] I. A. Ibragimov and Y. V. Linnik. *Independent and Stationary Sequences of Random Variables.* Wolters-Noordhoff Publishing, Groningen, The Netherlands, 1971.

[15] J. A. Jaquez. The physiological role of myoglobin: More than a problem in reaction-diffusion kinetics. *Math. Bios.*, 68:57–97, 1984.

[16] H. Kesten. Subdiffusive behavior of random walk on a random cluster. *Ann. Inst. Henri Poincaré*, 22:425–487, 1986.

[17] S. Kirkpatrick. Percolation and conduction. *Rev. Mod. Phys.*, 45:575, 1973.

[18] B. J. Last and D. J. Thouless. Percolation theory and electrical conductivity. *Phys. Rev. Lett.*, 27:1719–1721, 1971.

[19] C. D. Levermore, W. Nadler, and D. L. Stein. Random walks on a fluctuating lattice: A renormalization approach applied in one dimension. *Phys. Rev. E*, 51:2779–2786, 1995.

[20] L. M. Lust and J. Kakalios. Dynamical percolation model of conductance fluctuations in hydrogenated amorphous silicon. *Phys. Rev. Lett.*, 75, 1995.

[21] A. Nitzan and M. A. Ratner. Conduction in polymers: Dynamic disorder transport. *J. Phys. Chem.*, 98:1765–1774, 1994.

[22] T. Odagaki and M. Lax. Coherent-medium approximation in the stochastic transport theory of random media. *Phys. Rev. B*, 24:5284–5294, 1981.

[23] A. Perera, B. Gaveau, M. Moreau, and K. A. Penson. Memory effect in diffusions in a 2d fluctutating lattice. *Phys. Let. A*, 159:158–162, 1991.

[24] M. Settles, F. Post, D. Müller, A. Schulte, and W. Doster. Solvent damping of internal processes in myoglobin studied by specific heat spectroscopy and flash photolysis. *Bioph. Chem.*, 43:107–116, 1992.

[25] D. Stauffer. Scaling theory of percolation clusters. *Phys. Rep.*, 54:1, 1979.

[26] D. Stauffer and A. Aharony. *Introduction to Percolation Theory.* Taylor & Francis, London, 1992.

[27] R. B. Stinchcombe. The branching model for percolation theory and conductivity. *J. Phys. C*, 6:L1–5, 1973.

[28] R. B. Stinchcombe. Conductivity and spin-wave stiffness in disordered systems—an exactly soluble model. *J. Phys. C*, 6:179–203, 1973.

[29] J. P. Straley. The ant in the labyrinth: diffusion in random networks near the percolation threshold. *J. Phys. C*, 13:2991–3003, 1980.